Institut de Chimie Inorganique et Analytique
Université de Fribourg (Suisse)

A study of the photophysical and photochemical properties of metal complexes using Density Functional Theory

THESE

présentée à la Faculté des Sciences de l'Université de Fribourg (Suisse)
pour l'obtention du grade de *Doctor rerum naturalium*

MATTHIEU BUCHS
de
Jaun (FR)

Thèse No 1332

2001

Acceptéee par la Facultée des Sciences de l'Université de Fribourg (Suisse) sur la proposition du jury composé de Messieurs

Prof. Dr. Albert Gossauer, Université de Fribourg, président du Jury

Prof. Dr. Claude Daul, Université de Fribourg, directeur de thèse

Prof. Dr. Carl-Wilhelm Schläpfer, Université de Fribourg, rapporteur

Prof. Dr. Jacques Weber, Université de Genève, rapporteur

Fribourg, le 12 janvier 2001

Le directeur de thèse

Prof. Dr. Claude Daul

Le Doyen

Prof. Dr. Alexander von Zelewsky

Remerciements

Certaines personnes ont contribué à l'aboutissement de ce travail de longue haleine. J'aimerais ici les en remercier.

Un très grand merci, tout d'abord, à l'attention de mon directeur de thèse le Professeur Claude Daul. Merci pour m'avoir ouvert les portes de son groupe, pour son soutien durant ces quatre années de travail, pour ses conseils éclairés ainsi que pour un atmosphère de travail très agréable.

J'aimerais également remercier très chaleureusement le Professeur Jacques Weber, de l'Université de Genève, pour avoir accepté d'endosser le rôle d'expert externe et donc pour avoir lu et rapporté ma thèse.

Le Professeur Carl-Wilhelm Schläpfer a également accepté le rôle d'expert pour ce travail de thèse et j'aimerais ici l'en remercier. Mais j'aimerais également le remercier pour les discussions intéressantes dont il a été la source à l'occasion de nos séminaires du mardi matin.

En tant que président du département de chimie, le Professeur Albert Gossauer a officié comme président du jury de ma thèse. J'aimerais ici le remercier.

Pour ma place d'assistant au sein de l'institut de chimie inorganique et analytique, j'aimerais chaleureusement remercier le professeur Alexander von Zelewsky.

Outre les personnes précédemment citées, ces quatre années passées au sein de cet institut ont été l'occasion de rencontrer un grand nombre de personnes. J'aimerais leur dire merci pour les collaborations et les moments d'amitiés que nous avons partagés. Merci tout d'abord aux collègues du groupe de chimie théorique: David, Jean-Luc, Karel, Raf, Fabio, Gabriella, Ilaria. Merci également aux collègues des autres groupes: Professeur Peter Belser, Professeur Franzpeter Emmenegger, Manuel, Vincent, Nunzio, Sandrine, Marielle, Thomas, Simona, Mathias, Didier, Laure-Emmanuelle, Boris, Sarah ainsi que tous ceux partis durant mon travail. J'aimerais adresser un merci tout spécial aux trois collaborateurs indispensables de l'institut que sont Dr. Liz Kohl, Emerith Bruegger et Michel Piccand pour leur précieux aide et leur grande sympathie.

J’aimerais également remercier tout le personnel du service central du département de chimie: Hubert, Philippe, Lucienne, Noëlle, Alfonse,…

A Bruni j’aimerais dire un très grand merci. Merci pour tout, et en particulier pour son soutien et sa compréhension dans la dernière partie de mon travail de thèse.

Finalement, mon dernier mais peut-être plus grand merci ira à mes parents. Merci pour votre soutien tout au long de mes longues études.

Contents

Abstract

The first objective of this thesis is the calculation of excited state energies and properties of transition metal complexes using Density Functional Theory (DFT). To explore this wide topic, we did choose three different chemical systems.

The first one, presented in the chapter 4, is about the photodissociation of the tris(2,2'-bipyridine)ruthenium(II) ($[Ru(bpy)_3]^{2+}$) ion. Over the last two decades, there has been a vivid interest in the literature for this complexe ion because of its remarkable photochemical behavior. $[Ru(bpy)_3]^{2+}$ and complexes belonging to the same family are actually good candidates for solar energy conversion. Even if the electronic structure of the complexe begins to be well known, the understanding of the photosubstitution and photoracemization is still an unresolved problem. In very recent years, the photochemistry and photophysics of complexes with low-lying metal-to-ligand charge transfer (MLCT) states have attracted considerable interest. With the help of those studies, a mechanism of the photochemistry of $[Ru(bpy)_3]^{2+}$ is emerging and is presented in this work. This mechanism implies a complete reassessment of the role of metal centered excited states in the photochemical dissociation of metal-ligands bonds. The key step in this mechanism involves an elongation of the Ru-N bond length, which is possible since the lowest MLCT states have long life times. This leads to a transfer of the metal σ^* character to one of the lowest unoccupied π^* orbital. The result is an energy lowering of the MC transition, which is a fully dissociative state.

As a second chemical system, we were also interested, in chapter 5, by a molecule that attracted the chemist's interest for quite a while, i.e. nitroprusside. Due to this interest, many details on the nature of nitroprusside's ground state and its two metastable states were known. However, a clear picture of the reaction pathways between the three minima on the ground state potential energy curve was still missing. By studying the excited states corresponding to all three minima, we could setup, in this work, a model explaining the photochemistry and photophysics responsible for the population of the three different states on the ground state potential energy curve.

Last but not least, the third kind of transition metal complexes we were interested in are compounds showing nonlinear optical properties. The most important class of nonlinear optical (NLO) compounds are molecules possessing both electron donating and accepting groups which are electronically coupled. In this work, a computational chemistry approach is used to model some nonlinear optical parameters. Using time dependent DFT, we obtained good estimates for the NLO parameters for molecules of the family of the para-nitroaniline. Organometallic donating and accepting groups also exhibit interesting features which enables a tunning or even a switching of the NLO properties. In a second part of chapter 6, we thus extended our study to the computation of dipolar bimetallic sandwich-like complexes composed of sesquifulvalene and metal-ligand fragments.

Résumé

La chimie des complexes des métaux de transition est un domaine qui a considérablement évolué depuis ses débuts. Dans divers domaines de la chimie moderne, les composés de coordination sont sujets à de nombreuses applications et porteurs de nouveaux espoirs. Nombre de ces applications font intervenir une interaction entre la molécule et la lumière: télécommunication, développement de l'optique en informatique, conversion de l'énergie solaire en énergie électrique, …

Parallèlement, dans les domaines de la chimie computationnelle et de la chimie théorique, la théorie de la fonctionnelle de densité (TFD) s'affirme de plus en plus comme méthode de choix dans la modélisation de certains phénomènes chimiques. Dans cette méthode qui est décrite au chapitre 2, l'énergie d'un système électronique est déterminée, de façon univoque, par sa densité électronique.

Regroupant les deux thèmes précédemment cités, le but premier de cette thèse est le calcul des énergies ainsi que des propriétés des états excités de complexes métalliques à l'aide de la TFD. La méthodologie est décrite au chapitre 3. Les différentes méthodes ont été appliquées à trois différents systèmes chimiques.

Le premier complexe métallique étudié est le tris(2,2'-bipyridine)ruthénium(II). Le chapitre 4 de cette thèse présente une étude des états excités du $[Ru(bpy)_3]^{2+}$, un accent particulier ayant été mis sur les états excités de transfert de charge ainsi que sur les états excités centrés sur le métal et la photodissociation que leur population engendre. Cette molécule a suscité un grand intérêt parmi les chimistes depuis quelques décennies déjà en raison d'un comportement photochimique remarquable. Le $[Ru(bpy)_3]^{2+}$ ainsi que d'autres molécules de la même famille sont en effet potentiellement applicables à la conversion de l'énergie solaire en énergie électrique (photolyse de l'eau). Malgré cet intérêt et le grand nombre d'études sur la molécule, le mécanisme exact de la photochimie du $[Ru(bpy)_3]^{2+}$ n'est pas encore exactement connu. Le mécanisme que nous proposons ici implique une réévaluation complète du rôle des états excités centrés sur le métal lors de la dissociation photochimique de la liaison métal-ligand. L'étape clé de ce mécanisme implique une élongation de la liaison Ru-N lorsque le $[Ru(bpy)_3]^{2+}$ se trouve

dans sa configuration excitée de plus basse énergie. Par cette élongation, le caractère de l'orbitale σ* métallique est transféré sur une orbitale de type π* plus basse en énergie. Il en résulte un abaissement de l'énergie de la transition électronique centrée sur le métal, transition responsable de la photochimie du $[Ru(bpy)_3]^{2+}$.

Dans un deuxième temps, nous nous sommes intéressés à une autre molécule ayant suscité un grand intérêt chez les chimistes, le nitroprusside. Du fait de cet intérêt, de nombreux détails sur la nature de l'état fondamental du nitroprusside ainsi que sur la nature de ses deux états métastables ont été publiés. Malgré cela, un modèle clair des chemins réactionnels reliant l'état fondamental et les deux états métastables était toujours manquant. En étudiant les états excités de ces trois minima appartenant à la surface de potentiel de l'état fondamental, nous sommes arrivés à établir un modèle expliquant la photochimie et la photophysique reliant les trois différents minima entre eux.

Dans le dernier chapitre de la thèse, nous nous sommes intéressés à certains composés chimiques présentant des propriétés d'optique non-linéaire. La principale classe de composés présentant un intérêt en optique non-linéaire possède un groupe donneur d'électron et un groupe accepteur reliés entre eux. L'exemple typique est la para-nitroaniline. En utilisant la théorie de la fonctionnelle de densité dépendante du temps (TFDDT) dans notre modèle, nous avons obtenus de bonnes estimations des propriétés d'optique non-linéaire dans le cas de molécules de la famille de la para-nitroaniline. Dans une deuxième partie du chapitre 6, nous avons étendu la méthode a des composés organométalliques susceptibles de présenter d'intéressantes propriétés pour l'optique non-linéaire.

Chapter 1

Introduction

The coordination chemistry of transition metals has considerably progressed since its beginning with the work of Alfred Werner at the end of the 19th century. Nowadays, coordination compounds find numerous applications in modern chemistry, or are, at least, carrying new and important hopes. Many of these applications are based on the interaction of matter with light, e.g. in telecommunication, development of optical devices in data processing, conversion of light into electricity.

The consideration of new applications requires first a basic knowledge of the electronic structure and photophysical properties, as well as the photochemical properties of transition metal complexes, which are of potential interest. To carry out such investigations, several tools are available: experimental ones as well as theoretical ones. Amongst the former, such tools are represented by the various spectroscopical methods that are in use (RMN, UV-VIS, ESR, IR, etc.). In the field of theoretical chemistry, the application of quantum chemistry and quantum physics makes it also possible to study exhaustively the electronic structure of a molecule. A work that can be considerably facilitated using modern computer technology.

Currently, the rate of development in this technology is such that the power of computers doubles every 18 months. Thus, the use of computers in the various fields of physical science is of increasing importance. In chemistry, this even caused the creation of a new branch: computational chemistry, a field where computers are used as an “experimental” tool, like a NMR spectrometer for example. An important goal of computational chemistry is, as far as possible, to obtain results for a well defined chemical problem, e.g. by modelling this chemical problem using well established techniques, not necessarily by developing new theoretical methods. This requires still a strong interface between the traditional theoretical chemistry and computational chemistry.

In the field of computational chemistry, two approaches are generally considered, the empirical and the quantum approach. The methods based on an empirical approach are

very fast and consume little computer time (CPU) compared to the methods based on the quantum approach. Unfortunately those methods need to be parameterised and these parameters can only be obtained as results of an experiment or a quantum approach. In principle, an empirical approach allows a simple comparison of energy or geometry optimization. It is not possible to treat chemical reactions, formation or breaking of chemical bonds, since the electronic structure of the molecules is not taken into account.

Quantum mechanical methods are based on the explicit consideration of the electronic structure. These methods are substantially more CPU time consuming in comparison with empirical approaches for molecules of the same size. They can roughly be divided into two sub-fields: the semi-empirical methods and the non-empirical or ab initio methods.

Semi-empirical methods are approximate methods in which some intermediate results are taken from experiment. These methods can only be used for chemical species for which they were parameterised. Uncommon bonding situations can produce unreliable results.

In non-empirical or ab initio methods, the term ab initio means from first principles, without experimental parameters. However, it does not mean that the Schrödinger equation is solved exactly. The selected ab initio method will generally lead to a reasonable approximation to the exact solution of the Schrödinger equation.

Among ab initio methods there is Density Functional Theory (DFT). Although this theory has already emerged soon after the discovery of quantum sciences, it found only about thirty years ago its formal foundations and nowadays very popular and efficient for treating chemical problems. With this method, which will be described in chapter 2, the energy of an electronic system is completely and uniquely determined by its electronic density ρ.

Though DFT appears nowadays as an efficient tool to describe the electronic structure of molecules in their ground state, computation of excited states still remains a challenging task. And precisely, the calculation of excited state energies and properties of some transition metal complexes using DFT is the first objective of this thesis. The different procedures we used, either in a stationary DFT or in a Time-Dependent DFT (TDDFT) framework, are developed in chapter 3.

The first chemical problem we studied is the photodissociation of the tris(2,2'-bipyridine)ruthenium(II) ($[Ru(bpy)_3]^{2+}$) ion. Over the last two decades, there has been a vivid interest in the literature for this molecule because of its remarkable photochemical

behaviour. Nowadays, even though the electronic structure of metal complexes begins to be well known, the understanding of their photosubstitution and photoracemization is still an unresolved problem. In chapter 4, we present a mechanism implying a complete reassessment of the role of metal centred excited states in the photochemical dissociation of Ru-N bond in the $[Ru(bpy)_3]^{2+}$.

In chapter 5, we were also interested by a molecule that attracted chemists for quite a while: i.e. the nitroprusside. In our study, we have only treated nitroprusside $[Fe(CN)_5NO]^{2-}$ in its ionic form. The existence of two long-lived metastable states, easily obtained upon irradiation, is the principal reason of this interest. Indeed, those systems, which exhibit metastable states, are good candidates for optical information storage. Due to recent studies, we already know that the two metastable states and the ground state of nitroprusside correspond to three minima on the ground state potential energy surface. However, these studies did not include the excited states of all three minima, as well as a photochemical mechanism of transformation of one of these minima into the others. This consideration is the main goal of this work.

In chapter 6, we consider the study of nonlinear optical compounds. In this respect, the most important class of nonlinear (NLO) compounds are molecules possessing both electron donating and accepting groups which are electronically coupled. In this study, a computational chemistry approach is used to model some nonlinear optical parameters. Using TDDFT, we obtained good parameters for molecules of the family of the para-nitroaniline. In a second part of the study, we extended our work to the computation of dipolar bimetallic sandwich-like complexes composed of sesquifulvalenes and other metal-ligand fragments. Indeed, organometallic donating and accepting groups exhibit interesting features which allow a tuning or even a switching of NLO properties.

Chapter 2

Density Functional Theory

2.1 Introduction

A traditional way of procedure in science consists first of all to observe an experimental phenomenon, then to try to translate this observation into a mathematical law, and finally to apply this law in order to test its validity and its predictive quality. Thus, the atomic science passed from a planetary model with the Bohr atom to a quantum model following certain observations such as the *ultraviolet catastrophe*[1] and the *photoelectric effect*.

In 1925, this quantum behavior of atoms and molecules was translated, by Erwin Schrödinger, mathematically into the famous equation

$$H\Psi = E\Psi$$

Any problem concerning the electronic structure of matter can be solved in using *Schrödinger's wave equation*, so-called because it has the mathematical form of the classical wave equations due to the wave-particle duality of electrons.

This wave equation is up to now considered as exact. However, practically, this eigenvalue problem can only be solved exactly and analytically for a limited number of simple and rare cases : the hydrogen atom and molecules like H_2^+, Li^{2+}…

Approximations were, thus, brought. The best known and most popular one being the *Hartree-Fock approximation*. In this method, known as « ab-initio » (which means not exact), the wave function Ψ is written in a determinantal form called *Slater determinant*. The realisation of this Hartree-Fock method dates from the second half of the 20th century with the work of Roothaan[2].

These Hartree-Fock methods, which are frequently used hitherto, are nowadays in competition with another method, the *Density Functional Theory* (DFT).

2.2 History

The electronic density $\rho(\vec{r})$ represents the number of electrons per unit of volume at position $\vec{r}$ around the molecule or the atom. The idea, that this electronic density is of fundamental importance to discuss the ground state of an atom or of a molecule, is already very old. It is almost as old as quantum mechanics and goes back to the work of Thomas[3], Fermi[4], Dirac[5] and Wigner[6]

> *« Bei einem schweren Atom können die Elektronen als eine Art Atmosphäre um den Kern betrachtet werden, welche sich in einem Zustand vollständinger Entartung befindet. Man kann die Verteilung der Elektronen um den Kern angenähert durch eine statistische Methode berechnen ; diese wird auf die Theorie der Bildung der Elektronengruppen im Atom angewandet. Die Uebereinstimmung mit der Erfahrung ist befriedigend. »*[4]

This so-called *Thomas-Fermi theory* is the first method which proposes to use the electronic density instead of the wave function. It is thus the oldest form of the Density Functional Theory. According to this theory, the energy associated with a density $\rho(\vec{r})$ reads

$$E_{TF}[\rho(r)] = \int v(r)\rho(r)dr + \int \frac{3}{10}\left(3\pi^2\right)^{\frac{2}{3}}\rho^{\frac{5}{3}}(r)dr + \frac{1}{2}\int \frac{\rho(r)\rho(r')}{|r-r'|}drdr'$$

This approach is extremely simple and qualitatively correct for atoms. However it does not predict a binding energy for molecules, and the proof is not rigorous.

In the second half of the 20th century emerges the *Xα method*, also called *Hartree-Fock-Slater method*. The method arises from the work of J.C. Slater, who proposed in 1951, before the work of Hohenberg, Kohn and Sham (vide infra), to represent the potential of exchange and correlation by the cubic root of the electronic density[7].

This modification was motivated by the theory of the homogeneous electronic gas, introduced by Thomas and Fermi, and particularly characterized by the introduction of its exchange potential. Thus Slater simplifies the Hartree-Fock method in a way that the exchange potential is calculated locally from the third power of the density. This Hartree-Fock-Slater method, or Xα method, is running under a DFT principle.

Like the theory of Thomas and Fermi, the one introduced by Slater was rather intuitive and approximative. It was formally completed in 1964 by the work of Hohenberg and Kohn[8], and in 1965 by the work of Kohn and Sham[9].

Hohenberg and Kohn have shown in their work, that for a non degenerate ground state, the energy is a unique functional of its electronic density. This theory, derived from the electronic density when N, the number of electrons, is large, is known as the Density Functional Theory .

2.3 The Thomas-Fermi model

The essential purpose of the DFT is to replace the wave function of N-electrons $\Psi(x_1, x_2, \ldots, x_N)$ and the expensive part of the Hamiltonian in the Hartree-Fock method by a functional of the electronic density.

This theory began with the work of Thomas and Fermi in the Twenties. They realized that statistical considerations could be used to approximate the distributions of the electrons in an atom, by dividing the space into small cubes of edge l and of volume $\Delta V = l^3$, each cube containing a fixed number of electrons. Then it is assumed that the electrons in each cube move independently like fermions at 0 K and that the cubes are independent from each other.

The energy levels of a particle in an infinite three dimensional cell are given by[10] :

$$\varepsilon(n_x, n_y, n_z) = \frac{h^2}{8ml^2}\left(n_x^2, n_y^2, n_z^2\right) = \frac{h^2}{8ml^2} R^2$$

where n_x, n_y, n_z=1,2,3,…, and the second equality defines R. For great quantum numbers, for large R, the number of distinct energy levels smaller than ε can be approximated by the volume of a sphere with radius R in the space (n_x,n_y,n_z). Thus, we obtain the total energy of the electrons in the cell by summing over all the contributions of the variours energy states

$$\Delta E = 4\pi\left(\frac{2m}{h^2}\right)^{3/2} l^3 \int_0^{\varepsilon_F} \varepsilon^{3/2} d\varepsilon$$

$$\Delta E = \frac{8\pi}{5}\left(\frac{2m}{h^2}\right)^{3/2} l^3 \varepsilon_F^{5/2}$$

where ε_F is the Fermi level. All the states with an energy lower than ε_F are occupied, whereas all the states with an higher energy are empty.

The Fermi level is related to the number of electrons N in the cell through the formula

$$\Delta N = \frac{8\pi}{3}\left(\frac{2m}{h^2}\right)^{3/2} l^3 \varepsilon_F^{3/2}$$

from where we draw that

$$\Delta E = \frac{3h^2}{10m}\left(\frac{3}{8\pi}\right)^{2/3} l^3 \left(\frac{\Delta N}{l^3}\right)^{5/3}$$

This last equation is related to the total kinetic energy and to the electronic density

$$\rho = \frac{\Delta N}{\Delta V}$$

for each cell (various cells can have different ρ).

By adding the contributions of each cell, we obtain the total kinetic energy

$$T_{TF}[\rho] = C_F \int \rho^{5/3}(\vec{r}) d\vec{r}$$

with the constant C_F=2.871.

We encounter here one of the very important ideas of DFT, that is the *Local Density Approximation* (LDA). In this approximation, the electronic properties of a system are determined as a function of the electronic density, by applying local relations adapted to a homogeneous electronic system. The LDA can also be employed for other properties than the kinetic energy.

If we neglect the terms of exchange and correlation, thus by taking into account only the traditional electrostatic energies of attraction (electron-nuclei) and repulsion(electron-electron), we obtain a formula for the energy of an atom depending only on the electronic density

$$E_{TF}[\rho(\vec{r})] = C_F \int \rho^{5/3}(\vec{r}) d\vec{r} - Z\int \frac{\rho(\vec{r})}{\vec{r}} d\vec{r} + \frac{1}{2}\iint \frac{\rho(\vec{r}_1)\rho(\vec{r}_2)}{|\vec{r}_1 - \vec{r}_2|} d\vec{r}_1 d\vec{r}_2$$

This is the functional for the energy in the Thomas-Fermi theory for atoms.

Innumerable modifications of the Thomas-Fermi theory were proposed. Unfortunately, this primitive method does not work well when applied to molecules. There was no link between this theory and the molecular vision. This failure, added to the fact that the

precision for atoms was not as high as obtained through other methods, caused that the Thomas-Fermi model and the following ones were considered as oversimplified models without much importance for quantitative prediction in atomic and solid state physics.
The situation changes whith the communication of Hohenberg and Kohn[8] in 1964. They did postulate a fundamental theorem showing that, for ground states, the Thomas-Fermi model can be considered as an approximate model of an exact theory, the Density Functional Theory.

2.4 Hohenberg and Kohn theorems

In an electronic system described by the Hamiltonian

$$\hat{H} = \sum_{i=1}^{N}\left(-\frac{1}{2}\nabla_i^2\right) - \sum_{i=1}^{N}\sum_{\alpha}\frac{Z_\alpha}{r_{i\alpha}} + \sum_{i<j}^{N}\frac{1}{r_{ij}}$$

the energy of the ground state as well as its wave function are determined by the minimisation of the energy functional E[Ψ]. But, for a system with N electrons, the external potential

$$-\sum_{\alpha}\frac{Z_\alpha}{r_{i\alpha}} = v(\vec{r})$$

entirely defines the Hamiltonian. Thus, N and $v(\vec{r})$ determine all the molecular ground state properties.
Instead of N and $v(\vec{r})$, the first *Hohenberg-Kohn theorem* legitimates the use of the electronic density $\rho(\vec{r})$ as basic variable. The proof of this theorem is simple. Only the minimum energy principle for the ground state is taken into consideration. Using this, they show by *reductio ad absurdum* that, if there are two systems with N electrons and both of equal electronic density, the two systems have also the same external potential $v(\vec{r})$. Thus ρ determines N and v and by extension all properties of the ground state, such as the kinetic energy T[ρ], the potential energy V[ρ] and the total energy E[ρ]. For the formulae below, we write E_v instead of E to underline the dependence on v.

$$E_v[\rho] = T[\rho] + V_{ne}[\rho] + V_{ee}[\rho] = \int \rho(\vec{r})v(\vec{r})d\vec{r} + F_{HK}[\rho]$$

where

$$F_{HK}[\rho] = T[\rho] + V_{ee}[\rho]$$

and

$$V_{ee}[\rho] = J[\rho] + \text{nonclassical term}$$

where J[ρ] is the classical repulsion.
The nonclassical term is of fundamental importance ; it is the major part of the *exchange-correlation energy*. Let us note that $F_{HK}[\rho]$ is defined independently to the external potential $v(\vec{r})$; this means that $F_{HK}[\rho]$ is a universal functional of $\rho(\vec{r})$.
The second Hohenberg-Kohn theorem provides a variational principle. It stipulates that for an approximate density ρ' of a N-electrons system, we have

$$E_0 \leq E_v(\rho')$$

Assuming differentiability of $E_v[\rho]$, the variational principle requires that the ground state density satisfys the stationary condition

$$\delta\left\{E_v[\rho] - \mu\left[\int \rho(\vec{r})d\vec{r} - N\right]\right\} = 0$$

which gives the Euler-Lagrange equation

$$\mu = \frac{\delta E_v[\rho]}{\delta\rho(\vec{r})} = v(\vec{r}) + \frac{\delta F_{HK}[\rho]}{\delta\rho[\vec{r}]}$$

with μ being the chemical potential. This later equation is the basic working equation of Density Functional Theory.

2.5 Kohn-Sham equations

How can we find solutions for the previously discussed equations without making too crude approximations, i.e. without loosing too much precision, as it is the case in the Thomas-Fermi and its derived models. In 1965, Kohn and Sham invented an ingenious indirect approach to the kinetic energy functional T[ρ], called the *Kohn-Sham* (KS)

method. They thereby turned density functional theory into a practical tool for rigorous calculations.

To understand the Kohn-Sham method, it is convenient to begin with the exact formula for the ground state kinetic energy.

$$T = \sum_{i=1}^{N} n_i \left\langle \Psi_i \left| -\frac{1}{2}\nabla^2 \right| \Psi_i \right\rangle$$

where the Ψ_i and n_i are respectively, spin orbitals and their occupation numbers. Kohn and Sham showed that one can build a theory using simpler formulas, namely

$$T_s[\rho] = \sum_{i}^{N} \left\langle \Psi_i \left| -\frac{1}{2}\nabla^2 \right| \Psi_i \right\rangle$$

and

$$\rho(\vec{r}) = \sum_{i}^{N} \sum_{s} |\Psi_i(\vec{r}, s)|^2$$

corresponding to the exact formula for the ground state kinetic energy, but having $n_i=1$ for N orbitals and $n_i=0$ for the rest. This representation of kinetic energy and density is true for the determinantal wave function that exactly describes N noninteracting electrons. In analogy with the Hohenberg and Kohn definition of the universal functional $F_{HK}[\rho]$, Kohn and Sham introduced a corresponding noninteracting reference system, with the Hamiltonian

$$\hat{H}_s = \sum_{i}^{N} \left(-\frac{1}{2}\nabla_i^2 \right) + \sum_{i}^{N} v_s(r_i)$$

in which there are no electron-electron repulsion terms, and for which the ground state electron density is exactly ρ. For this system there will be an exact determinantal ground state wave function

$$\Psi_s = \frac{1}{\sqrt{N!}} \det\left[\Psi_1 \quad \Psi_2 \quad \ldots \quad \Psi_N\right]$$

The quantity $T_s[\rho]$, although uniquely defined for any density, is not the exact functional for the kinetic energy $T[\rho]$. The idea of Kohn and Sham is to set up a problem of interest in such a way that $T_s[\rho]$ is exactly its kinetic energy component. The resultant theory turns out to be of independent particle form. Nevertheless, it is exact. We can write

$$F[\rho] = T_s[\rho] + J[\rho] + E_{XC}[\rho]$$

where

$$E_{XC}[\rho] = T[\rho] - T_s[\rho] + V_{ee}[\rho] - J[\rho]$$

The E_{XC} quantity is called the *exchange-correlation energy* ; it contains the difference between T and T_s, presumably fairly small, and the nonclassical part of $V_{ee}[\rho]$. The Euler equation becomes

$$\mu = v_{eff}(\vec{r}) + \frac{\delta T_s[\rho]}{\delta \rho(\vec{r})}$$

where the KS effective potential is defined by

$$v_{eff}(\vec{r}) = v(\vec{r}) + \frac{\delta J[\rho]}{\delta \rho(\vec{r})} + \frac{\delta E_{XC}[\rho]}{\delta \rho(\vec{r})} = v(\vec{r}) + \int \frac{\rho(\vec{r}')}{|\vec{r} - \vec{r}'|} d\vec{r}' + v_{XC}(\vec{r})$$

with the *exchange-correlation potential*

$$v_{XC}(\vec{r}) = \frac{\delta E_{XC}[\rho]}{\delta \rho(\vec{r})}$$

The Kohn-Sham method works as follows : For a given $v_{eff}(\vec{r})$, we obtain $\rho(\vec{r})$, that satisfies the Euler equation by solving the N one electron equations

$$\left[-\frac{1}{2} \nabla^2 + v_{eff}(\vec{r}) \right] \psi_i = \varepsilon_i \psi_i$$

We start with a guessed $\rho(\vec{r})$, construct $v_{eff}(\vec{r})$ from the KS effective potential definition, and then find a new $\rho(\vec{r})$. This approach is called *self-consistent.* The three previous equations are the celebrated Kohn-Sham equations. They are still rigorously exact ! But the exact form of the exchange-correlation potential $v_{XC}[\rho]$ is not known. Thus approximations are necessary for practical calculations.

The simplest approximation is the *local density approximation* (LDA), which was introduced by Kohn and Sham

$$E_{XC}^{LDA}[\rho] = \int \rho(\vec{r}) \varepsilon_{XC} d\vec{r}$$

where ε_{XC} indicates the exchange and correlation energy per particle of a uniform electron gas of density ρ. The exchange and correlation potential then becomes

$$v_{XC}^{LDA}(\vec{r}) = \frac{\delta E_{XC}^{LDA}}{\delta \rho(\vec{r})} = \varepsilon_{XC}\left(\rho(\vec{r})\right) + \rho(\vec{r})\frac{\partial \varepsilon_{XC}(\rho)}{\partial \rho}$$

and the KS orbital equations

$$\left[-\frac{1}{2}\nabla^2 + v(\vec{r}) + \int \frac{\rho(\vec{r}')}{|\vec{r}-\vec{r}'|}d\vec{r}' + v_{XC}^{LDA}(\vec{r})\right]\psi_i = \varepsilon_i \psi_i$$

The self-consistent solution of this equation defines the *Kohn-Sham local density approximation* (KS-LDA), which in the literature is usually simply called the LDA method.

2.6 LDA and GGA methods

The Local Density Approximation (LDA) is applicable to systems with sufficiently soft variations of the density but cannot be formally justified for highly inhomogeneous systems such as atoms and molecules. The essential justification for its use in atomic and molecular systems comes from its success in numerical applications.

The exchange-correlation energy for the homogeneous electron gas can be written as

$$E_{XC}^{LDA} = E_X^{LDA} + E_C^{LDA}$$

with the first term known by the *Dirac exchange energy*

$$E_X^{LDA} = -\frac{2}{3}\left(\frac{3}{4\pi}\right)^{1/3}\int \left[\rho_x(r)\right]^{4/3} dr$$

The second term, representing the correlation energy, is not known analytically. However, approximations of increasing accuracy have been developped. The well known Vosko, Wilk and Nusair[11] (VWN) local approximation uses *Padé interpolations* to fit the correlation energy from accurate *Monte-Carlo numerical simulations* on the homogeneous electron gas due to Cerperley and Alder[12].

The LDA remained the approximation of choice of E_{XC} for many years. In fact, depending on the properties to compute, the LDA remains a valuable method. It has been shown, for example, that the LDA method gives suprisingly good results, sometimes better than newer methods, in the case of molecular geometries[13], vibrational frequencies and single-particle properties. However it also appears that the first generation of DFT

methods based on LDA considerably overestimates bond energies, resulting in a typical tendency to overbind[14].

To avoid this problem, due to the fact that an atomic or molecular density is not homogeneous, Becke et al.[15] introduced nonuniformity information to the LDA method. This lead to the so called Generalized Gradient Approximation (GGA) method.

In this method, which takes the following general form,

$$E_{XC}^{GGA} = \int f\left(\rho(\vec{r}), \nabla\rho(\vec{r})\right)d\vec{r}$$

the expression for the exchange and correlation energy contains both the density and the gradient of the density, which is a real measure for the inhomogeneity of the electronic density of finite systems[16].

2.7 Practical implementations

The ADF[17, 18] (*Amsterdam Density Functional*) program package has been employed in all the calculations inside the thesis. It is a Density Functional program written in Fortran and working under the Kohn-Sham formalism. As we have seen before, this implies a one-electron picture of many-electron systems. In ADF, as it is also in most other modern DFT codes, the one-electron orbitals are written as linear combinations of a set of basic functions. The basic functions employed in ADF are Slater-type exponential basis function centered on the atoms.

One other problem emerging from the computation of many-electron systems is the number of electrons involved. When dealing with transition metal complexes, this number of electrons become quickly large. However, it is well established that only valence electrons participate in chemical bonds. Thus, in ADF, the so-called *frozen core approximation* is used[19, 20]. It is assumed that molecular orbitals describing inner-shell electrons remain unperturbed in going from a free atom to a molecule. This *core electrons* can then be exclude from the variational procedure. They are pre-calculated in an atomic calculation (*create mode* in ADF) and kept *frozen* thereafter.

ADF is based on a fragment approach : the molecular system to be computed is built up from fragments, the molecular one-electron orbitals are calculated as linear combination

of fragment orbitals and final results (e.g. bonding energy) are given in terms of fragment properties.

The ADF package is, since 1970, in continuous development. The latest version used in this thesis, ADF2000.02, offers, among others, functionalities as *geometry optimization*, *transition state search*, *linear transit*, *intrisinc reaction coordinate*, *frequencies calculation*, *QM/MM method*, *Time-Dependent DFT* for the computation of *excitation energies* and *(hyper) polarizabilities*, …

A more detailed description of the program and of all the functionalities available with respect of the latest version can be found on the website of the *Scientific Computing & Modelling NV (SCM)* company (http://www.scm.com), the company in charge of the distribution and of the development of the code since 1995.

2.8 Further formal treatment of DFT

The theoretical treatment of DFT in this thesis remained rather general. It is used as a basis for the continuation of this work where DFT has been used as a computational tool. For further theoretical deepening, the reader is requested to refer to the book of Parr and Yang[10].

Time-Dependent DFT (TDDFT) has also been used in this thesis for the computation of excited state energies and hyperpolarizabilities. An introduction will be given in the next chapter « Calculation of excited states using Density Functional Theory ».

2.9 References

(1) Planck, M., *Verh. dt. phys. Ges.* **1900**, *2*, 202.

(2) Roothaan, C. C. J., *Reviews of Modern Physics* **1951**, *23*, 69.

(3) Thomas, L. H., *Proc. Camb. Phil. Soc.* **1926**, *23*, 542.

(4) Fermi, E., *Z. Phys.* **1928**, *48*, 73.

(5) Dirac, P. A. M., *Proc. Camb. Phil. Soc.* **1930**, *26*, 376.

(6) Wigner, E., *Phys. Rev.* **1932**, *40*, 749.

(7) Slater, J. C., *Physical Review* **1951**, *81*, 385.

(8) Hohenberg, P.; Kohn, W., *Physical Review B* **1964**, *136*, 864.

(9) Kohn, W.; Sham, L. J., *Physical Review A* **1965**, *140*, 1133.

(10) Parr, R. G.; Yang, W., *Density Functional Theory of Atoms and Molecules*; ed.; Oxford University Press: 1989;
(11) Vosko, S. H.; Wilk, L.; Nusair, M., *Can. J. Phys.* **1980**, *58*, 1200.

(12) Ceperley, D. M.; Alder, B. J., *Phys. Rev. Lett.* **1980**, *45*, 566.

(13) Bray, M. R.; Deeth, R. J.; Paget, V. J.; Sheen, P. D., *Int. J. Quant. Chem.* **1996**, *61*, 85.

(14) Ziegler, T., *Can. J. Chem.* **1995**, *73*, 743.

(15) Becke, A. D., *J. Chem. Phys.* **1992**, *96*, 2155.

(16) Ziegler, T., *Chem. Rev.* **1991**, *91*, 651.

(17) Baerends, E. J.; Bérces, A.; Bo, C.; Boerrigter, P. M.; Cavallo, L.; Deng, L.; Dickson, R. M.; Ellis, D. E.; Fan, L.; Fischer, T. H.; Fonseca Guerra, C.; van Gisbergen, S. J. A.; Groeneveld, J. A.; Gritsenko, O. V.; Harris, F. E.; van den Hoek, P.; Jacobsen, H.; van Kessel, G.; Kootstra, F.; van Lenthe, E.; Osinga, V. P.; Philipsen, P. H. T.; Post, D.; Pye, C.; Ravenek, W.; Ros, P.; Schipper, P. R. T.; Schreckenbach, G.; Snijders, J. G.;

Sola, M.; Swerhone, D.; te Velde, G.; Vernooijs, P.; Versluis, L.; Visser, O.; van Wezenbeek, E.; Wiesenekker, G.; Wolff, S. K.; Woo, T. K.; Tiegler, T.,
(18) Fonseca Guerra, C.; Snijders, J. G.; te Velde, G.; Baerends, E. J., *Theor. Chem. Acc.* **1998**, *99*, 391.

(19) Baerends, E. J.; Ellis, D. E.; Ros, P., *Chem. Phys.* **1973**, *2*, 41.

(20) Baerends, E. J.; Ros, P., *Chem. Phys.* **1973**, *2*, 52.

Chapter 3

Calculation of Excited States using Density Functional Theory

3.1 Introduction

Many interesting chemical problems involve both the ground and the excited states of molecules. In this respect, calculations of excited states are of fundamental importance in chemistry. Thus, since Density Functional Theory (DFT) has provided an extremely successful description of ground state properties of atoms, molecules and solids ; the DFT formalism had to be extended to excited states in order to describe photochemical and photophysical processes.

Traditionally however, the description of excited by DFT has been controversed. Conditions justifying and limiting the application of the Kohn-Sham formula to the calculation of excited states have been the subject of numerous papers[1-3].

3.2 Energies of multiplets

Following the proposition, in 1977, of Ziegler and co-workers, we can replace the energy of a single-determinant by the corresponding statistical energy as obtained in DFT[4]. However, the individual multiplet state arising from an open-shell configuration cannot, in general, be expressed by a single-determinant.

Following results from Daul[5, 6], it is possible to write the energy of a multiplet as a weighted sum of single-determinant energies. The multiplet splitting of a given configuration is thus obtained to fisrt order.

Daul exploited the symmetry to its largest extent to simplify the relation between the multiplet splitting and the single-determinant energies.

The multiplet wave functions[6]

$$\Psi_i = |\alpha \Gamma m_\Gamma S m_S\rangle$$

arising from a given configuration α and caracterized by : Γ is the label of the irreducible representation of the space part of the wave function, m_Γ its component in case of degenerecy, S is the spin part of the wave function with component m_S in case of spin multiplicity larger than 1.

Ψ_i are easily obtained by vector coupling as

$$\Psi_i = \sum_\mu A_{i\mu} \phi_\mu$$

a linear combination of single-determinants where

$$\phi_\mu = |\chi_1 \quad \chi_2 \quad \chi_3 \quad \ldots|$$

is a single-determinant wave function of spin orbitals χ ; and $A_{i\mu}$ is an orthogonal square matrix of symmetry coefficients.

The energies of the single-determinant ϕ_μ are directly provided by the DF or Hartree-Fock calculations. The energy of the multiplet can then be expressed as a weighted sum of single-determinant energies.

The procedure can be applied to all symmetry point groups, keeping thus computational effort to a minimum.

3.2.1 Example

Let us take a small example to illustrate the computation of multiplets energies : the HOMO-LUMO transition in the $[Ru(bpy)_3]_{2+}$ molecule[7, 8]. In this example, orbitals involved do not show any degeneracy and the system can then be compared to a nonsymmetrical system. There is no benefit from the use of the symmetry as explained by Daul, but the exemple help in the understanding of the general method.

The ground state is a closed-shell system, with a doubly occupied nondegenerate HOMO of a_1 symmetry. The ground state $^1A_1$ can thus be expressed as the following single-determinant

$$\left|{}^{+}a_1\ {}^{-}a_1\right|$$

Let us consider the single excitations from this doubly occupied nondegenerate a_1 orbital to the empty nondegenerate LUMO of a_2 symmetry. It results in four different configurations that determine two different spin states.

The triplet state can be expressed in three different state functions (degenerate in energy as one omits the spin-orbit coupling), the singlet state only in one.

$${}^3\Psi_{MS=+1} = \left|{}^{+}a_1\ {}^{+}a_2\right| \qquad {}^3\Psi_0 = \frac{1}{\sqrt{2}}\left(\left|{}^{+}a_1\ {}^{-}a_2\right| + \left|{}^{-}a_1\ {}^{+}a_2\right|\right) \qquad {}^3\Psi_{-1} = \left|{}^{-}a_1\ {}^{-}a_2\right|$$

$${}^1\Psi_0 = \frac{1}{\sqrt{2}}\left(\left|{}^{+}a_1\ {}^{-}a_2\right| - \left|{}^{-}a_1\ {}^{+}a_2\right|\right)$$

Both ${}^3\Psi_{+1}$ and ${}^3\Psi_{-1}$ are single-determinants, it is then possible to get directly the energy of this triplet excited state from a DF (or Hartree-Fock) computation. However, the singlet excited state cannot be expressed as a single-determinant and thus cannot be obtained as the result of a DF computation. The method to obtain the energy of the singlet state consists in starting from a definite virtual state

$${}^x\Psi_0 = \left|{}^{+}a_1\ {}^{-}a_2\right| = \frac{1}{\sqrt{2}}\begin{vmatrix} a_1(1)\alpha(1) & a_1(2)\alpha(2) \\ a_2(1)\beta(1) & a_2(2)\beta(2) \end{vmatrix}$$

$$= \frac{1}{\sqrt{2}}\left[a_1(1)a_2(2)\alpha(1)\beta(2) - a_2(1)a_1(2)\beta(1)\alpha(2)\right]$$

one has then to define ${}^1\Psi_0$ as a function of ${}^x\Psi_0$ and ${}^3\Psi_1$.

After some easy mathematics, we find for this virtual state

$${}^x\Psi_0 = \frac{1}{\sqrt{2}}\left\{{}^1\Psi_0 + {}^3\Psi_0\right\}$$

We can then calculate the energy for this state by introducing the operator for the energy

$$E\left({}^x\Psi_0\right) = \left\langle {}^x\Psi_0 \middle| H \middle| {}^x\Psi_0 \right\rangle = \frac{1}{2}\left\{E\left({}^1\Psi_0\right) + E\left({}^3\Psi_0\right)\right\}$$

Thus we find for the singlet state energy

$$E\left({}^1\Psi_0\right) = 2 \cdot E\left({}^x\Psi_0\right) - E\left({}^3\Psi_1\right)$$

For more examples, I encourage the reader to look at the paper of Daul[6].

3.3 Energy of single-determinant

As we have seen, the calculation of multiplet energies requires the energies of excited determinants, e.g. (occupied spin-orbital no. i) → (empty spin-orbital no. j), to be computed. If either one of the two orbitals i or j belongs to a degenerate irreducible representation in a given symmetry point group, this symmetry has to be lowered to a point group where the degenerate irreducible representation splits.
Independently from this orbital degeneracy of either i or j, the single-determinant energy of a given configuration is calculated, in DFT, by occupying the Kohn-Sham (KS) orbitals issued from the self-consistent procedure (SCF).
Those KS orbitals can be obtained by two different procedures. Either the KS equations are solved self-consistently for the symmetrically averaged density of all the configurations involved in this excitation, or the KS equations are solved self-consistently for the symmetrically averaged density of the reference configuration only (a transition state). These self-consistent KS orbitals are then kept frozen for computation of all the single-determinants. The first procedure is called *ΔSCF* and the second the *Transition State* procedure. Both procedures should in principle give similar energies[9].
Next to those « ground state » procedures, there is a new promizing procedure to compute excited states energies for closed shell systems using *Time-Dependent Density Functional Theory* (TDDFT). A short description of each three methods will follow.

3.3.1 ΔSCF procedure[9]

In the *ΔSCF* procedure, the KS equations have to be solved for the symmetrically averaged density of each configurations, corresponding to the ground state and to each excited state. For example, the electronic transition $t_2^3 \rightarrow t_2^2 e^1$ requires two different SCF computations for the two following electronic configurations

$\left|t_2^3\right\rangle$ where $\eta_{t_2}^{\uparrow} = \eta_{t_2}^{\downarrow} = \frac{1}{2}$

and

$|t_2^2 e^1\rangle$ where $\eta_{t_2}^{\uparrow} = \eta_{t_2}^{\downarrow} = \frac{1}{3}$ and $\eta_e^{\uparrow} = \eta_e^{\downarrow} = \frac{1}{4}$

The so obtained KS orbitals for each configurations are then kept frozen, and all needed single-determinants airsing from the corresponding configuration are calculated. From the single-determinants energies, we can then obtain the multiplet energies. Excitation energies are finally calculated by taking the differences between ground state and excited state multiplet energies.

3.3.2 Transition state procedure[9]

A slightly simplified calculation scheme is suggested from Slater's Transition State (TS) method[10]. The KS orbitals are no more obtained self-consistently for each configuration, but only for one reference configuration, which is located exactly halfway between the ground and the excited state configuration. The electronic transition from the initial to the final state may be described by means of a continuous redistribution of the occupation numbers along a continuous ensemble of transition states which might be mapped onto intervall $\lambda \in [0,1]$, where $\lambda=0$ corresponds to (i) and $\lambda=0$ to (f). Along all points of this path, the energy is a continuous and differentiable function of the occupation numbers ($n_{i\sigma}$) and of λ, namely

$$E = E\left[\{n_{i\sigma}(\lambda)\}\right]$$

At the boundary points, where $\lambda=0$ and $\lambda=1$, we obtain E_i and E_f respectively. The intermediate points should verify the following condition

$$\frac{\partial \chi_{i\sigma}}{\partial n_{j\sigma'}} = \frac{\partial \chi_{i\sigma}}{\partial \lambda} = 0 \qquad \text{for all i,j and } \sigma,\sigma' = \uparrow,\downarrow$$

Following Slater's idea, let us expand the energy of any arbitrary TS in a Taylor series, in terms of power of λ as

$$E\left[\{n_{i\sigma}(\lambda)\}\right] = E(\lambda) = E(\lambda_0) + \left(\frac{dE}{d\lambda}\right)_{\lambda_0} \delta\lambda + \frac{1}{2}\left(\frac{d^2E}{d\lambda^2}\right)_{\lambda_0} \delta^2\lambda + \frac{1}{6}\left(\frac{d^3E}{d\lambda^3}\right)_{\lambda_0} \delta^3\lambda + R_3(\lambda)$$

where $\delta\lambda = \lambda - \lambda_0$. Slater showed that this expansion can be terminated at third order without significant loss of accuracy[10].

Let us now consider a reference situation which is located exactly halfway between the initial and the final states, λ_0=1/2. When using the Talyor expansion, we find for ΔE_{if}

$$\Delta E_{if} = E_f - E_i = \left(\frac{dE}{d\lambda}\right)_{\lambda=\frac{1}{2}} + \frac{1}{24}\left(\frac{d^3E}{d\lambda^3}\right)_{\lambda=\frac{1}{2}}$$

We notice that the second derivatives cancel. The TS concept is attractive because of this point, and also because the third-order term is reduced by a factor 1/24. Neglecting this last term, one gets an approximate working formula :

$$E_f - E_i \cong \left(\frac{dE}{d\lambda}\right)_{\lambda=\frac{1}{2}}$$

This formula indicates that the energy difference between the initial and final states is reasonably well approximated by the derivative of the energy vs. λ at the point where λ=1/2. This derivative can be expressed by the corresponding ratio of centered differences

$$\left(\frac{dE}{d\lambda}\right)_{\lambda=\frac{1}{2}} \cong E\left[\rho^{\left(\lambda=\frac{1}{2}\right)}\left\{n_{i\sigma}^{(f)}\right\}\right] - E\left[\rho^{\left(\lambda=\frac{1}{2}\right)}\left\{n_{i\sigma}^{(i)}\right\}\right]$$

Daul showed that this expression is almost exact[9].

Thus the only density, i.e. the only self-consistent computation, we need is the one from the TS where λ=1/2.

For example, the electronic transition $t_2^3 \rightarrow t_2^2e_1$ requires one SCF, the TS, computation with the following occupation

$\left|t_2^{2.5}e^{0.5}\right\rangle$ where $\eta_{t_2}^{\uparrow} = \eta_{t_2}^{\downarrow} = \frac{5}{12}$ and $\eta_e^{\uparrow} = \eta_e^{\downarrow} = \frac{1}{8}$

These self-consistent KS orbitals are kept frozen, and all needed single-determinants are calculated using the KS orbitals of the TS, with a definite occupation. Excitation energies are finally calculated by taking the differences between ground state and excited state multiplet energies.

3.3.3 Excited states energies using time-dependent DFT

As already mentionned, conditions justifying and limiting the application of the stationary Kohn-Sham formula to the calculation of excited states have been the subject of numerous papers[1-3]. Actually, the treatment of excitations within a time-independent DFT framework presents some formal and practical difficulties. The formal problem relies on the second Hohenberg-Kohn theorem which provides the energy variational principle. This theorem does not apply to all excited states (only the lowest excited state of each symmetry), and becomes a practical problem in the commonly encountered case of spin or spatial multiplets which have the same charge density (to first order) but different energies.

The usual solutions[4, 6] have been presented in the previous parts of this chapter. Even if those techniques have shown good results, often in very good agreement with experiments (also in this thesis), theoretical works on excited states in DFT are still an important field of research. In this respect time-dependent DFT (TDDFT) is a very promising tool.

TDDFT, based on the Runge-Gross theorem[11], is thoroughly reviewed in[12, 13]. For a more quantum chemical oriented field, Casida published a review paper[14].

The formalism of time-dependent DFT generalizes Kohn-Sham theory to include the case of a time-dependent, local external potential. A practical computational formulation of time-dependent DFT can be developed using time-dependent response theory. Thus TDDFT provides a first principles method for the calculation of excitation energies and many related response properties within a density functional framework.

The starting point of such a time-dependent quantum chemical problem is provided by the Schrödinger time-dependent equation

$$i\frac{\partial}{\partial t}\Psi(t) = \hat{H}(t)\Psi(t)$$

where the hamiltonian H consists of the kinetic energy, the Coulomb interaction and the time-dependent external potential. Runge-Gross[11] derived the analogues of the Hohenberg-Kohn theorems for stationary DFT. According to them, a set of time-dependent Kohn-Sham equations has been introduced

$$i\frac{\partial}{\partial t}\phi_j(r,t)=\left(-\frac{\nabla^2}{2}+v_s[\rho](r,t)\right)\phi_j(r,t)$$

The potential v_s is usually called the time-dependent KS potential and written as

$$v_s[\rho](r,t)=v(r,t)+\int d^3r'\frac{\rho(r',t)}{|r-r'|}+v_{XC}[\rho](r,t)$$

where v(r,t) is the nuclear potential, the 2nd term represents the classical coulomb repulsion potential and the 3rd term is the time-dependent exchange-correlation potential. This potential is defined as

$$v_{XC}[\rho](r,t)=\frac{\delta A_{XC}[\rho]}{\delta\rho(r,t)}$$

The time-dependent exchange-correlation functional A_{XC} is the analogue of E_{XC} in the static case. It is a functional of the density as a function of space and time. As this functional is still unknown, it can be approximated, in the adiabatic limit

$$A_{XC}[\rho]=\int dt E_{XC}[\rho]\Big|_{\rho=\rho(r,t)}$$

Note that, whereas A_{XC} is a functional of the full space- and time- dependent density, E_{XC} is a functional only of the space-dependent density at the specified time t.

The time-dependent generalization of the DFT formalism offers a rigorous route to the calculation of the dynamic response of the charge density. This allows the determination of the electronic excitation spectrum in the usual dipole approximation, because the poles of the dynamic polarizability determine the excitation energies.

For the determination of properties like polarizability and excitation energy, only the knowledge of the linear density response of the system is required, which considerably simplifies the problem.

Following Gross and co-workers[13], we consider an external potential v_{ext} of the form

$$v_{ext}(r,t)=\begin{cases} v_0(r) & t\le t_0 \\ v_0(r)+v_1(r,t) & t>t_0 \end{cases}$$

Expanding the density ρ(r,t) as a functional of the external potential v_{ext} in a functional Taylor series

$$\rho(r,t)=\rho_0(r)+\rho_1(r,t)+\rho_2(r,t)+\ldots$$

where ρ_0 is the unperturbed density of $t<t_0$, which can be obtained from the ground state KS equations in the potential $v_0(r)$. In general, the first-order time-dependent density can be calculated from the exact linear response function χ

$$\rho_1(r,t) = \int dr' \int dt' \, \chi(r,t;r',t') v_1(r',t')$$

where the density-density response function is given by

$$\chi(r,t;r',t') = \left. \frac{\delta \rho[v_{ext}](r,t)}{\delta v_{ext}(r',t')} \right|_{v_0}$$

which has to be evaluated at the initial (ground state) potential v_0.

Similarly for the KS system of noninteracting electrons, the first-order change in the density can be expressed as

$$\rho_1(r,t) = \int dr' \int dt' \, \chi_s(r,t;r',t') v_{s,1}(r',t')$$

where χ_s is the noninteracting linear density-density response function, and $v_{s,1}(r,t)$ is the KS potential in first-order of the external field

$$v_{s,1}(r,t) = v_1(r,t) + \int dr' \frac{\rho_1(r',t)}{|r-r'|} + \int dr' \int dt' \, f_{XC}[\rho_0](r,t;r',t') \rho_1(r',t')$$

Here the xc kernel f_{XC} has been introduced. It is the functional derivative of the time-dependent xc potential $v_{XC}(r,t)$ with respect to the time-dependent density $\rho(r,t)$

$$f_{XC}(r,t;r',t') = \frac{\delta v_{XC}(r,t)}{\rho(r',t')}$$

This kernel determines the first-order change in the time-dependent xc potential due to the applied electric perturbation. Previous equations constitute an exact representation of the linear density response. In other words, the exact linear density response $\rho_1(r,t)$ of an interacting system can be written as the linear density response of a noninteracting system to the effective perturbation $v_{s,1}(r,t)$. Combining the two equations for $\rho_1(r,t)$ and $v_{s,1}(r,t)$ and taking the Fourier transform with respect to time, the exact frequency-dependent linear density response is seen to be

$$\rho_1(r,\omega) = \int dr' \, \chi_s(r,r',\omega) v_1(r',\omega) +$$
$$\int dr' \int dr'' \, \chi_s(r,r',\omega) \left(\frac{1}{|r'-r''|} + f_{XC}[\rho_0](r',r'',\omega) \right) \rho_1(r'',\omega)$$

The KS response function is known in terms of the unperturbed KS orbitals $\phi_j(r)$, their occupation numbers f_j and their orbital energies ε_j

$$\chi_s(r,r';\omega)=\sum_{j,k}(f_k-f_j)\frac{\phi_j(r)\phi_k^*(r)\phi_j^*(r')\phi_k(r')}{\omega-(\varepsilon_j-\varepsilon_k)+i\eta}$$

If we make use of the fact that there is no contribution from j and k if j and k are both occupied or both virtual, we can simply write for the response function

$$\chi_s(r,r';\omega)=\sum_{i}^{occ}\sum_{a}^{virt}\phi_a(r)\phi_i(r)\phi_a(r')\phi_i(r')\times\left(\frac{2(\varepsilon_i-\varepsilon_a)}{(\varepsilon_i-\varepsilon_a)^2+\omega^2}\right)$$

This is the form which is actually implemented in the Amsterdam Density Functional (ADF) program package[15-17].

Finally, since the dynamic polarizability, $\alpha(\omega)$, describes the response of the dipole moment to a time-dependent electric field, it may be calculated from the response of the charge density obtained from time-dependent density functional theory. This allows the determination of the electronic excitation spectrum in the usual dipole approximation.

$$\alpha(\omega)=\sum_i\frac{f_i}{\omega_i^2-\omega^2}=\frac{2}{3}\sum_i\frac{\omega_i\mu_i^2}{\omega_i^2-\omega^2}$$

The linear dipole polarizability tensor $\alpha(\omega)$ has the poles at the vertical excitation energies ω_i. The strengths of the poles are given by the oscillator strengths f_i, or equivalently, by the transition dipole moment μ_i.

3.4 Oscillator strengths in stationary DFT

The intensity of an optical transition is determined by its electrical transition dipole moment

$$\text{Intensity}\propto\left|\left\langle\Psi_i\left|\sum_j^N r_j\right|\Psi_f\right\rangle\right|^2$$

where Ψ_i and Ψ_f are the wave functions of the ground and excited state respectively, r_j the coordinate of the *i*th electron and *N* the number of electrons.

We can write[18]

$$\left\langle\Psi_i\left|\sum_j^N r_j\right|\Psi_f\right\rangle=\frac{1}{\sqrt{D_{ii}D_{ff}}}\sum_{k,l}^N\langle a_k|r|b_l\rangle D_{ab}(kl)$$

where $D_{ab}(kl)$ denotes the cofactor of the element $\langle a_k | b_l \rangle$ in the determinant $Dab = |\langle a_k | b_l \rangle \ldots \langle a_k | b_l \rangle|$. If Ψ_i and Ψ_f can be approximate in single-determinant, where all the spin orbitals are derived from the same calculation, it can be shown that the previous equation can be reduce to

$$\left\langle \Psi_i \left| \sum_j^N r_j \right| \Psi_f \right\rangle = \langle a_m | r | b_n \rangle$$

where a_m is occupied in Ψi and not occupied in Ψf, whereas b_n is occupied in Ψf and empty in Ψi. This expression is evaluated in the *Dipole* module that is now part of the ADF[16, 17] program package. The oscillator strength is finally obtained by multiplying the latest equation with the energy of the corresponding transition.

3.5 References

(1) Kohn, W., *Physical Review A* **1986**, *34*, 737.

(2) Theophilou, A. K., *Journal of Physics C* **1979**, *12*, 5419.

(3) von Barth, U., *Physical Review A* **1979**, *20*, 1693.

(4) Ziegler, T.; Rauk, A.; Baerends, E. J., *Theoret. Chim. Acta* **1977**, *43*, 261.

(5) Daul, C., *J. Chim. Phys* **1989**, *86*, 703.

(6) Daul, C., *Int. J. Quant. Chem.* **1994**, *52*, 867.

(7) Daul, C.; Baerends, E. J.; Vernooijs, P., *Inorg. Chem.* **1994**, *33*, 3538.

(8) Buchs, M.; Daul, C., *Chimia* **1998**, *52*, 163.

(9) Daul, C. A.; Koclo, K. G.; Stückl, A. C., *Recent Advances in Density Functional Theory* **1997**, *2*, 61.

(10) Slater, J. C., *Quantum Theory of Molecules and Solids*; ed.; McGraw-Hill: 1974;
(11) Runge, E.; Gross, E. K. U., *Phys. Rev. Lett.* **1984**, *52*, 997.

(12) Gross, E. K. U.; Kohn, W., *Adv. Quantum Chem.* **1990**, *21*, 255.

(13) Gross, E. K. U.; Dobson, J. F.; Petersilka, M., *Density Functional Theory*; R.F. Nalewajski ed.; Heidelberg, 1996;
(14) Casida, M. E., *Recent Advances in Density-Functional Methods*; ed.; World Scientific: Singapore, 1995;
(15) van Gisbergen, S. J. A.; Snijders, J. G.; Baerends, E. J., *Comput. Phys. Commun.* **1998**, *114*, 368.

(16) Baerends, E. J.; Bérces, A.; Bo, C.; Boerrigter, P. M.; Cavallo, L.; Deng, L.; Dickson, R. M.; Ellis, D. E.; Fan, L.; Fischer, T. H.; Fonseca Guerra, C.; van Gisbergen, S. J. A.; Groeneveld, J. A.; Gritsenko, O. V.; Harris, F. E.; van den Hoek, P.; Jacobsen, H.; van Kessel, G.; Kootstra, F.; van Lenthe, E.; Osinga, V. P.; Philipsen, P. H. T.; Post, D.; Pye, C.; Ravenek, W.; Ros, P.; Schipper, P. R. T.; Schreckenbach, G.; Snijders, J. G.; Sola, M.; Swerhone, D.; te Velde, G.; Vernooijs, P.; Versluis, L.; Visser, O.; van Wezenbeek, E.; Wiesenekker, G.; Wolff, S. K.; Woo, T. K.; Tiegler, T.,
(17) Fonseca Guerra, C.; Snijders, J. G.; te Velde, G.; Baerends, E. J., *Theor. Chem. Acc.* **1998**, *99*, 391.

(18) McWeeny, R., *Methods of Molecular Quantum Mechanics*; ed.; Academic Press: San Diego, 1996; pp. 66.

Chapter 4

A Density Functional Study of the Photochemistry and Photophysics of the $[Ru(bpy)_3]^{2+}$

4.1 Introduction

The tris(2,2'-bipyridine)ruthenium(II), $[Ru(bpy)_3]^{2+}$, has been one of the most studied molecule for the last three decades. Reasons for this vivid interest have to be found in its unique combination of chemical stability, redox properties, reactivity of the excited state, luminescence as well as suitable lifetime of the excited state. For all those reasons, Ru^{II} with polypyridine ligands are still playing a key role in the development of photochemistry, photophysics, photocatalysis, electrochemistry, photoelectrochemistry, chemical luminescence, electrochemical luminescence as well as electron transfer and energy transfer[1]. Applications, or potential applications, of molecules of the $[Ru(bpy)_3]^{2+}$ family are found in many various domains.

Such molecules are used in optical devices for data processing[2, 3]. In pharmacology, i.e. the $[Ru(bpy)_3]^{2+}$ complexe has been used for the determination of codein, heroin and dextromethorphan[4, 5]. $[Ru(bpy)_3]^{2+}$ has also been studied when intercalated in DNA[6, 7]. In the same way the complexe has been used for the treatment of some cancers[8]. A molecule derived from the $[Ru(bpy)_3]^{2+}$, the $Rh(DIP)_3$ complexe (DIP=4,7-diphenylphenanthroline), has also shown interesting properties for a possible treatment of the VIH virus[9]. In a more chemically oriented application, $[Ru(bpy)_3]^{2+}$ and molecules of this family are also used for photoinduced asymetric synthesis[10]. Another field of application is the data processing where molecules of the $[Ru(bpy)_3]^{2+}$ family have been studied for their interesting properties in 'electronic shift-register memory'[11]. The storage elements are based on chains of molecules capable of electron transfer. In such a system, the information is moved, or modified, by photoinduced electron transfer reactions.

Molecules like $[Ru(bpy)_3]^{2+}$ have also been used and studied in a very important and promising scientific field right before entering the 21st century : the conversion of solar energy to electric energy.

Electron-transfer quenching of molecular excited states is of potentially importance for conversion of excited state energy into stored chemical redox energy[12]. When the molecule is excited with solar light, we speak about solar energy conversion. The excited states of metal complexes like $[Ru(bpy)_3]^{2+}$ are especially appealing in this respect because these complexes absorb light appreciably in the visible.

Moreover, excited states of the $[Ru(bpy)_3]^{2+}$ can be quenched by both electron-transfer and energy-transfer processes[13]. It has been found, for example, that net electron transfer occurs from $[Ru(bpy)_3]^{2+}*$ to oxidants such as $Fe(OH_2)_6^{3+}$ and $Ru(NH_3)_6^{3+}$. Generally speaking those Ru-types compounds have been extensively studied for solar energy conversion because their intense absorption bands in the visible region of the spectrum are also long-lived electronic excited states. These excited states, which are of metal-to-ligand charge transfer type (MLCT), are easily oxidized and reduced, and the products of oxidation and reduction are kinetically stable[14].

We obtain then the following reaction scheme[15]

$$\left[Ru(bpy)_3\right]^{2+} \xrightarrow{h\upsilon} \left[Ru(bpy)_3\right]^{2+*}$$
$$\left[Ru(bpy)_3\right]^{2+*} + Q \longrightarrow \left[Ru(bpy)_3\right]^{3+} + Q^-$$
$$\left[Ru(bpy)_3\right]^{3+} + A \longrightarrow \left[Ru(bpy)_3\right]^{2+} + A^+$$

This scheme represents an inorganic model for photosynthesis, with Q an oxidant responsible of an oxidative quenching. $[Ru(bpy)_3]^{3+}$ is a strong oxidant, thermodynamically capable of oxidizing water to O_2 (A in the upper scheme). The upper scheme can also be operated with a reductive quenching step instead of an oxydative one.

$$\left[Ru(bpy)_3\right]^{2+*} + Q \longrightarrow \left[Ru(bpy)_3\right]^{+} + Q^+$$

In this case, we obtain $[Ru(bpy)_3]^+$ which is a strong reductant, thermodynamically capable of reducing water to H_2. It should then be possible to photolyse water with such a system.

Photochemical cleavage of water by a system involving monolayers of $[Ru(bpy)_3]^{2+}$ derivatives has indeed been reported[16], but the results have not been confirmed by further work[17]. However, those type of Ruthenium compounds are still very good « sensitizers », and can convert light to electricity by an heterogeneous charge-transfer reaction when bound to TiO_2 films[18, 19]. For all the reasons expressed previously in this chapter, Ru^{II} with polypyridine ligands are still playing a key role in modern photochemistry, photophysics and related fields.

To understand the photochemical and the photophysical properties of a molecule, it is important to study their excited states. The electronic structure of the $[Ru(bpy)_3]^{2+}$ has already been the subject of a large number of studies[20-28]. And, despite the apparent simplicity of $[Ru(bpy)_3]^{2+}$ and related compounds, their spectroscopy, photophysics and photochemistry have proven to be rather complicated, resulting in controversial and often conflicting interpretations of experimental results[29]. As an example, let us just mention the question of the localization or delocalization of the excited electron in the lowest excited state. This question is still up to date. In the gas phase, the problem of localization or delocalization is due to a competition between the Jahn-Teller effect and an electrostatic interaction. If the Jahn-Teller effect is strong, the system will be localized, and if the Jahn-Teller effect is small compared to the electrostatic effect, the system will be delocalized. Until now, nobody has determined which of the two effects is the strongest, neither in the lowest singlet MLCT nor in the lowest triplet MLCT. The reason for this is that nobody succeeded to study the $[Ru(bpy)_3]^{2+}$ in the gas phase so far.

In condensed phase, the problem is different. The molecular structure around the complexe can induce, depending on the medium, an inhomogeneity which can destroy the ideal D_3 symmetry of the complex. The three ligands are then no more equivalent. This inhomogeneity is in favor of the Jahn-Teller effect in the competition with the electrostatic interaction. This inhomogeneity is the strongest factor[30, 31] in solution and in frozen glasses, and there the lowest excited ^{3}MLCT state in $[Ru(bpy)_3]^{2+}$ is localized. The situation in crystal depends on the counter ion.

Another noteworthy point is the photochemical stability of the $[Ru(bpy)_3]^{2+}$, and thus the characterization of the ligand field transitions. This stability is of fundamental importance for applications. Indeed, although $[Ru(bpy)_3]^{2+}$ is normally considered as photochemically inert towards ligand substitution, there is increasing evidence that this is not the case.

Especially if the pH of the solution is acid and/or at high temperature[32]. In the before mentioned study, the authors have found experimentally that the photoactive set of levels are located 3600cm^{-1} above the lowest MLCT state. This is not in agreement with the computation of the d-d* transition energies using Density Functional Theory[33]. In recent years, the photochemistry and the photophysics of complexes with low-lying MLCT states have attracted considerable interest[34-38]. With the help of those studies, a mechanism of the photochemistry of the $[Ru(bpy)_3]^{2+}$ will be presented in this work. This mechanism implies a reassessment of the role of the ligand-field excited state in the photochemical dissociation of metal-ligand bonds.

4.2 Computational methods

The ADF[39, 40] program package has been employed in all the calculations. The Vosko, Wilk and Nusair[41] (VWN) functional for exchange and correlation energies was used in the Local Density Approximation (LDA). The nonlocal corrections using the Becke[42] exchange and Perdew[43] correlation (GGA or Generalized Gradients Approximation) have been used for all gradient corrected calculations. We used a set of basis functions present in the program database. All atoms were described by a triple-ζ STO basis set and the core electrons of Ru(1s-3d), N(1s), C(1s) were kept frozen.

To evaluate the intensities of optical transitions in a time-independent framework, we calculated the oscillator strength using the Dipole program which is now part of the ADF program package.

Using the time-dependent density functional theory (TDDFT) formalism, the transition energies have been performed using the Davidson algorithm.

For the structure of the $[Ru(bpy)_3]^{2+}$, quasi-relativistic computations have also been performed, using the Pauli formalism. This approach is called quasi-relativistic in the sense that the first-order scalar relativistic Pauli Hamiltonian is diagonalized in the space of the non-relativistic solutions[44].

4.3 Results and discussion

4.3.1 Geometry optimization

	X-ray[45]	LDA	GGA	GGA+Pauli
Ru-N	2.056(2)	2.050	2.122	2.078
N-C(1)	1.354(3)	1.352	1.368	1.368
N-C(5)	1.354(4)	1.336	1.349	1.348
C(1)-C(2)	1.369(5)	1.386	1.399	1.400
C(1)-C(1')	1.474(5)	1.448	1.463	1.470
C(2)-C(3)	1.374(5)	1.380	1.390	1.393
C(3)-C(4)	1.348(5)	1.386	1.394	1.395
C(4)-C(5)	1.362(5)	1.378	1.393	1.391
C(3)-H(3)	0.85(4)	1.094	1.089	1.090
C(4)-H(4)	0.88(3)	1.093	1.090	1.088
C(5)-H(5)	0.88(3)	1.094	1.089	1.087
N-Ru-N'	78.7°(1)	77.9°	76.8°	78.4°
N-C(1)-C(1')-N'	5.9°/6.6°(19)[46]	7.1°	5.8°	4.5°
Ru-N-C(1)	115.9°(2)	116.7°	116.2°	115.7°
Ru-N-C(5)	126.0°(2)	124.7°	125.5°	125.1°
N-C(1)-C(1')	114.6°(1)	114.6°	115.3°	115.0°
C(1)-C(2)-C(3)	120.2°(3)	119.6°	119.8°	119.7°
C(2)-C(3)-C(4)	119.2°(3)	118.6°	118.6°	118.9°
C(3)-C(4)-C(5)	119.5°(3)	119.2°	119.1°	118.8°
C(4)-C(5)-N	122.4°(3)	122.4°	122.8°	122.6°

Table 1. Comparison between calculated and experimental structural parameters ($[Ru(bpy)_3](PF_6)_2$) for the ground state of $[Ru(bpy)_3]^{2+}$ with atom labeling in Fig. 1 (bond distances in Å and bond angles in degree, estimated standard deviations in parentheses)

As already mentionned, the $[Ru(bpy)_3]^{2+}$ ion has been one of the most studied molecule for the last three decades. Thus a great number of investigations have been carried on.

Also a DFT study on the electronic structure of the complexe has been performed[47], but without prior optimization of the geometry. We therefore performed a DFT calculation to optimize the structure of this complexe. In order to reduce the computational effort, we optimized the structure of the complexe in D_3 symmetry, after having previously optimized the structure of the cis-bipyridine ligand in C_{2v} symmetry. In the optimization of the complete complexe in D3 symmetry, non additional criteria have been set on the bipyridine ligands however.

Results of the optimization can be found in Table 1. The best results are obtained with the LDA method, especially for the metal-ligand bond length. Our calculations are thus in agreement with the conclusion, often pointed out, that for Werner type of complexes, GGA functionals lead to structural parameters in worse agreement with the experiment than the LDA[48].

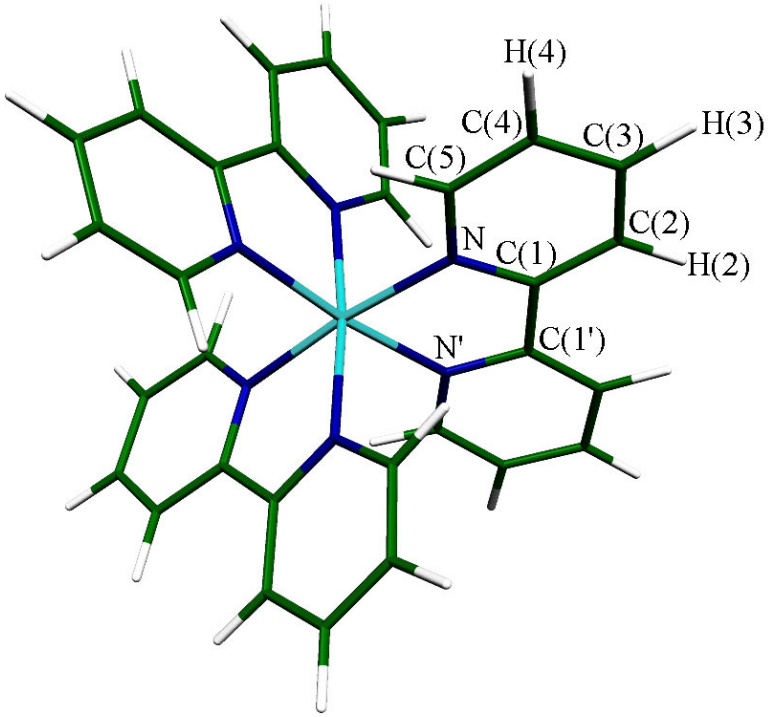

Figure 1. Molecular conformation of $[Ru(bpy)_3]^{2+}$ with the atom labeling used in Table 1

When introducing relativistic corrections, we see that the metal-ligand bond length becomes shorter. At a first glance, this is surprising with respect to the d-orbital expansion due to the s- and p-orbital contraction. This particular point has been satisfactorily explained by Ziegler and coworkers[49].

Another interesting feature of the final geometry is the bpy distortion. While the symmetry of the $[Ru(bpy)_3]^{2+}$ remains D_3 (initial criteria) during the optimization, we observe that the bpy ligand deviates from planarity, as exhibited by the dihedral angle between the two pyridine cycles of the bpy ligand. This feature has already been observed by X-ray structure determination[46]. In this study, the value of the dihedral angle is 5.9° at room temperature and 6.6° at 105K, which is in reasonable agreement with the angle of 7.1° as obtained in our calculation.

4.3.2 Molecular orbital scheme

Despite the fact that there are still unsolved problems in understanding all details of the resolved emission $[Ru(bpy)_3]^{2+}$ spectrum, the overall molecular orbital of such a complex is well known[1] and in perfect agreement with our molecular orbital scheme of the $[Ru(bpy)_3]^{2+}$ as depicted in Fig. 2.

In Fig. 2 we see two sets of levels of empty molecular orbitals. Following a one-electron excitation, promotion of an electron from the HOMO to the lowest set of unoccupied orbitals gives rise to a MLCT state, whereas the promotion of one electron from the HOMO to the upper set of unoccupied orbitals gives rise to a Ligand-Field or Metal Centerd (MC) state. The left part of Fig. 2 represents a complete, but simplified, molecular orbital diagram for the complexes of the form $M(LL)_3^{2+}$ (with M=Fe, Ru, Os)[1]. Ru^{2+} is a d^6 ion and the polypyridine ligands are usually colorless molecules possessing σ-donor orbitals localized on the nitrogen atoms and π donor and π^* acceptor orbitals delocalized on aromatic rings.

The right part of Fig. 2 shows a more detailed diagram of the frontier orbitals of $[Ru(bpy)_3]^{2+}$ that have been calculated in this work.

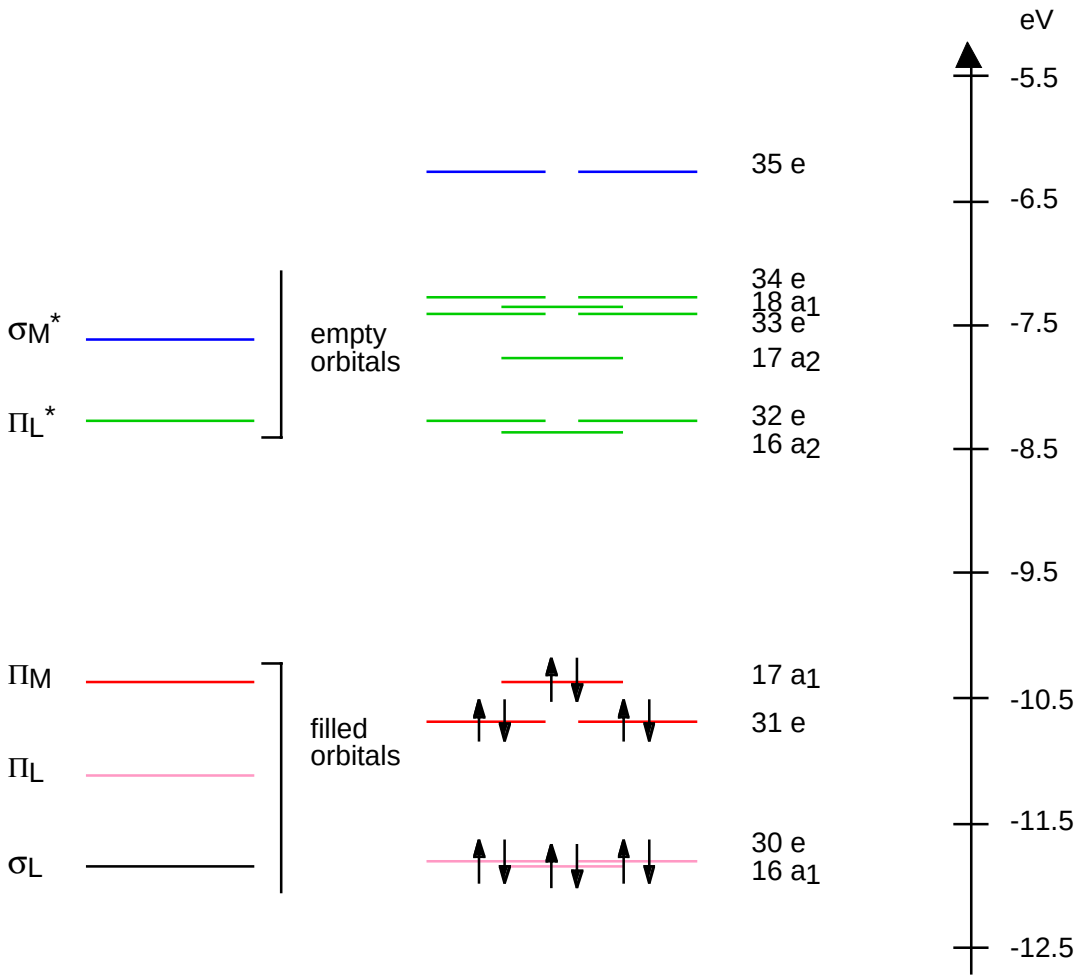

Figure 2. Molecular orbital scheme of the $[Ru(bpy)_3]^{2+}$.

	$d_{x^2-y^2}$	d_{z^2}	d_{xy}	d_{xz}	d_{yz}	$p_x(N)$ $p_y(N)$	$p_z(N)$	$p_x(C)$ $p_y(C)$	$p_z(C)$	Energies (eV)
35 e_θ	24%	0%	0%	0%	30%	15%	5%	4%	3%	-6.618
35 e_ε	0%	0%	24%	30%	0%	15%	5%	4%	3%	-6.618
34 e_θ	1%	0%	0%	0%	1%	10%	8%	46%	34%	-7.306
34 e_ε	0%	0%	1%	1%	0%	10%	8%	46%	34%	-7.306
18 a_1	0%	4%	0%	0%	0%	12%	8%	41%	33%	-7.355
33 e_θ	1%	0%	0%	0%	2%	6%	3%	45%	39%	-7.430
33 e_ε	0%	0%	1%	2%	0%	6%	3%	45%	39%	-7.430
17 a_2	0%	0%	0%	0%	0%	4%	4%	51%	40%	-7.712
32 e_θ	4%	0%	0%	0%	5%	15%	8%	31%	30%	-8.282
32 e_ε	0%	0%	4%	5%	0%	15%	8%	31%	30%	-8.282
16 a_2	0%	0%	0%	0%	0%	12%	11%	42%	34%	-8.354
17 a_1	0%	79%	0%	0%	0%	1%	1%	11%	2%	-10.324
31 e_θ	43%	0%	0%	0%	28%	1%	1%	6%	10%	-10.589
31 e_ε	0%	0%	43%	28%	0%	1%	1%	6%	10%	-10.589
30 e_θ	0%	0%	0%	0%	0%	0%	0%	52%	39%	-11.742
30 e_ε	0%	0%	0%	0%	0%	0%	0%	52%	39%	-11.742
16 a_1	0%	0%	0%	0%	0%	0%	0%	52%	39%	-11.769

Table 2. Orbital contributions, calculated within the GGA approximation

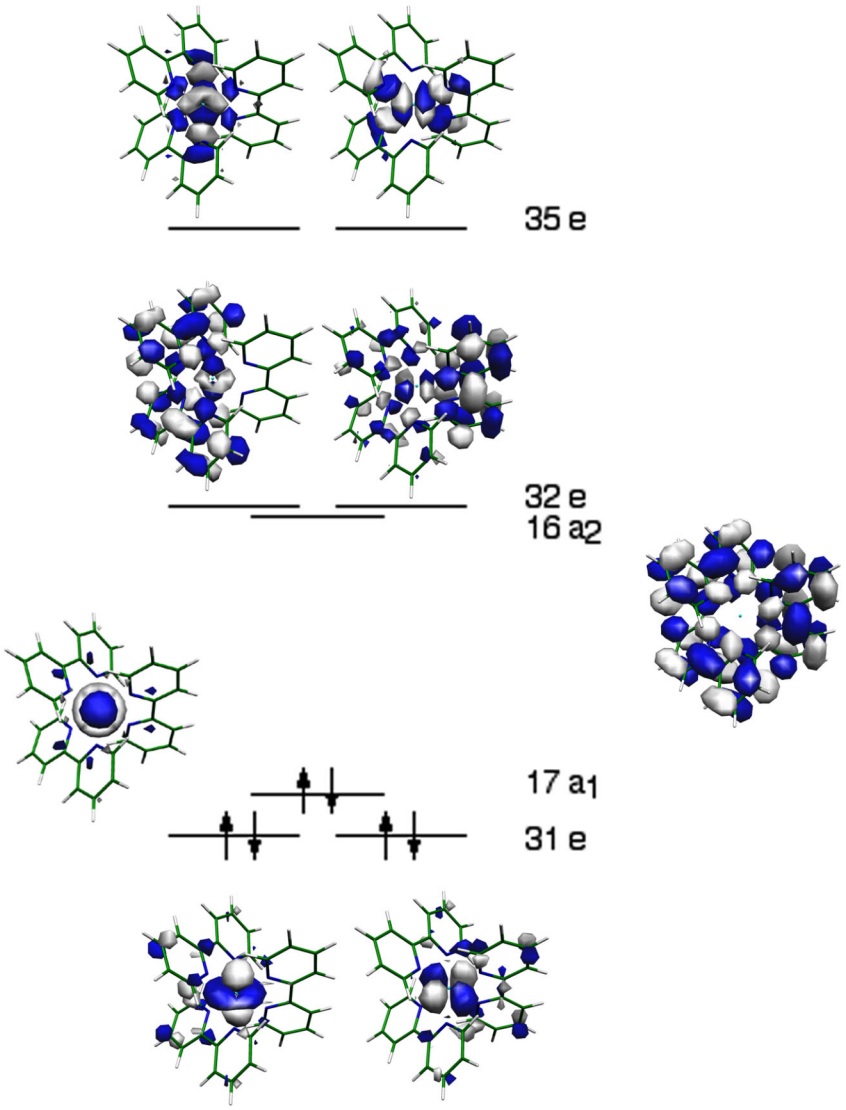

Figure 3. Frontier Molecular orbitals of the [Ru(bpy)3]2+ in 3D

Table 2 shows the *Symmetrized Fragments Orbitals* (SFO) contributions of the frontier molecular orbitals. The ADF program package that we used in this study works on a system of fragments. By defining the atoms as being the fragments, we can then have the atomic orbital contributions to the different molecular orbitals. As already depicted in

Fig. 2, we clearly see in Table 2 the metallic caracter of the highest set of occupied molecular orbitals. We also see clearly the ligand π^* character of the lowest set of unoccupied molecular orbitals. Finally, we observe that the σ_M^* of Fig. 2 are the 35e orbitals. The Fig. 3 gives a 3D-representation of the relevant frontier molecular orbitals.

4.3.3 Energies of the excited states

4.3.3.1 MLCT states

Using the ΔSCF method as described in chapter 3 of this thesis, energies of the lowest MLCT excitation ($^{1,3}A_2$), arising from the transition of one electron in the HOMO ($17a_1$) to the LUMO ($16a_2$), have been computed using different functionals. Results are shown in Table 3.

	LDA	GGA	GGA+Pauli	Exp.[20]
$\Delta E(^1A_2)$	19486	19000	18043	18950
$\Delta E(^3A_2)$	19159	18641	17874	18470

Table 3. Excitation energies of the lowest MLCT. (values in cm^{-1})

In Table 3, the agreement between the experimental values and the calculated ones are very good. Contrary to geometry where the LDA structure was closer to experiment, GGA energies correspond best with the experimental values. Note that no correction for any solvent effect has been included.

Due to the results obtained for the lowest excited state of the $[Ru(bpy)_3]^{2+}$, the further excitation energies that have been calculated using the ΔSCF in this chapter have been calculated using the nonlocal gradient corrections of Becke[42] for the exchange and of Perdew[43] for the correlation.

Table 4 shows the computed energies of the lowest set of MLCT states of the $[Ru(bpy)_3]^{2+}$. The states are arising from the promotion of one electron from the metal t_{2g} orbitals of the ruthenium ($e + a_1$ in symmetry D_3) to the lowest unoccupied π^* orbitals of

the bipyridine ligands (a_2 + e in D_3 symmetry). It results a state of 12 states, 6 that are singlet in character and 6 that are triplet.

MLCT transitions		E(ΔSCF) cm^{-1}	E(TDDFT /GGA)	E(exp.)[20]	f(ΔSCF) a.u.	f(TDDFT)
$17a_1 \rightarrow 16a_2$	$^1A_2$	19000	16744	18950	$2.97 \cdot 10^{-4}$	$0.15 \cdot 10^{-2}$
	$^3A_2$	18641	16377	18470		-
$31e \rightarrow 16a_2$	^1E	20250	19319	21500 (strong)	$1.21 \cdot 10^{-1}$	0.56
	^3E	19936	18639	20450		-
$17a_1 \rightarrow 32e$	^1E	20151	17688		$4.5 \cdot 10^{-7}$	$0.17 \cdot 10^{-2}$
	^3E	19533	16889			-
$31e \rightarrow 32e$	$^1A_1$	22422	22237		$8.44 \cdot 10^{-2}$	0
	$^3A_1$	19988	18389			-
	^1E	22477	21204	23300 (strong)	$8.45 \cdot 10^{-2}$	0.19
	^3E	21724	18976			-
	$^1A_2$	24113	19622	26130	0	$0.14 \cdot 10^{-3}$
	$^3A_2$	23459	19422			-

Table 4. Excitation energies for the lowest MLCT of the $[Ru(bpy)_3]^{2+}$

From inspection of Table 4 it appears that the MLCT excitation energies are a slightly better described when using the ΔSCF approach than with time-dependent DFT one. Using this former method, the worst result is obtained when computing the energy of the $^1A_2$ state arising from the transfer of one electron from the 31e orbital to the 32e orbital. In this case the deviation is $2017cm^{-1}$. This turns out to be quite acceptable, bearing in mind that the general accuracy of the method is usually around $2500cm^{-1}$[50].

The computation of excitation energies using TDDFT does not give better results in this case. This is not so surprising as it seems. Indeed, many recent results show that the improvement of the TDDFT over the ΔSCF method depends on the type of excitation under consideration, and is not so evident as one thought some years ago. Moreover, nowadays, the founder of TDDFT is reconsidering the ΔSCF method[51].

The excitation energies shown in Table 4 and obtained with the TDDFT approach have been calculated using the GGA functional of Becke[42] for the exchange and Perdew[43] for the correlation. It is important to note that it was not necessary to use a functional with a correct asymptotic behavior, e.g. the LB94 functional[52]. However, it is known that LB94 functional improves the description of the exchange and correlation potential upon Becke-Perdew's one only in the outer molecular region, but it doesn't affect the inner region. We are then, a priori, not expecting better results for the present case, and so it is exactly as one can see in Table 5.

MLCT transitions		E(TDDFT/GGA)	E(TDDFT/LB94)	E(exp.)
$17a_1 \rightarrow 16a_2$	$^1A_2$	16744	15648	18950
	$^3A_2$	16377	15297	18470
$31e \rightarrow 16a_2$	^1E	19319	18230	21500 (strong)
	^3E	18639	17536	20450
$17a_1 \rightarrow 32e$	^1E	17688	16586	
	^3E	16889	15769	
$31e \rightarrow 32e$	$^1A_1$	22237	21102	
	$^3A_1$	18389	17220	
	^1E	21204	20108	23300 (strong)
	^3E	18976	17841	
	$^1A_2$	19622	18497	26130
	$^3A_2$	19422	18302	

Table 5. Excitation energies for the lowest MLCT states of the $[Ru(bpy)_3]^{2+}$ using the LB94 functional.

4.3.3.2 LC states

$\pi\rightarrow\pi^*$ transitions		E(ΔSCF) cm^{-1}	E(TDDFT /GGA)	E(exp.)[53]	f(ΔSCF) a.u.	f(TDDFT)
$16a_1\rightarrow16a_2$	$^1A_2$	28916	28397		$4.37\cdot10^{-1}$	$0.54\cdot10^{-1}$
	$^3A_2$	27647	28383			-
$30e\rightarrow16a_2$	^1E	31054	28200		$1.33\cdot10^{-1}$	0.22
	^3E	29769	26512			-
$16a_1\rightarrow32e$	^1E	31680	28826		$1.36\cdot10^{-1}$	$0.1\cdot10^{-1}$
	^3E	30602	28807			-
$30e\rightarrow32e$	$^1A_1$	39650	28658		$1.37\cdot10^{-1}$	0
	$^3A_1$	40196	28651			-
	^1E	34147	28826	34000	$6.95\cdot10^{-1}$	0.14
	^3E	32439	28322			-
	$^1A_2$	26417	34658	36000 (strong)	0	2.68
	$^3A_2$	24682	26695			-

Table 6. Excitation energies for the lowest $\pi\rightarrow\pi^*$ transitions (LC) of the $[Ru(bpy)_3]^{2+}$

Concerning the $\pi\rightarrow\pi^*$ transitions, as depicted in Table 6, our theoretical results are in less good agreement with the experimental ones. This is specially true for the excitation arising from the promotion of one electron of the 30e orbital to the 32e orbital. The $^1A_2$ state arising from this transfer is badely described by the ΔSCF approach. In this case, an improvement is achieved when using the TDDFT approach. The main reason for this discrepancy has to be seeked in the large Coulomb interaction responsible for multiplet splitting of the $e(t_{2g})\rightarrow e(\pi^*)$ many fold (13233cm^{-1} between $^1A_1$ and $^1A_2$).

4.3.3.3 Ligand-Field states

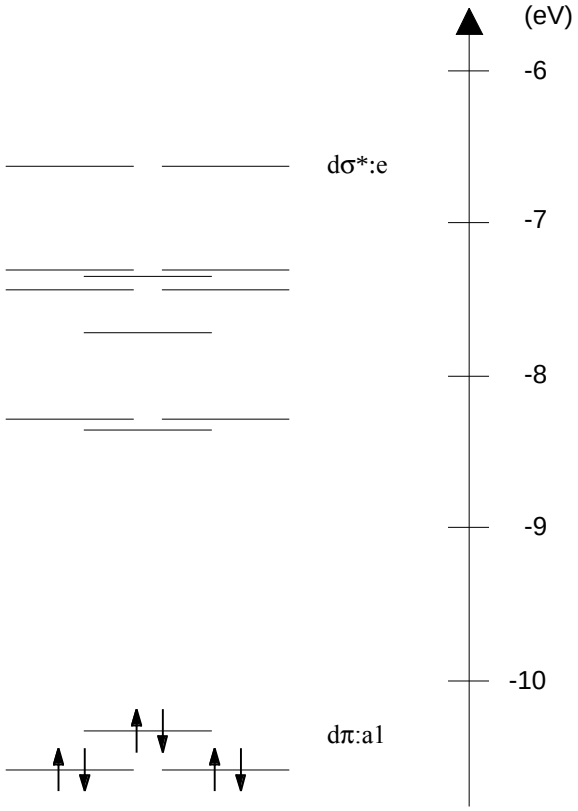

Figure 4. Location of the metal-ligand σ* antibonding orbital

Our previous results, which are in agreement with spectroscopical data, suggest that the lower set of energy levels in $[Ru(bpy)_3]^{2+}$ are metal-to-ligand charge-transfer (MLCT) states. These levels are photoinert, whereas the upper set of excited states, which have been experimentally found to be ~3600cm^{-1} above the lower set[13], give rise to ligand substitution photochemistry. According to the accepted picture of the photochemical dissociation of metal-ligand bonds, those states should be ligand-field states.

	$\Delta E(^3E)$	$\Delta E(^1E)$
$d\pi : a_1 \rightarrow d\sigma^* : e$	32327	35542

Table 7. Excitation energies for the lowest d→d* transition of the $[Ru(bpy)_3]^{2+}$

Using the ΔSCF method described in chapter 3 of this thesis, we have calculated the energy of the lowest d-d transition within the GGA approximation. The two orbitals involved in this transition are emphasized in Fig. 4. In Table 7 we give the results obtained for the calculation of the singlet and the triplet states. This calculation yields a value of 32327cm^{-1} for the energy of the triplet ^{3}E state, assuming the same geometry as the ground state, that is within the Franck-Condon approximation. There is, thus, a large difference between the predicted and the experimental values for this transition. How shall we interpret this result ? In view of the calculated MLCT energies, it seems however that our model describes pretty well the system.

Is it really necessary to consider the involvement of ligand field states for the interpretation of the photochemistry of the $[Ru(bpy)_3]^{2+}$?

4.3.4 Photochemistry of the $[Ru(bpy)_3]^{2+}$

Although $[Ru(bpy)_3]^{2+}$ is normally considered as photochemically inert towards ligand subsitution, there is increasing evidence that this is not the case. Especially if the pH of the solution is acid and/or at high temperature [32].

And despite numerous studies in this field, the understanding of the photosubstitution and photoracemization of the $[Ru(bpy)_3]^{2+}$ is still not completely achieved. Moreover, our first computation for the energy of the ligand-field state is also in bad agreement with the general accepted interpretation for photochemical dissociation. In recent years, the photochemistry of complexes with low-lying metal-to-ligand charge-transfer (MLCT) states have attracted considerable interest. With the help of those studies[34-38], a mechanism of the photochemistry of the [Ru(bpy)3]2+ is slowly emerging. This mechanism implies a reassessment of the role of ligand-field excited states in the photochemical dissociation of metal-ligand bonds.

This accepted picture of photochemical dissociation of metal-ligand bonds assigns a predominant role to a ligand-field excitation. The argument may be illustrated using the well-known qualitative molecular orbital energy diagram of an octahedral d^6 transition metal complex.

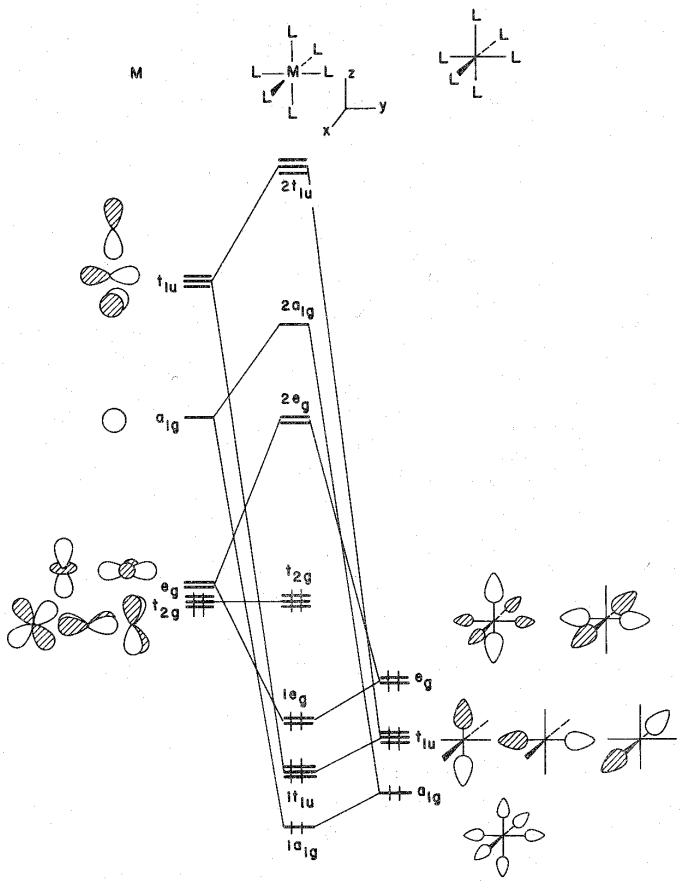

Figure 5[54]. Molecular orbital diagram of an octahedral ML6 complex, where L is an arbitrary σ donor ligand

On the left side of the interaction diagram there are the nine atomic orbitals of the valence shells of a transition metal. d_{z^2} and $d_{x^2-y^2}$ orbitals have e_g symmetry whereas d_{xy}, d_{xz} and d_{yz} transform as a t_{2g} irrep. At higher energies are the metal s- and p-levels. We are only concerned by the d-shell, so that interaction with the empty shells of s and p electrons on the metal can be neglected. On the right side of the figure are drawn the symmetry adapted linear combinations of the σ orbitals. There are six of them and their relative ordering is set by the number of nodes within each members. The a_{1g} and t_{1u} combinations match with the metal s- and p-orbital and give rise to a bonding and to an antibonding combination, thus yielding the molecular level $1a_{1g}$, $1t_{1u}$ and $2a_{1g}$, $2t_{1u}$ respectively. The e_g ligand set is stabilized by interacting with metal z^2 and x^2-y^2 which yields the MO's $1e_g$ and $2e_g$ respectively. Here the six M-L bonding orbitals are concentrated on the ligands

whereas the six corresponding M-L antibonding levels are heavily confined on the metal atom. Finally there is a t_{2g} centered on the metal. It is nonbonding when L has only a σ donor function ; however, it will play an important role when the ligands have functions (π acceptor or π donor) that can enter into π bonding with the metal. The HOMO t_{2g} and LUMO $2e_g$ of Fig. 5 are better depicted in Fig. 6.

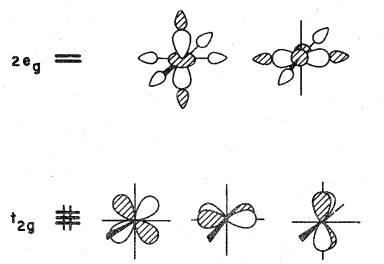

Figure 6[54]. HOMO t_{2g} and LUMO $2e_g$ of an octahedral ML_6 complex where L is an arbitrary σ donor ligand.

When the $2e_g$ orbitals, which are strongly M-L antibonding, are populated, we would expect that the complex will distort so as to lengthen the M-L distances or perhaps one or two M-L bonds might completely break.

In case of $[Ru(bpy)_3]^{2+}$, and actually with many other complexes, it is important to take into account the π-effects as well. How does the primary interaction diagram change when π functions are added to the surrounding ligands ? Let us start by replacing one of the generalized σ donor ligands in ML_6 by a carbonyl group which yields an ML_5CO complex.

As mentionned previously the σ donor orbital of CO along with the five σ levels of the L_5 grouping produce a splitting pattern in ML_5CO analogous to that in the Fig. 5. What does change is the t_{2g} level as shown in Fig. 7. Two members of t_{2g} set, i.e. xz and yz have the correct symmetry to interact with π and π* of CO. They become an e-set of orbitals in the reduced symmetry of the complex, the C_{4v}.

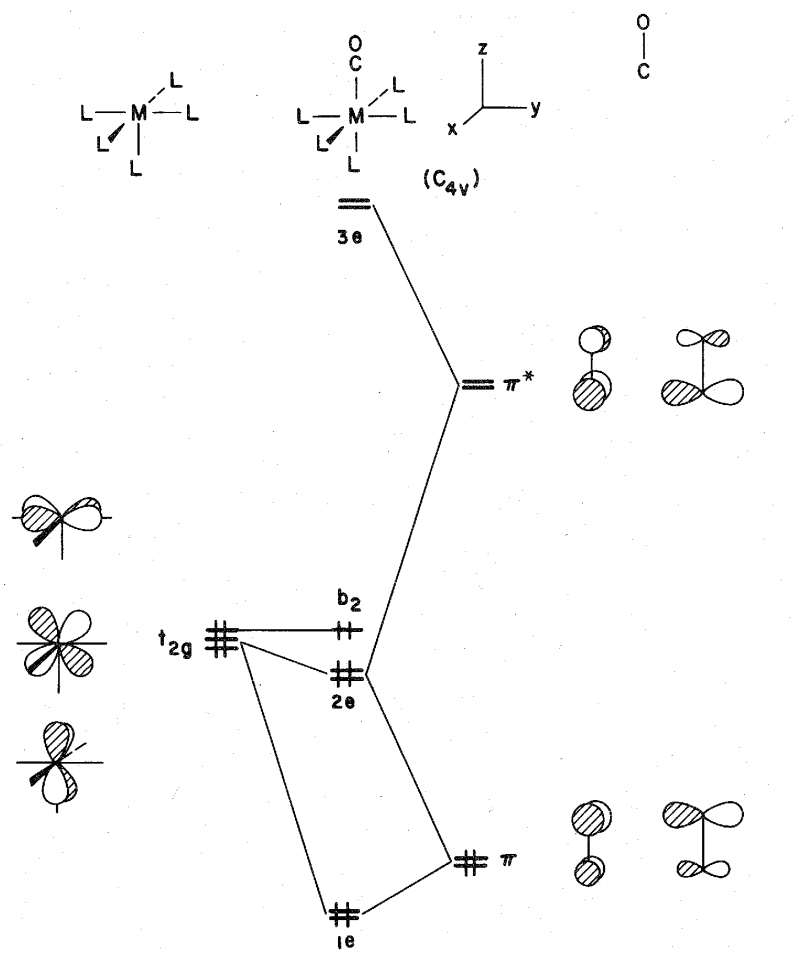

Figure 7[54]. An interaction diagram for the π components in a ML_5CO complex where L is an arbitrary σ donor.

Electron density is transferred from the filled metal t_{2g} orbitals is transferred to the empty π* orbital of CO. We call this effect π-backbonding.

When we merge the two previous interaction diagram into a single one, which take into account at the same time the σ effect and the π effect of the ligands, we then obtain Fig. 8, the MO diagram of the $Cr(CO)_6$ complexe in this case.

The lowest transition, a Ligand-Field or MC transition, will populate the e_g* set of orbitals and the corresponding excited state potential energy curve (PEC) along the metal-CO dissociation coordinate is dissociative

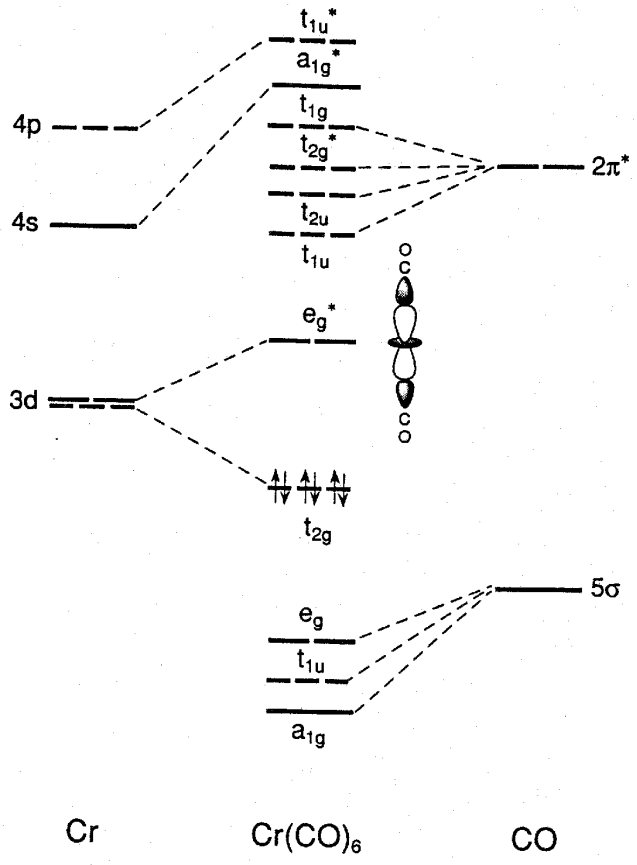

Figure 8[38]. Typical qualitative MO level diagram for a d^6 metal complex with ligands possessing both σ and π character.

Experimentally, Van Houten and Watts have found that the photoactive set of levels which is responsible for the photochemistry of the $[Ru(bpy)_3]^{2+}$ lies 3600cm^{-1} above the lowest MLCT state[13], i.e. ~19000cm^{-1} + 3600cm^{-1} above the ground state. We calculated (see chap. 4.3.3.3) the energy of the lowest d-d transition whithin the Franck-Condon approximation. We obtained an energy of 33000cm^{-1} for the ^3E state. There is thus a large difference between the calculated and the experimental values for this transition.
The same discrepancy has been found recently and has been the subject of refined studies[34-38].
The excitation spectrum of $Cr(CO)_6$ contains at low-energy a low-intensity shoulder that was assigned a long time ago to the excited ligand field state $^1T_{1g}$ belonging to the $t_{2g}^5e_g^1$

configuration. Moreover there was no reason for a revision of this assignment, since irradiation in the low-energy shoulder, presumably populating the lowest LF state, leads to photodissociation of CO, in perfect agreement with this qualitative picture. However, it has recently been found[38] that the relation between the lowest LF excited state at equilibrium geometry and the photochemistry is less straight forward than assumed in the « standard model ». The LF excitation to a metal-CO antibonding e_g-type orbital was predicted to lie at higher energy than this low-energy shoulder.

The same behavior was found in other metal complexes such as $Mn_2(CO)_{10}$[34, 35], *fac*-$Mn(Cl)(CO)_3(H\text{-}DAB)$[36] and $MnCl(CO)_5$[37].

The main conclusion drawn in these studies was that it is not necessary to excite to LF states in order to induce photodissociation of ligands, and that such dissociation, when observed, does not prove that the excitation was to a LF state. The σ-antibonding character of the e_g-type orbital proved to be not only strong but also short ranged. As a consequence, as soon as the metal-ligand bond length increases, the « pushing-up » effect due to the σ-antibonding character diminishes quickly, hence both the orbital energy and the excitation energy lower rapidely. The initially high-lying LF state is therefore characterized by a strongly dissociative potential energy curve (PEC), which, after fairly small metal-ligand bond lengthening, leads to crossing with the PECs of the MLCT states lying lower in energy for the ground state geometry. In the accepted picture, metal-ligand dissociation occurs from LF excited states because they are dissociative. This is actually fully corroborated by calculations. But they are actually so strongly dissociative that, even if they are too high to be populated directly by irradiation into the lowest absorption band, they cross soon with the lowest excited states and the lowest excited state of the PEC becomes dissociative. In other words, photochemical metal-ligand dissociation may take place regardless of the nature of the excited state into which the excitation takes place at ground state geometry.

Looking at the energy of the unoccupied orbitals of the $[Ru(bpy)_3]^{2+}$ as a function of the metal-ligand bond length, as depicted in Fig. 9, we clearly see the strong dissociative character of the σ*-antibonding e_g-type of orbital. By a mechanism of avoided crossing, the metal character of the σ* orbital in the ground state geometry is transferred to a π* orbital of the same symmetry with dominant ligand character.

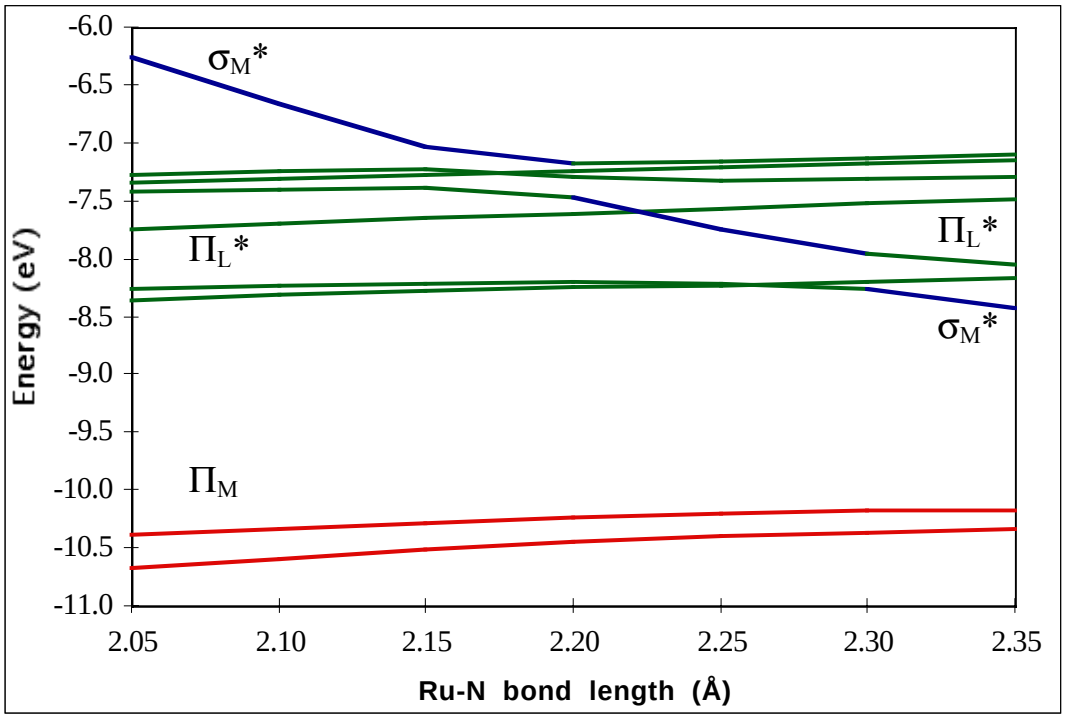

Figure 9. Energy of the frontier orbitals as a function of the metal-ligand bond length

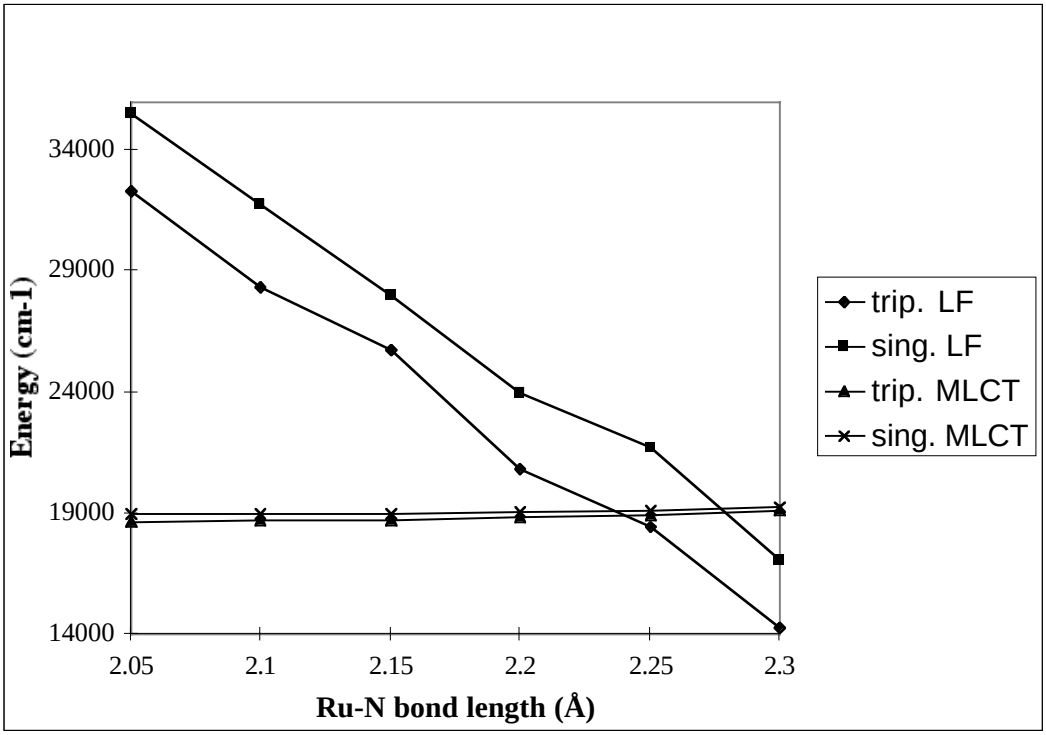

Figure 10. Transition energies of the lowest MLCT and lowest LF states

The labeling of the orbital in Fig. 9 corresponds to the labeling of the orbital in Fig. 2 and the energies of the orbitals therein have been calculated using the GGA functional.

As a result of the behavior of the unoccupied orbitals as depicted in Fig. 9, the energy of the lowest LF transition is strongly lowered when increasing the ruthenium to nitrogen bond lengths. The resulting state becomes fully dissociative as depicted in Fig. 10.

With sufficiently large ruthenium to nitrogen bond lengths, the energy of the lowest LF state becomes even lower than the energy of the lowest MLCT state. Energies in Fig. 10 have been obtained using the GGA functional.

It is important to notice here, that Fig. 9 and Fig. 10 have been obtained when elongating all the ruthenium to nitrogen bonds simultaneously. That is in conserving the D_3 symmetry of the $[Ru(bpy)_3]^{2+}$ during the whole procedure. This fully symmetrical model seems, at first glance, not very realistic. And indeed, Van Houten and Watts[32] have found, when investigating experimentally the photodissociation of the $[Ru(bpy)_3]^{2+}$, the presence of a photoproduct where one Cl^- and one monodentate bpy ligand are bound to Ru(II) : $[Ru(bpy)_2 \cdot (bpy)(Cl)]^+$.

In our calculations, when we look at the energy of the unoccupied orbitals of the $[Ru(bpy)_3]^{2+}$ as a function of one, and only one, ruthenium to nitrogen bond, the dissociative character of the metallic σ^*-antibonding orbital is poor. However, to obtain the experimental difference of 3600 cm^{-1} between the LF and the MLCT state, an increase of less than 0.15 Å is needed for all the ruthenium to nitrogen bond lengths. Thus we suggest the following explanation for the photochemistry of the $[Ru(bpy)_3]^{2+}$.

The initial excitation is a MLCT one. Intersystem crossing (ISC) to a nominal triplet state (^{3}MLCT) occurs with high efficiency. Assuming that the photochemical reaction occurs from a set of LF levels, there should be a thermal equilibrium between the lowest LF state and the lowest MLCT state. This lowest MLCT state is an extremely long-lived one. It decays with a radiative rate constant of $6.8 \cdot 10^5$ s^{-1} and with a radiationless rate constant of $1.22 \cdot 10^6$ cm^{-1}. This feature should allow for a vibrational motion which does correspond to a totally symmetrical stretching mode relative to all the ruthenium to nitrogen bonds. As soon as the lengthening of the Ru-N bonds is large enough (less than 0.15 Å), one electron from the MLCT state will be allowed to thermally populate the

lowest LF state. As a result, one ruthenium to nitrogen bond will break, and produce the intermediate with one monodentate bpy ligand of the $[Ru(bpy)_3]^{2+}$ photochemistry.

4.4 Conclusion

This work shows once more that Density Functional Theory is an efficient tool to describe the electronic structure of transition metal complexes. We obtain for both the geometry and the energy of the lowest MLCT states a good agreement with the experiment. Further more, in this work, DFT helps us to understand, or at least to give some answers, in the photochemical behavior of the $[Ru(bpy)_3]^{2+}$ which is still not completely understood by experimentalists. In this respect DFT is a tool with predictive value. Hence we may anticipate that computational chemistry can be generalized as a usefull tool for understanding chemical problems.

On the other hand, we see in this work that excited states computation remains a challenging task for DFT. If good results are obtained for MLCT states, LC states seem to be less well described. For formal problems with a theoretical background involving the computation of excited states, researchers are now more focussed on TDDFT. In our case however, we don't see any real improvement of the TDDFT method in the computation of the excited states in general and of LC states in particular. This will probably be confirmed in the next few years.

4.5 References

(1) Juris, A.; Balzani, V.; Baribelletti, F.; Campagna, S.; Belser, P.; von Zelewsky, A., *Coord. Chem. Rev.* **1988**, *84*, 85.

(2) Hsueh, Y. T.; Smith, R. L.; Northrup, M. A., *Proc. Electrochem. Soc.* **1995**, *95*, 117.

(3) Hench, L. L., *Ceram. Trans.* **1991**, *19*, 265.

(4) Greenway, G. M.; Knight, A. W.; Knight, P. J., *Analyst* **1995**, *120*, 2549.

(5) Knight, A. W.; Greenway, G. M.; Chesmore, E. D., *Anal. Proc.* **1995**, *32*, 125.

(6) Kojima, H.; Sato, N.; Kawamoto, Y.; Iyoda, J., *Chem. Lett.* **1989**,
(7) Stradowski, C.; Goerner, H.; Currell, L. J., *Biopolymers* **1987**, *26*, 189.

(8) Bhattacharyya, B. D., *Indian J. Cryog.* **1990**, *15*, 711.

(9) Barton, J. K., *PCT Int. Appl. WO 90 05*, 732.

(10) Ohkubo, K.; Hamada, T.; Watanabe, M.; Fukushima, M., *Chem. Lett.* **1993**, 1651.

(11) Hopfield, J. J.; Onuchic, J. N.; Beratan, D. N., *Science* **1988**, *241*, 817.

(12) Durham, B.; Meyer, T. J., *J. Am. Chem. Soc.* **1978**, *100*, 6286.

(13) Van Houten, J.; Watts, R. J., *J. Am. Chem. Soc.* **1976**, *98*, 4853.

(14) Petersen, J. D.; Gahan, S. L.; Rasmussen, S. C.; Ronco, S. E., *Coord. Chem. Rev.* **1994**, *132*, 15.

(15) Young, R. C.; Meyer, T. J.; Whitten, D. G., *J. Am. Chem. Soc.* **1975**, *97*, 4781.

(16) Sprintschnik, G.; Sprintschnik, H. W.; Kirsch, P. P.; Whitten, D. G., *J. Am. Chem. Soc.* **1976**, *98*, 2337.

(17) Sprintschnik, G.; Sprintschnik, H. W.; Kirsch, P. P.; Whitten, D. G., *J. Am. Chem. Soc.* **1977**, *99*, 1285.

(18) Nazeeruddin, M. K.; Kay, A.; Rodicio, I.; Humprhy-Baker, R.; Müller, E.; Liska, P.; Vlachopoulos, N.; Grätzel, M., *J. Am. Chem. Soc.* **1993**, *115*, 6382.

(19) Wang, Z. S.; Huang, C. H.; Zhang, B. W.; Hau, Y. J.; Xie, P. H.; Qian, H. J.; Ibrahim, K., *New J. Chem.* **2000**, *24*, 567.

(20) Felix, F.; Ferguson, J.; Güdel, H. U.; Ludi, A., *J. Am. Chem. Soc.* **1980**, *102*, 4096.

(21) Daul, C. A.; Weber, J., *Chem. Phys. Lett.* **1981**, *77*, 593.

(22) Belser, P.; Daul, C. A.; von Zelewsky, A., *Chem. Phys. Lett.* **1981**, *79*, 596.

(23) Kober, E. M.; Meyer, T. J., *Inorg. Chem.* **1981**, *21*, 3967.

(24) Ferguson, J.; Herren, F., *Chem. Phys.* **1983**, *76*, 45.

(25) Kober, E. M.; Meyer, T. J., *Inorg. Chem.* **1984**, *23*, 3877.

(26) Ferguson, J.; Krausz, E.; Vrbancich, J., *Chem. Phys. Lett.* **1986**, *131*, 463.

(27) Daul, C. A.; Schlaepfer, C. W., *J. Chem. Soc. Dalton Trans.* **1988**, 393.

(28) Damrauer, N. H.; Cerullo, G.; Yeh, A.; Boussie, T. R.; Shank, C. V.; McCusker, J. K., *Science* **1997**, *275*, 54.

(29) Cushing, J. P.; Butoi, C.; Kelley, D. F., *J. Phys. Chem. A* **1997**, *101*, 7222.

(30) Riesen, H.; Wallace, L.; Krausz, E., *J. Phys. Chem.* **1995**, *99*, 16807.

(31) Krausz, E.; Riesen, H., *Comments on Inorg. Chem.* **1995**, *18*, 395.

(32) Van Houten, J.; Watts, R. J., *Inorg. Chem.* **1978**, *17*, 3381.

(33) Buchs, M.; Daul, A. C., *Chimia* **1998**, *52*, 163.

(34) Rosa, A.; Ricciardi, G.; Baerends, E. J.; Stufkens, D. J., *Inorg. Chem.* **1995**, *34*, 3425.

(35) Rosa, A.; Ricciardi, G.; Baerends, E. J.; Stufkens, D. J., *Inorg. Chem.* **1996**, *35*, 2886.

(36) Rosa, A.; Ricciardi, G.; Baerends, E. J.; Stufkens, D. J., *J. Phys. Chem.* **1996**, *100*, 15346.

(37) Wilms, M. P.; Baerends, E. J.; Rosa, A.; Stufkens, D. J., *Inorg. Chem.* **1997**, *36*, 1541.

(38) Pollak, C.; Rosa, A.; Baerends, E. J., *J. Am. Chem. Soc.* **1997**, *119*, 7324.

(39) Baerends, E. J.; Bérces, A.; Bo, C.; Boerrigter, P. M.; Cavallo, L.; Deng, L.; Dickson, R. M.; Ellis, D. E.; Fan, L.; Fischer, T. H.; Fonseca Guerra, C.; van Gisbergen, S. J. A.; Groeneveld, J. A.; Gritsenko, O. V.; Harris, F. E.; van den Hoek, P.; Jacobsen, H.; van Kessel, G.; Kootstra, F.; van Lenthe, E.; Osinga, V. P.; Philipsen, P. H. T.; Post, D.; Pye, C.; Ravenek, W.; Ros, P.; Schipper, P. R. T.; Schreckenbach, G.; Snijders, J. G.; Sola, M.; Swerhone, D.; te Velde, G.; Vernooijs, P.; Versluis, L.; Visser, O.; van Wezenbeek, E.; Wiesenekker, G.; Wolff, S. K.; Woo, T. K.; Tiegler, T.,
(40) Fonseca Guerra, C.; Snijders, J. G.; te Velde, G.; Baerends, E. J., *Theor. Chem. Acc.* **1998**, *99*, 391.

(41) Vosko, S. H.; Wilk, L.; Nusair, M., *Can. J. Phys.* **1980**, *58*, 1200.

(42) Becke, A. D., *Phys. Rev. A* **1988**, *38*, 3098.

(43) Perdew, J. P., *Phys. Rev. B* **1986**, *33*, 8822.

(44) Ziegler, T.; Tschinke, V.; Baerends, E. J.; Snijders, J. G.; Ravenek, W., *J. Phys. Chem.* **1989**, *93*, 3050.

(45) Rillema, D. P.; Jones, D. S.; Woods, C.; Levy, H. A., *Inorg. Chem.* **1992**, *31*, 2935.

(46) Biner, M.; Bürgi, H.-B.; Ludi, A.; Röhr, C., *J. Am. Chem. Soc.* **1992**, *114*, 5197.

(47) Daul, C.; Baerends, E. J.; Vernooijs, P., *Inorg. Chem.* **1994**, *33*, 3540.

(48) Bray, M. R.; Deeth, R. J.; Paget, V. J.; Sheen, P. D., *Int. J. Quant. Chem.* **1996**, *61*, 85.

(49) Ziegler, T.; Snijders, J. G.; Baerends, E. J., *Chem. Phys. Lett.* **1980**, *75*, 1.

(50) Daul, C. A.; Doclo, K. D.; Stückl, A. C., *Recent Advances in Density Functional Theory* **1997**, *2*, 61.

(51) Casida, M. E., On-line Workshop Proceedings of the Joint ITP/INT Workshop on Time-Dependent Density Functional Theory, Santa Barbara, 1999,
(52) van Leeuwen, R.; Baerends, E. J., *Phys. Rev. A* **1994**, *49*, 2421.

(53) Mason, S. F., *Inorg. Chem. Acta* **1968**, *14*, 89.

(54) Albright, T. A.; Burdett, J. K.; Whangbo, M. H., *Orbital Interactions in Chemistry*; ed.; John Wiley & Sons: New York, Chichester, Brisbane, Toronto, Singapore, 1985; 447.

Chapter 5

A Density Functional Study of the Nitroprusside

5.1 Introduction

The nitroprusside ion is a transition metal nitrosyl compound of iron that attracts the chemists interest for more than 30 years. The crystal structure of sodium nitroprusside $[Fe(CN)_5NO]Na_2 \cdot 2H_2O$ has been determined in 1963 by X-ray diffraction techniques[1].

The sodium nitroprusside (SNP) is an interesting molecule under very different topics. Pharmacologically and commercially known as Nipride, the SNP is a powerful vasodilator and is generally used in treatments of hypertensive emergencies and severe cardiac failure. SNP can produce nitric oxide which activates guanylate cyclase. Guanylate cyclase results in increased concentrations of cyclic-GMP in smooth muscle, leading to vasodilation in veins and arteries[2].

In the sixties, SNP has attracted the attention of chemists and physicists for two reasons[3-6] : (i) NO^+ creates a strong crystal field potential at the central metal ion and thus dominates the splitting of the energy levels of the d-orbitals ; the $[Fe(CN)_5NO]^{2-}$ ion actes as model compound to study the chemical bonding of nitrosyl group to transition metal ions, the important feature being the presence of low lying ligand level π^* NO, getting inserted into the d-orbital splitting ; and (ii) SNP was used as a Mössbauer reference standard because of its negative chemical shift as well as for its large quadrupole splitting.

Another interesting property of SNP is the occurrence of metastable states. Nitrosyl transition metal complexes are in general extensively studied because of their long-lived metastable states which are easily obtained by irradiation with light. In the case of SNP, the existence of the metastable states were discovered in 1977 using Mössbauer spectroscopy[7]. It was subsequently found that similar long-lived states can be generated by irradiation of other nitrosyl complexes : of Ni[8-10], of Ru[11-13], of Os[14] and of other iron complexes[15, 16] as well.

In the case of the SNP, two light-induced metastable states have been observed[7, 17-21]. They are produced by blue light irradiation and annihilated by red light irradiation. In crystaline SNP, metastable states have lifetimes greater than 10^4s. at temperature below 140K[22]. Because of this property, they attracted the interest of many researchers as potential candidates for functional material of memory devices[23-25] in which information can be optically written, read and erased.

Notwithstanding quite extensive studies, the nature of the two metastable states has for long time been subject of debate. In 1990, Güdel pointed out that the life time of the metastable states is inconsistent with any one-electron transfer model, and that either a large structural change, or a multi-electron promotion is required to explain the stability of the species[26]. Mössbauer[27] and ESR[28] evidences indicate that both metastable states are diamagnetic. The geometries of the two metastable states of SNP and that of its ground state have been analysed by X-ray diffraction at 50K by Carducci and coworkers[21]. Structural changes are mainly confined to the Fe-N-O group. In this respect, the ground state is linear, of symmetry C_{4v}, with the iron bound to the nitrogen. One of the two metastable states is also linear, but with the iron bound to the oxygen atom (isonitrosyl, η^1). In the litterature, this metastable state is often labeled as MS_I. The second metastable state, which has C_s symmetry, has the NO bound sideways (η^2). This metastable state is generally labeled as MS_{II}. Calorimetry and Raman experiments show that MS_I and MS_{II} lie 1.1 and 1.0 eV, respectively, above the ground state[22].

Two theoretical studies have been carried out including density functional theory calculation[10, 29]. They showed that the ground state and the two metastable states of SNP correspond to three minima on the ground state potential energy surface. However, these studies did not include the excited states and the corresponding potential energy curves of the nitroprusside ion. The consideration of these states is the main goal of this work.

5.2 Computational methods

The Density Functional Theory (DFT) within the Kohn-Sham formalism has been used throughout this work. The ADF[30, 31] program package has been employed in all the calculations. The Vosko, Wilk and Nusair[32] (VWN) functional for exchange and

correlation energies was used in the Local Density Approximation (LDA). The nonlocal corrections using the Becke[33] exchange and Perdew[34] correlation (B88P86) have been used in all gradient corrected calculations (GGA or Generalized Gradients Approximations). We used a set of basis functions present in the program database. All atoms were described by a triple-ζ STO basis set and the core electrons of Fe (1s-2p), C(1s), N(1s), O(1s) were kept frozen.

In the time-dependent density functional theory (TDDFT) formalism, the calculations were performed with the RESPONSE module of the ADF program. In this regards, excitation energies and oscillator strengths have been computed using the iterative DAVIDSON method. In TDDFT, either the B88P86 functional or the asymptotically correct Van Leeuwen-Baerends potential[35] (LB94) have been used.

5.3 Results and discussion

5.3.1 Ground state

5.3.1.1 Geometry and electronic structure of the GS

We first optimized the geometry of the nitroprusside ion, $[Fe(CN)_5NO]^{2-}$, in its ground state. In Table 1 the optimized geometry for the ideal C_{4v} symmetry is compared to the crystal structure[21], obtained by X-ray diffraction. The complex ion is slightly distorded in the solid. The symmetry is C_s. Thus, in the crystal structure, two different bond lengths are observed for the equatorial C atoms.

The results of the calculation are in good agreement with the experimental structural parameters. The LDA functional, which is known to overbind, gives too short bond lengths whereas the B88P86 functional yields bond lengths that are slightly too long. However, deviations between the optimized and the experimental structure are small. The arithmetic average of the deviations is 1.90pm in the case of the LDA optimization, with a maximal error of 2.9%. In the case of the GGA optimization, this average amounts to 2.15pm, with a maximum error of 3.2%.

	LDA / VWN	GGA / B88P86	Exp.[21]
Fe-N	1.616	1.642	1.6656(7)
N-O	1.159	1.170	1.1331(10)
Fe-C_{ax}	1.915	1.957	1.9257(9)
Fe-C_{eq}	1.907	1.959	1.9310/1.9403(6)
C_{ax}-N_{ax}	1.164	1.172	1.159(12)
C_{eq}-N_{eq}	1.166	1.173	1.1603/1.1622(8)
Fe-C_{ax}-N_{ax}	180.0	180.0	179.78(8)
Fe-C_{eq}-N_{eq}	175.0	175.0	178.34/176.49(6)
Fe-N-O	180.0	180.0	176.03(7)
N-Fe-C_{ax}	180.0	180.0	176.63(4)
N-Fe-C_{eq}	95.2	94.5	93.40/97.65(2)
C_{eq}-Fe-C_{eq} (trans)	169.6	171.1	168.91(3)
C_{eq}-Fe-C_{eq} (cis)	89.5	89.7	90.25/88.20(2)

Table 1. Structural parameters of the ground state of $[Fe(CN)_5NO]^{2-}$ (distances in Å)

On the whole, these results are satisfactory because one expects the errors of the same order of magnitude if the crystal environnement is neglected. It is thus justified to study the ground state of the nitroprusside in its ionic form.

As shown in Fig. 1 and in Table 2, the nitroprusside ground state is a $^1A_1$ closed shell state, corresponding to a pseudo octahedral $t_{2g}^6e_g^0$ occupation. This is in agreement with the ESR study[28]. Due to the C_{4v} symmetry, the t_{2g} ligand field orbitals are split into b_2 (dxy) + e (dxz, dyz) orbitals. The Highest Occupied Molecular Orbital (HOMO) is the $2b_2$ orbital and has mainly a d_{xy} iron character, as displayed in Table 2. With respect to the nitrosyl group, the $2b_2$ orbital is nonbonding.

	d_{x2-y2}	d_{z2}	d_{xy}	d_{xz}	d_{yz}	N(s)	N(p)	C(s)	C(p)	O(s)	O(p)	eV
5 b_1	46%	0%	0%	0%	0%	0%	0%	36%	14%	0%	0%	-1.711
13 a_1	0%	49%	0%	0%	0%	6%	0%	29%	0%	0%	0%	-2.100
10 e_θ	0%	0%	0%	27%	0%	0%	45%	0%	0%	0%	24%	-3.658
10 e_ε	0%	0%	0%	0%	27%	0%	45%	0%	0%	0%	24%	-3.658
2 b_2	0%	0%	69%	0%	0%	0%	26%	0%	0%	0%	0%	-5.633
9 e_θ	0%	0%	0%	0%	0%	0%	53%	7%	22%	0%	0%	-6.529
9 e_ε	0%	0%	0%	0%	0%	0%	53%	7%	22%	0%	0%	-6.529
8 e_θ	0%	0%	0%	28%	0%	0%	45%	0%	16%	0%	0%	-6.593
8 e_ε	0%	0%	0%	0%	28%	0%	45%	0%	16%	0%	0%	-6.593

Table 2. Orbital contributions to the MO's of the nitroprusside ground state

In Table 2 we also see that the Lowest Unoccupied Molecular Orbital (LUMO) : 10e, is a π^* antibonding combination between the iron d_{xz}, d_{yz} AOs and the nitrosyl π^* orbitals. The largest amplitude of this molecular orbital is on the p_x and p_y atomic orbitals of the nitrogen atom of the NO group. This is in agreement with previous DFT calculations[29]. The energy of the 10e π^* orbital lies between the d-π^* and the d-σ^* metallic orbitals. The degenerate 8e orbital, consisting primarily of the metal d_{xz}, d_{yz} and the π^* orbitals of the NO ligand, is bonding with respect to the Fe and N atoms and is antibonding between N and O. This electronic situation corresponds to the usual π-back bonding model used in describing the bonding of NO^+ or CO with transition metals.

This electronic structure is generally observed for nitrosyl compounds[36] and is the reason for their interesting properties.

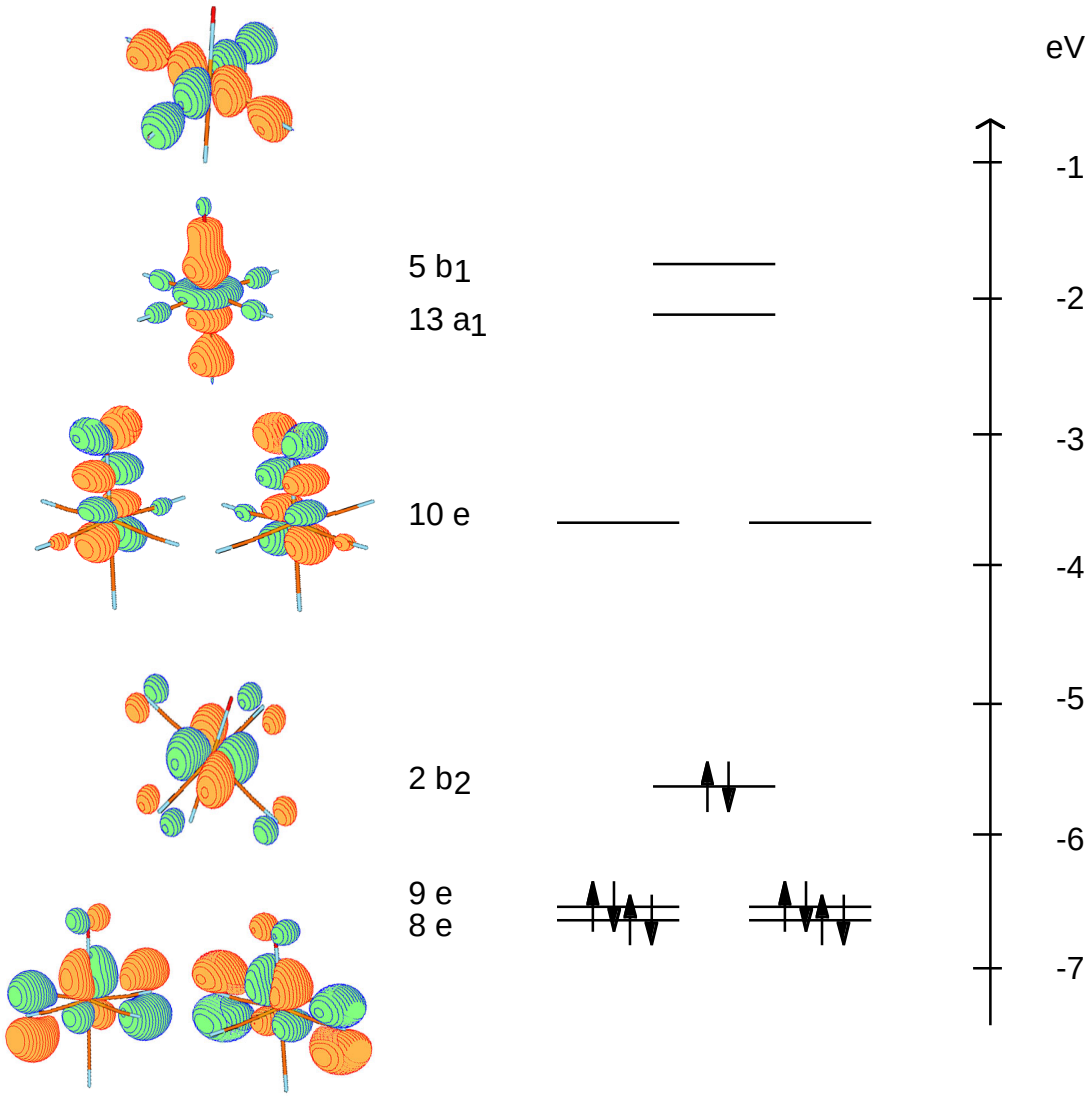

Figure 1. Frontier molecular orbitals of $[Fe(CN)_5NO]^{2-}$ in its ground state geometry

			ΔSCF (GGA)	TDDFT(GGA)	TDDFT(LB94)	exp.[3]
$2\ b_2 \rightarrow 10\ e$	MLCT	^1E	18601	17341	15431	20080
		^3E	16923	14661	12628	
$2\ b_2 \rightarrow 13\ a_1$	MC	$^1B_2$	32658	32098	31635	
		$^3B_2$	26105	26260	26006	
$2\ b_2 \rightarrow 5\ b_1$	MC	$^1A_2$	29740	32654	31785	30300
		$^3A_2$	25359	29320	28562	
$9\ e \rightarrow 10\ e$	LC	$^1A_1$	29738	23733	21465	
		$^3A_1$	22496	22690	19430	
		$^1A_2$	27599	22942	19999	
		$^3A_2$	26003	22918	19967	
		$^1B_1$	29738	23313	20722	
		$^3B_1$	22496	22804	19437	
		$^1B_2$	27599	23043	20175	
		$^3B_2$	26003	22917	19664	
$8\ e \rightarrow 10\ e$	MLCT	$^1A_1$	30151	29235	27136	25380
		$^3A_1$	29603	17790	16144	
		$^1A_2$	30512	23617	22225	
		$^3A_2$	30429	23616	22223	
		$^1B_1$	30151	25231	23636	
		$^3B_1$	29603	21398	20208	
		$^1B_2$	30512	25014	23465	
		$^3B_2$	30429	21452	20304	
$9\ e \rightarrow 13\ a_1$	LMCT	^1E	37494	36281	35248	
		^3E	35686	34548	33431	
$9\ e \rightarrow 5\ b_1$	LMCT	^1E	53288	39980	39327	
		^3E	51954	37911	35816	
$8\ e \rightarrow 13\ a_1$	MC	^1E	40417	36843	37340	37800
		^3E	39025	35354	35530	
$8\ e \rightarrow 5\ b_1$	MC	^1E	44131	41099	40574	42000
		^3E	42276	38417	38043	

Table 3. Lowest excitation energies of the $[Fe(CN)_5NO]^{2-}$. (values in cm^{-1})

5.3.1.2 Excited states in the GS geometry

Calculations of the excited states energies of the nitroprusside ion have been done either in the time-dependent or time-independent framework. For the lowest excitation, arising from the promotion of one electron of the HOMO to the LUMO, the calculation of the transition energy is best carried out with the ΔSCF method as described in the chapter 3 of this thesis. In this case, i.e. the transition is of MLCT type, TDDFT underestimates largely the excitation energy. The same behavior of TDDFT has been found for the lowest MLCT states of the $[Ru(bpy)_3]^{2+}$ (see chapter 4). For states which are higher in energy and for which we have experimental transition energies, the TDDFT method gives results in slightly better agreement with experience.

Long-living metastable states of SNP have been observed when the molecule is excited below 150K by the green radiation of the argon ion laser at 514.4nm ($19436cm^{-1}$)[7]. The wavelength dependance of the formation of the metastable states indicates that this state is a relaxed byproduct of the charge-transfer transition 3d $\rightarrow \pi^*$ (NO). Those experimental evidences combined with the results of our calculation of the electronic structure and of the transition energies in the $[Fe(CN)_5NO]^{2-}$ indicate clearly that the metastable states occur after the excitation of one electron from the $2b_2$ (Fe : d_{xy}) orbital to the 10e (NO : π^*) orbital. The resulting state, $|9e^4\ 2b_2^1\ 10e^1\ ;^1E\rangle$, is Jahn-Teller, or pseudo Rehner-Teller active, i.e. considering only the Fe-N-O part. This state will then be split as a consequence, giving rise to two non-degenerate states.

Pressprich et al.[20] have predicted the higher-energy state to have a linear Fe-N-O geometry and the lower-energy state a bent Fe-N-O geometry. The symmetry of both excited states are thus C_s. We computed the energy of both states resulting from this excited configuration in C_s symmetry, i.e. $|12a''^1\ 26a'^1\ ;^1A''\rangle$ and $|12a''^1\ 13a''^1\ ;^1A'\rangle$. Note that the HOMO $2b_2$ orbital in the ground state geometry (C_{4v}) becomes a'' (12) in Cs symmetry, whereas the LUMO 10e orbital splits into a' (26) and a'' (13). We let the geometry of the excited states relax and obtained thus the geometries as given in Table 4 and 5. As predicted by Pressprich et al., the structure bent is more stable than the other one. The calculated energy difference is 0.2614 eV ($2108\ cm^{-1}$).

$\|^1A''\rangle$	excited / LDA	excited / GGA	GS / LDA	GS / GGA
Fe-N	1.790	1.837	1.616	1.642
N-O	1.180	1.191	1.159	1.170
Fe-N-O	141.1	141.5	180.0	180.0

Table 4. Geometry of the $|^1A''\rangle$ excited state (bond lengths in Å, angles in °)

$\|^1A'\rangle$	excited / LDA	excited / GGA	GS /LDA	GS / GGA
Fe-N	1.792	1.848	1.616	1.642
N-O	1.185	1.195	1.159	1.170
Fe-N-O	177.3	177.3	180.0	180.0

Table 5. Geometry of the $|^1A'\rangle$ excited state (bond lengths in Å, angles in °)

Fig. 2 gives a better picture of both size and extent of the Jahn-Teller stabilization energy for the excited $|12a''^1\ 26a'^1\ ;1A''\rangle$ state. The figure represents the energy of the excited state with respect to the Fe-N-O angle. This angle has been kept fixed at different values between 180° and 120°, but the rest of the molecule, the $Fe(CN)_5$ part, was free to relax for each step.

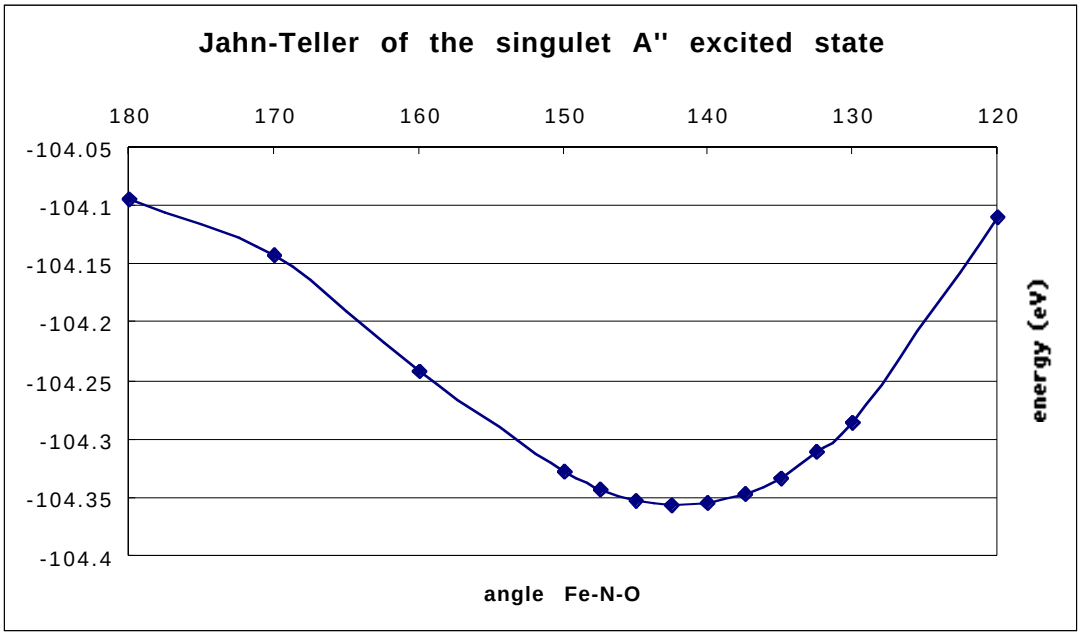

Figure 2. Jahn-Teller stabilization for the excited $|12a''^1\ 26a'^1\ ;1A''\rangle$ state

We then computed the Jahn-Teller stabilization energy (E_{JT}) of the $^1A''$ excited state using the methodology described in the paper of Daul et al[37]. We obtained the value E_{JT}=0.3273 eV (2640 cm^{-1}).

5.3.2 Metastable states

5.3.2.1 Geometry and electronic structure of the metastable states

Nitrosyl compounds are known for the existence of metastable states. This property has been discovered in 1977 in the case of nitroprusside[7]. The geometries of both metastable states have been analysed by X-ray diffraction technique at 50K by Carducci et al[21]. As shown by previous theoretical studies[10, 29], the two metastable states of the nitroprusside correspond to two minima on the ground state potential energy surface (PES).

The nitroprusside ground state has C_{4v} symmetry with Fe-N-O atoms aligned. A rotation of the nitrosyl group leads to a first metastable state with C_s symmetry (cf. Fig. 3), where the Fe-N-O angle is approximately 80°. This metastable state, with C_s symmetry and NO bound sideways (η^2), is generally labeled as MS_{II} in the litterature. Carrying on the rotation we obtain a second metastable state, generally labeled as MS_I, where the NO is O bound and the Fe-O-N part aligned. This 2nd metastable state, generally labeled as MS_I, has also C_{4v} symmetry. The ground state and the two metastable states of nitroprusside are depicted in Fig. 3.

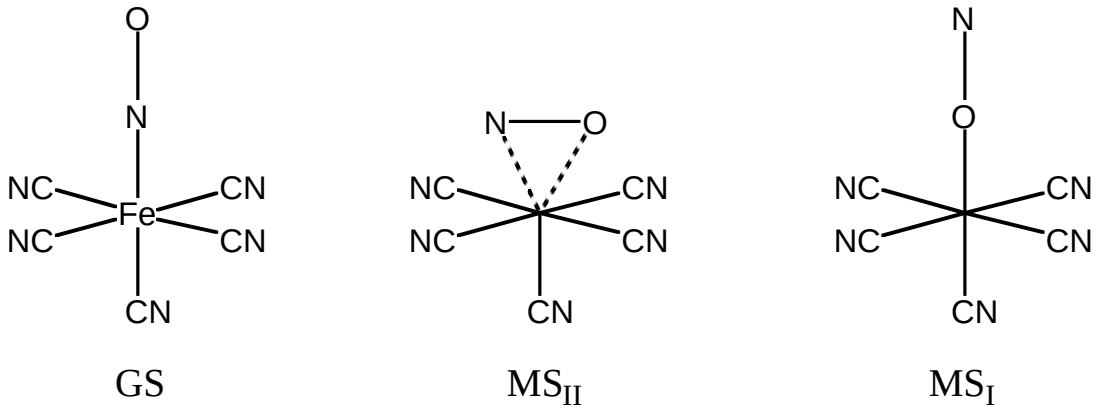

Figure 3. Ground state and metastable states of the nitroprusside ion

The optimized structural parameters compared to the experimental one are given in Table 6 and 7 for both metastable states.

MS_I	LDA (VWN)	GGA (B88P86)	Exp.[21]
Fe-O	1.697	1.731	1.715(5)
O-N	1.151	1.163	1.140(7)
Fe-C_{ax}	1.875	1.921	1.926(6)
Fe-C_{eq}	1.906	1.960	1.940/1.947(4)
C_{ax}-N_{ax}	1.166	1.172	1.149(7)
C_{eq}-N_{eq}	1.168	1.175	1.154/1.161(4)
Fe-C_{ax}-N_{ax}	180.0	180.0	179.3(4)
Fe-C_{eq}-N_{eq}	175.2	175.5	178.6/176.6(3)
Fe-O-N	180.0	180.0	174.9(4)
O-Fe-C_{ax}	180.0	180.0	177.1(3)
O-Fe-C_{eq}	94.3	93.6	93.0/97.0(2)
C_{eq}-Fe-C_{eq} (trans)	171.3	172.9	170.0(3)
C_{eq}-Fe-C_{eq} (cis)	89.7	89.8	90.1(2)/88.5(1)

Table 6. Most relevant structural parameters of the MS_I of $[Fe(CN)_5NO]^{2-}$ (bond length in Å, angle in °)

MS_{II}	LDA (VWN)	GGA (B88P86)	Exp.[21]
Fe-N	1.794	1.834	1.893(19)
Fe-O	1.989	2.057	2.067(15)
N-O	1.204	1.210	1.14(2)
Fe-C_{ax}	1.871	1.917	1.820(13)
Fe-N-O	80.5	82.2	82.0(13)
N-Fe-C_{ax}	155.6	155.3	158.7(6)

Table 7. Most relevant structural parameters of the MS_{II} of $[Fe(CN)_5NO]^{2-}$ (bond length in Å, angle in °)

In the case of the metastable state MS_I with C_{4v} symmetry, where the oxygen atom is bound to the iron atom, we obtain a good agreement between the experimental and the calculated structure. For bond lengths, the averaged deviation is 1.75pm in the case of the LDA optimization, with a maximum of 2.3% of error. In the case of the GGA optimization, the mean deviation drops to 1.05pm, with a maximum error of 1.4%.
Turning to the metastable state MS_{II} with C_s symmetry, the mean deviation between optimized and experimental bond lengths is 5.63pm when using the LDA fonctional, with a maximum of 4.2% of error. Within the GGA approximation, the arithmetical average of the deviation is 4.48pm, with a maximal error of 4.6%. The angle Fe-N-O is 80.53° (LDA) or 82.22° (GGA), which is in very good agreement with the experimental value of 82.0° (cf. Table 7).
The complete composition and the energies of the frontier orbitals of both MS_I and MS_{II} can be found in Tables 8 and 9 respectively. The HOMO for MS_I is the $2b_2$ orbital with the major contribution from the d_{xy} atomic orbital of the iron atom. As in the ground state, the z-axis coincides with C_4 axis and the x and y axis are both in the direction of the CN groups.

	d_{x2-y2}	d_{z2}	d_{xy}	d_{xz}	d_{yz}	N(s)	N(p)	C(s)	C(p)	O(s)	O(p)	eV
5 $b_1(0)$	46%	0%	0%	0%	0%	0%	0%	36%	14%	0%	0%	-1.60
13 $a_1(0)$	0%	54%	0%	0%	0%	0%	0%	26%	0%	0%	0%	-2.38
10 $e_\theta(0)$	0%	0%	0%	25%	0%	0%	47%	0%	0%	0%	26%	-4.46
10 $e_\varepsilon(0)$	0%	0%	0%	0%	25%	0%	47%	0%	0%	0%	26%	-4.46
2 $b_2(2)$	0%	0%	70%	0%	0%	0%	26%	0%	0%	0%	0%	-5.54
9 $e_\theta(2)$	0%	0%	0%	41%	0%	0%	45%	0%	6%	0%	0%	-6.30
9 $e_\varepsilon(2)$	0%	0%	0%	0%	41%	0%	45%	0%	6%	0%	0%	-6.30
8 $e_\theta(2)$	0%	0%	0%	0%	0%	0%	55%	8%	24%	0%	0%	-6.55
8 $e_\varepsilon(2)$	0%	0%	0%	0%	0%	0%	55%	8%	24%	0%	0%	-6.55

Table 8. Population and energy of the frontier MO's of MS_I nitroprusside (occupations in brackets)

The MS_{II} state has only C_s symmetry as can be seen in Fig. 3. In this respect, the labels of the orbitals are a' and a''. Descenting from C_{4v} to C_s symmetry, the HOMO: $2b_2$ for the

ground state becomes 12a''. The major atomic orbital contribution of the 12a'' stems from the d_{xy} orbital of iron, as it is also the case for the HOMO of the ground state and of MS_I.

	d_{x2-y2}	d_{z2}	d_{xy}	d_{xz}	D_{yz}	N(s)	N(p)	C(s)	C(p)	O(s)	O(p)	eV
28a'(0)	44%	0%	0%	0%	0%	0%	0%	0%	28%	0%	0%	-1.69
27a'(0)	0%	32%	7%	0%	7%	0%	14%	24%	0%	0%	0%	-1.82
26a'(0)	0%	12%	0%	0%	28%	0%	17%	0%	0%	0%	21%	-3.51
13a''(0)	0%	0%	9%	8%	0%	0%	56%	0%	0%	0%	26%	-4.24
12a''(2)	0%	0%	39%	32%	0%	0%	17%	0%	0%	0%	9%	-5.47
11a''(2)	0%	0%	20%	32%	0%	0%	27%	0%	0%	0%	9%	-5.87
25a'(2)	0%	0%	0%	0%	0%	0%	55%	0%	10%	0%	0%	-6.21
10a''(2)	0%	0%	0%	0%	0%	0%	54%	10%	19%	0%	0%	-6.49
9a''(2)	0%	0%	0%	0%	0%	0%	64%	0%	32%	0%	0%	-6.68
24a'(2)	0%	0%	0%	0%	15%	0%	44%	0%	17%	0%	9%	-6.74

Table 9. Population and energy of the frontier MO's of MS_{II} nitroprusside (occupations in brackets)

Both metastable states have a ^1A closed shell. Thus, they both lie on the potential energy surface of the nitroprusside ground state. In Fig. 4 the potential energy curve which connects the three minima (the ground state and the two metastable states) is depicted. The angle on the x-axis corresponds to the difference between 180° and the value of the Fe-N-O angle.

Relative energies between the ground state MS_I and MS_{II} have been calculated to be 1.608eV and 1.421eV, respectively. In a previous paper, Delley[29] has calculated the same relative energies to be 1.677eV and 1.368eV. The small difference between those two results from the nature of the functional and from the basis sets used for the calculation. Experimentally, it was found that these energies are 1.1eV and 1.0eV[22] respectively.

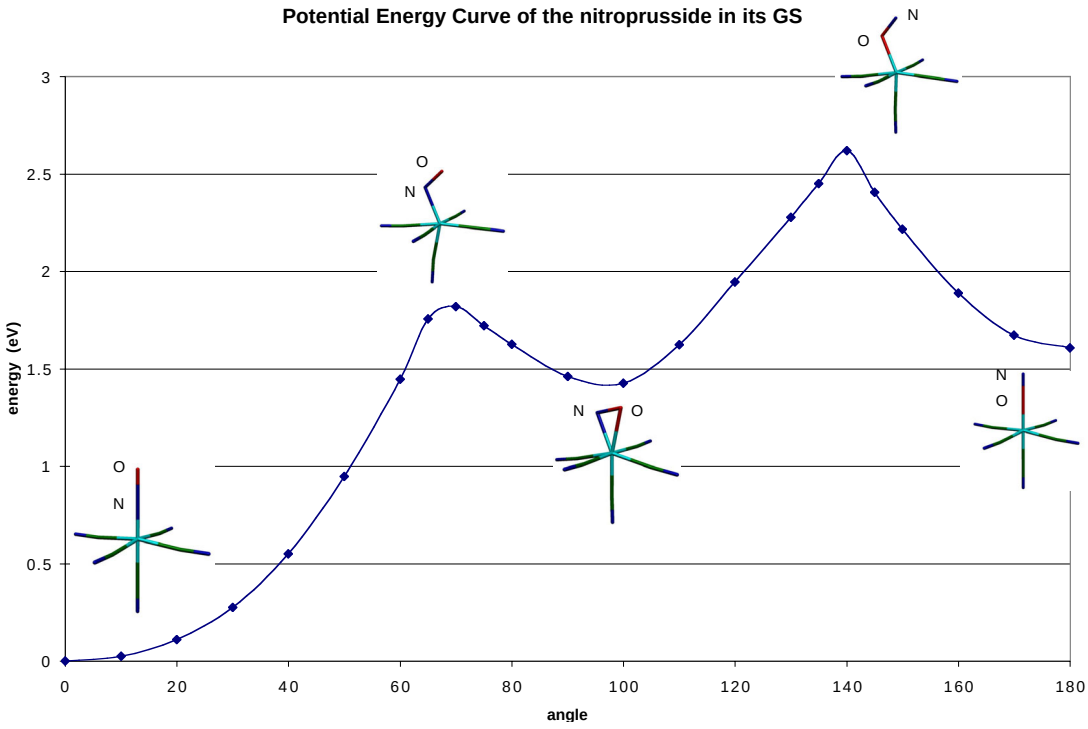

Figure 4. Potential energy curve of the nitroprusside ion in its ground state

The experimental activation energies are also known[23]. E_{a1}, the activation energy for MS_I to return to MS_{II} is 0.7eV, and E_{a2}, the activation energy for MS_{II} to go back to the ground state is 0.5eV. In our calculation, we obtain 1.19eV and 0.39eV for E_{a1} and E_{a2}, respectively.

Comparing Fig. 4 and Fig. 5, the main contribution to the stability is due to the interactions of the nitrosyl π^* orbitals with the occupied d_{yz} orbital of iron. The overlap between the π^* orbitals of NO and the d_{yz} orbital of the iron has a maximum for an Fe-N-O angle of 180°, 0° and ca 90°. This is respectively the case for the ground state, MS_I and MS_{II}.

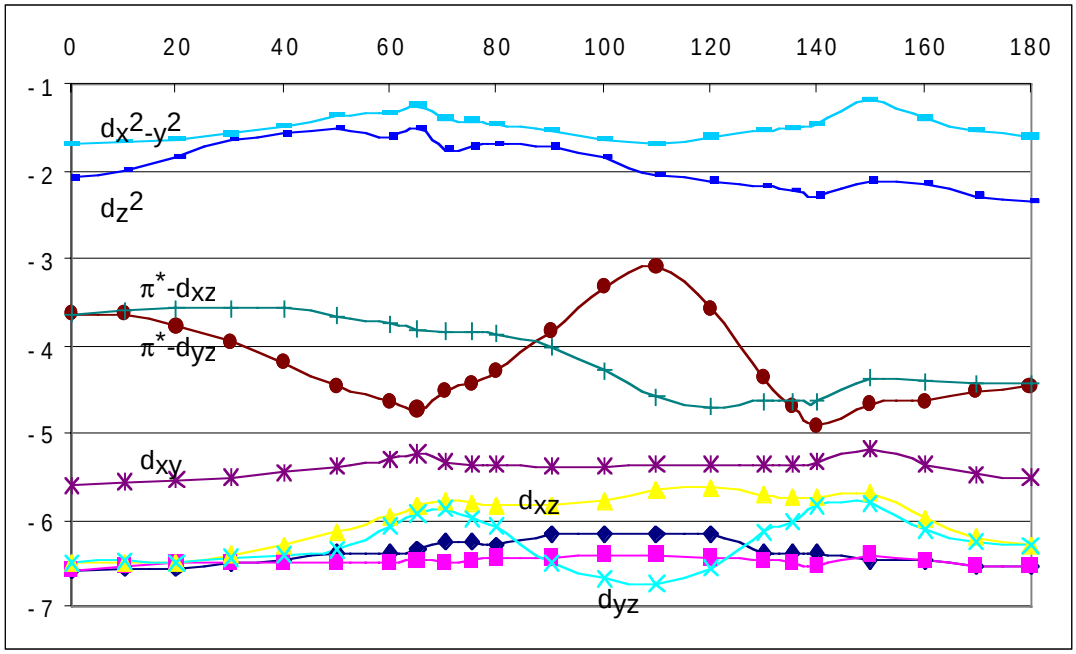

Figure 5. Frontier molecular orbitals along the Fe-N-O angle (energy in eV along the y-axis)

The angle on the x-axis of Fig. 5 corresponds to the difference between 180° and the value of the Fe-N-O angle, as it is also in Fig. 4.

5.3.2.2 Excited states of MS_I

As mentioned in the introduction, nitroprusside has attracted the interest of many researchers as potential candidate for functional material in memory devices in which information can be optically written, read and erased. Chemically speaking, the information is written when an external stimulation induces a structural transition. We have already seen previously in this work how the molecule can transit from the ground state to the MS_{II} state. The lowest electronic excitation of the molecule in the ground state gives rise to a Jahn-Teller active excited state. As a result of the Jahn-Teller distortion, the nitrosyl group will bent. Electronic relaxation of this bent excited state will then populate MS_{II}. The electronic structure of MS_I is very close to the one of the ground state

as can be seen in Fig. 5 and in Table 8. The major difference is the splitting between the HOMO ($2b_2$) and the LUMO (10e), a splitting which is smaller in MS_I than in the ground state. The consequence of this smaller splitting is that the lowest electronic transition will appear in a much lower energy.

		ΔSCF (GGA)	TDDFT (LB94)
$2b_2 \rightarrow 10e$	^1E	10377	8322
	^3E	9057	5843

Table 10. Lowest excited state energy of MS_I (energies in cm^{-1})

This can be seen in Table 10, where the excitation energy of MS_I is given in cm^{-1}. As it was the case for other MLCT transitions in our work, TDDFT values are much lower in energy than ΔSCF values. Until now, those kind of transitions were best described using the ΔSCF method. However, experimental values are not known. The only experimental parameter we know is that irradiation with light in the range 600-1200nm ($8333cm^{-1}$-$16667cm^{-1}$) depopulates MS_I[21].

As it was also the case for nitroprusside in its ground state geometry, the $|9e^4\ 2b_2^1\ 10e^1\ ;^1E\rangle$ excited state of MS_I is Jahn-Teller active. The π*-NO levels will also split by a Jahn-Teller distortion, giving rise to two states with lower symmetry, $^1A'$ and $^1A''$. The excited state $|12a''^1\ 26a'^1\ ;^1A''\rangle$ is the most stable of the two. Due to the Jahn-Teller distortion, its geometry is quite different from MS_I as can be seen in Table 11. The FeON angle deviates from linearity and becomes bent.

	$\|12a''^1\ 26a'^1\ ;^1A''\rangle$	$\|9e^4\ 2b_2^2\ ;^1A_1\rangle$ (MS_I)
Fe-O	2.025	1.731
O-N	1.190	1.163
Fe-O-N	139.8	180.0

Table 11. Geometry of the $|^1A''\rangle$ excited state arrising from MS_I (bond lengths in Å, angles in °)

We computed the Jahn-Teller stabilization energy (E_{JT}) of the excited $^1A''$ state using the same methodology as previously. We obtained the value E_{JT}=0.1445eV ($1165cm^{-1}$).

The Fe-O bond length becomes longer in this excited state (^{1}A'') since the antibonding π*NO-dyz orbital is populated. With an Fe-O-N angle around 140°, the excited ^{1}A'' state has a geometry very close to the geometry of the transition state between MS_I and MS_{II} (see Fig. 4). By relaxing electronically, ^{1}A'' should drop on the ground state potential energy curve around the transition state and then populates MS_{II}. This corresponds to the first step of the erasure mechanism.

5.3.2.3 Excited states of MS_{II}

We have already seen how nitroprusside can change from the ground state to MS_{II}, through an excited state. In the same way, we have seen how nitroprusside can pass from MS_I to MS_{II}, again through its excited state. To complete this work, we need to investigate its transition from MS_{II} either to MS_I or either how it returns to the ground state. To understand this, we need to study the excited states of MS_{II}. Experimentally[21] it is known that irradiation with visible light (350-600nm) converts MS_{II} to MS_I, as it allows the ground state to convert to MS_{II}. The photoreaction of MS_{II} to the ground state needs an irradiation with light in the range of 600-1200nm, as it is also the case for the transition from MS_I to MS_{II}.

The electronic structure of MS_{II} can be seen from inspection of Table 9 and in Fig. 5. To see this it is necessary to take a value of 100° on the x-axis (equivalent to an angle Fe-N-O of 80°).

		ΔSCF (GGA)	TDDFT (LB94)
12 a'' → 13 a''	^{1}A'	11033	8691
	^{3}A'	10626	6128
11 a'' → 13 a''	^{1}A'	14170	16819
	^{3}A'	11459	6778
12 a'' → 26 a'	^{1}A''	15933	16325
	^{3}A''	12568	12776
25 a' → 13 a''	^{1}A''	19228	13406
	^{3}A''	16984	12452
10 a'' → 13 a''	^{1}A'	23030	14355
	^{3}A'	22738	13468

Table 12. Lowest electronic transitions of MS_{II} metastable state (value in cm^{-1})

According to Table 12, we see that the promotion of one electron out of the HOMO 12 a'' into the 26 a' orbital occurs at approximately 16000 cm^{-1}. According to Fig. 5, the orbital 26 a' is the orbital labeled π^* :d_{yz}. It is the orbital that undergoes the biggest changes when rotating the nitrosyl part. We let relax the geometry of the excited $|12a''^1\ 26a'^1\ ;^1A''\rangle$ state. The geometry given in Table 13 is thus obtained.

	$\|12a''^1\ 26a'^1\ ;^1A''\rangle$	$\|12a''^2\ ;MS_{II}\rangle$	$\|2b_2^2\ ;GS\rangle$
Fe-N	1.836	1.834	1.642
N-O	1.191	1.210	1.170
Fe-N-O	141.7	82.2	180.0

Table 13. Geometry obtained, after relaxation, of the excited $|12a''^1\ 26a'^1\ ;^1A''\rangle$ state arising after excitation from MS_{II} (bond lengths in Å, angle in °)

Comparison with the geometry of MS_{II} indicates that the major change in the geometry of the excited $|12a''^1\ 26a'^1\ ;^1A''\rangle$ state is the variation of the Fe-N-O angle. In MS_{II} the nitrosyl is bound sideways (η^2) whereas in the excited $|12a''^1\ 26a'^1\ ;^1A''\rangle$ state the nitrosyl is N bound. Hence the ring has opened.

As a consequence $|12a''^{1}\ 26a'^{1};^{1}A''\rangle$ will relax electronically and fall onto the ground state potential energy curve depicted in Fig. 4. $|^{1}A''\rangle$ will fall near the transition state between the ground state and MS_{II}. It will then populate both the ground state and MS_{II}.
When looking at Table 4, we notice another excited $|^{1}A''\rangle$ state which originates from the geometry relaxation of the excited $|^{1}E\rangle$ state to the ground state. This $|^{1}A''\rangle$ arising from the ground state has the same geometry than $|^{1}A''\rangle$ arising from MS_{II}. They have also the same occupation and are nothing but an unique state.
The photochemical pathway from the ground state to MS_{II} passes through this excited $|^{1}A''\rangle$ state. The reverse photochemical pathway from MS_{II} to the ground state goes also through the same excited $|^{1}A''\rangle$ state. The difference between both photochemical reactions is the irradiation energy needed. It has been found experimentally[21] that irradiation with light in the range of 350-600 nm (16668-28571 cm^{-1}) will excite the ground state and populate fractionally MS_{II}. This is in agreement with the excitation energy we obtain for the $|2b_2^{2};^{1}A_1\rangle \rightarrow |2b_2^{1}\ 10e^{1};^{1}E\rangle$ transition i.e. 18601 cm^{-1} (cf. Table 3). Irradiation with light in the range of 600-1200 nm (8333-16667 cm^{-1}) will excite MS_{II} and then repopulate the ground state. This is also in agreement with the excitation energy we get for the $|12a''^{2};^{1}A'\rangle \rightarrow |12a''^{1}\ 26a'^{1};^{1}A''\rangle$ transition in MS_{II} of 15933 cm^{-1} (cf. Table 12).
The last open question to complete the whole scheme is the photochemical reaction from MS_{II} to MS_{I}. When looking at the diagram on Fig. 5, it seems that the explanation should also involve the π^*NO-d_{yz} orbital (26 a'). This orbital 26 a' has maximal energy for an Fe-N-O angle of around 70°. This Fe-N-O angle is so close to the one of the MS_{II} metastable state that the excited $|12a''^{1}\ 26a'^{1};^{1}A''\rangle$ state could also relax, at least to a small extent, towards MS_{I}. It is known experimentally that MS_{I} cannot be directly populated from the ground state, because no plateau could be measured[19]. All excited molecules are relaxing from the π^*NO-d_{yz} orbital into MS_{II} and from there are transferred into MS_{I} with the same excitation wavelength (350-600 nm). This is in agreement with our finding and with the profile of the correlation diagram of π^*NO-d_{yz} as can be seen in Fig. 5.
Irradiation of the ground state with light of appropriate energy will generate an excited state with an electron in the π^*NO-d_{yz} orbital. This excited state can immediately decay to the ground state or be geometrically distorted and form MS_{II}. This excited state cannot

directly populate MS_I because of the behavior of the Kohn-Sham eigenvalue of $\pi^*NO\text{-}d_{yz}$ orbital as a function of the maximal Fe-N-O angle (around 70-80°). At this point, where the geometry is very near to MS_{II}, a second excitation is needed in order to populate MS_I. This excitation correponds also to the promotion of one electron out of the HOMO into the $\pi^*NO\text{-}d_{yz}$ (26 a') orbital. In Table 12, this excitation energy has been calculated to occur at around 15933 cm^{-1} using the ΔSCF/GGA method. This value is very close to the experimental one : 600nm which is at the limit between the irradiation wavelength needed to go from the ground state to MS_I and the irradiation wavelength needed for the reverse reaction. Moreover, this value of 15933 cm^{-1} does not take into account the population of a higher vibrational level, or a slight distortion of the molecular surrounding of MS_{II}, a distortion that is plausible with regard to the broad character of the d_{yz} orbital around this point as can be seen in Fig. 5.

Within our model, we believe that the same electronic transition is responsible for the population of the ground state and of MS_I from MS_{II}. $|12a''^1\ 26a'^1\ ;^1A''\rangle$ (MS_{II}*) will relax, with different quantum yields, either to the ground state or to MS_I.

5.4 Conclusion

In this work, we did demonstrate the ability of Density Functional Theory not only to reproduce well experimental findings, but also to enable the understanding of chemical problems. Since the experimental work of Carducci et al[21] and the theoretical one of Delley et al[29], many details on the nature of nitroprusside ground state and metastable states were known. However, a clear picture of the reaction pathways between the three minima on the ground state potential energy curve was still missing. This is probably due to a lack, or default, of data for the excited states of the $[Fe(CN)_5NO]^{2-}$ ion. The use of femtosecond spectroscopy to investigate the photophysics and photochemistry of nitroprusside would certainly be of great help in this respect.

In our work we have first determined and analysed the three minima on the ground state potential energy curve : the ground state and the two metastable states. In this respect our results are in good agreement with the experimental findings and with previous theoretical studies. As a second part of the work, we studied the excited states of

nitroprusside. We are here also in agreement with data available for the excited states of nitroprusside in its ground state structure. No, or very view data however were available concerning excited states of nitroprusside in its metastable states. By analysing the electronic structure and the excited states of both metastable states of the nitroprusside ion, we could setup a model explaining the photochemistry and photophysics responsible for the population of the three different states on the ground state potential energy curve.

Our model is in good agreement with experimental findings. The ground state and the two metastable states of nitroprusside are all three states of ^{1}A symmetry. In this respect they all belong to the same ground state potential energy curve. They have the same electronic configuration, with the d_{xy} orbital of the iron being the HOMO. Depending on the symmetry, C_{4v} in the case of the ground state and MS_I and C_s for MS_{II}, this orbital transforms as b_2 or a'' respectively.

The major contribution to the total energy of nitroprusside along the reaction path from GS to MS_I and MS_{II} is due to the overlap between the π*NO-d_{yz} and the d_{yz} orbital of the iron. When the overlap is big, the splitting between both orbitals is important, the Kohn-Sham eigenvalue of the d_{yz} orbital is low and the configuration has then a minimum energy. This is the π-backbonding principle.

Photochemical pathways between the three different states involve always the electronic occupation of the π*NO-d_{yz} orbital. Depending on the HOMO-LUMO gap, the energy needed to promote one electron into this π*NO orbital is more or less important. For MS_I this splitting is smaller than that of the ground state and this is the reason why irradiation energy needed to populate the metastable states from the ground state is higher than in the case of the reverse reaction. As can be seen from our work, in MS_{II}, the same transfer of an electron into the π*NO orbital is responsible for the population of either the ground state or MS_I, with different quantum yields. This has never been proposed in previous studies.

Beside to this setup of a photochemical model connecting satisfactorily the ground state and the metastable states of nitroprusside, this work is also the occasion to demonstrate that the computation of excited states remains a challenging task for DFT. Especially, in the case of the lowest transitions, the ΔSCF and the new TDDFT procedures give very different results. For excited states with large transition energies, results coming from the two procedures are in better agreement. The problem with the lowest transitions, where

ΔSCF is in bether agreement with experience, can be a problem of the TDDFT. This method has difficulty to treat states that meet one of the two criteria evidenced by Casida et al. in their work[38]. TDDFT exhibits some « fallen states » where the excitation energy is close to the IP of the molecule or if the transition involves virtual molecular orbitals that are close to the HOMO.

5.5 References

(1) Manoharan, P. T.; Hamilton, W. C., *Inorg. Chem.* **1963**, *2*, 1043.

(2) Stoelting, R. K., *Pharmacology and Physiology in Anesthetic Practice*; ed.; Lippincott-Raven: 1999; pp. 315.

(3) Manoharan, P. T.; Gray, H. B., *J. Am. Chem. Soc.* **1965**, *88*, 3340.

(4) Gray, H. B.; Manoharan, P. T.; Pearlman, J.; Riley, R. F., *Chem. Comm.* **1965**, 62.

(5) Manoharan, P. T.; Gray, H. B., *Inorg. Chem.* **1966**, *5*, 823.

(6) Sweinhart, J. H., *Coord. Chem. Rev.* **1967**, *2*, 385.

(7) Hauser, U.; Oestreich, V.; Rohrweck, H. D., *Z. Phys. A* **1977**, *280*, 125.

(8) Field, C. N.; Green, J. C.; Mayer, M.; Nasluzov, V. A.; Rösch, N.; Siggel, M. R. F., *Inorg. Chem.* **1996**, *35*, 2504.

(9) Li, X.; Tse, J. S.; Bancroft, G. M.; Puddephatt, R. J.; Tan, K. H., *Inorg. Chem.* **1996**, *35*, 2515.

(10) Coppens, P.; Fomitchev, D. V.; Carducci, M. D.; Culp, K., *J. Chem. Soc., Dalton Trans.* **1998**, 865.

(11) Fomitchev, D. V.; Coppens, P.; Li, T.; Bagley, K. A.; Chen, L.; Richter-Addo, G. B., *Chem. Commun.* **1999**, 2013.

(12) Morioka, Y.; Ishikawa, A.; Tomizawa, H.; Miki, E., *J. Chem. Soc., Dalton Trans.* **2000**, 781.

(13) Kawano, M.; Ishikawa, A.; Morioka, Y.; Tomizawa, H.; Miki, E.; Ohashi, Y., *J. Chem. Soc., Dalton Trans.* **2000**, 2425.

(14) Baraldo, L. M.; Bessega, M. S.; Rigotti, G. E.; Olabe, J. A., *Inorg. Chem.* **1994**, *33*, 5890.

(15) Scheidt, R. W.; Duval, H. F.; Neal, T. J.; Ellison, M. K., *J. Am. Chem. Soc.* **2000**, *122*, 4651.

(16) Cheng, L.; Novozhilova, I.; Kim, C.; Kovalevsky, A.; Bagley, K. A.; Coppens, P.; Richter-Addo, G. B., *J. Am. Chem. Soc.* **2000**, *122*, 7142.

(17) Zöllner, H.; Krasser, W.; Woike, T.; Haussühl, S., *Chem. Phys. Lett.* **1989**, *161*, 497.

(18) Rüdlinger, M.; Schefer, J.; Chevrier, G.; Furer, N.; Güdel, H. U.; Haussühl, S.; Heger, G.; Schweiss, P.; Vogt, T.; Woike, T.; Zöllner, H., *Z. Phys. B* **1991**, *83*, 125.

(19) Woike, T.; Krasser, W.; Zöllner, H.; Kirchner, W.; Haussühl, S., *Z. Phys. D* **1993**, *25*, 351.

(20) Pressprich, M. R.; White, M. A.; Vekhter, Y.; Coppens, P., *J. Am. Chem. Soc.* **1994**, *116*, 5233.

(21) Carducci, M. D.; Pressprich, M. R.; Coppens, P., *J. Am. Chem. Soc.* **1997**, *119*, 2669.

(22) Zöllner, H.; Woike, T.; Krasser, W.; Haussühl, S., *Z. Kristallogr.* **1989**, *188*, 139.

(23) Woike, T.; Kirchner, W.; Schetter, G.; Barthel, T.; Kim, H.; Haussühl, S., *Opt. Commun.* **1994**, *106*, 6.

(24) Haussühl, S.; Schetter, G.; Woike, T., *Opt. Commun.* **1995**, *114*, 219.

(25) Güida, J. A.; Piro, O. E.; Aymonino, P. J., *Inorg. Chem.* **1995**, *34*, 4113.

(26) Güdel, H. U., *Chem. Phys. Lett.* **1990**, *175*, 262.

(27) Woike, T.; Kirchner, W.; Kim, H.; Haussühl, S.; Rusanov, V.; Angelov, V.; Ormandjiev, S.; Bonchev, T.; Schroeder, A. N. F., *Hyperfine Interact.* **1993**, *7*, 265.

(28) Terrile, C.; Nascimento, O. R.; Moraes, I. J.; Castellano, E. E.; Piro, O. E.; Güida, J. A.; Aymonino, P. J., *Solid State Commun.* **1990**, *73*, 481.

(29) Delley, B.; Schefer, J.; Woike, T., *J. Chem. Phys.* **1997**, *107*, 10067.

(30) Baerends, E. J.; Bérces, A.; Bo, C.; Boerrigter, P. M.; Cavallo, L.; Deng, L.; Dickson, R. M.; Ellis, D. E.; Fan, L.; Fischer, T. H.; Fonseca Guerra, C.; van Gisbergen, S. J. A.; Groeneveld, J. A.; Gritsenko, O. V.; Harris, F. E.; van den Hoek, P.; Jacobsen, H.; van Kessel, G.; Kootstra, F.; van Lenthe, E.; Osinga, V. P.; Philipsen, P. H. T.; Post, D.; Pye, C.; Ravenek, W.; Ros, P.; Schipper, P. R. T.; Schreckenbach, G.; Snijders, J. G.; Sola, M.; Swerhone, D.; te Velde, G.; Vernooijs, P.; Versluis, L.; Visser, O.; van Wezenbeek, E.; Wiesenekker, G.; Wolff, S. K.; Woo, T. K.; Tiegler, T.,
(31) Fonseca Guerra, C.; Snijders, J. G.; te Velde, G.; Baerends, E. J., *Theor. Chem. Acc.* **1998**, *99*, 391.

(32) Vosko, S. H.; Wilk, L.; Nusair, M., *Can. J. Phys.* **1980**, *58*, 1200.

(33) Becke, A. D., *Phys. Rev. A* **1988**, *38*, 3098.

(34) Perdew, J. P., *Phys. Rev. B* **1986**, *33*, 8822.

(35) van Leeuwen, R.; Baerends, E. J., *Phys. Rev. A* **1994**, *49*, 2421.

(36) Enemark, J. H.; Feltham, R. D., *Coord. Chem. Rev.* **1974**, *13*, 339.

(37) Bruyndonckx, R.; Daul, C.; Manoharan, P. T.; Deiss, E., *Inorg. Chem.* **1997**, *36*, 4251.

(38) Casida, M. E.; Jamorski, C.; Casida, K. C.; Salahub, D. R., *J. Chem. Phys.* **1998**, *108*, 4439.

Chapter 6

A Density Functional Study of Molecules showing Nonlinear Optical Properties : the Sesquifulvalene complexes

6.1 Introduction

Materials with nonlinear optical (NLO) properties are very promising species with potential applications in photonic devices, i.e. for optical data acquisition, storage, transmission and processing of data. Nonlinear optics involves the study of phenomena caused by the interaction of anisotropic materials with nearly monochromatic, polarized, electromagnetic radiation, such as light produced by high-power lasers[1]. For this reason, research in nonlinear optics started really with the development of the lasers, in the sixties. However, the « nonlinear » effect, i.e. that certain materials become doubly refracting when placed in regions of strong fields, was already discovered in 1875 by John Kerr[2].

Linear optical properties give rise to such familiar phenomena as refraction, light-scattering and absorption. The most prominent NLO features are frequency doubling or event tripling, i.e. second and third harmonic generation (SHG and THG) of incident light, and the linear electro-optical effect (Pockels-effect) which describes the change of refractive index of matter as a function of the strength of an applied external electric field[3]. Our interest, due to a collaboration with Jürgen Heck's synthetic group, is focused on the study of organometallic molecules suitable for SHG characterized by a large first hyperpolarizability tensor β.

With a few exceptions[4], the majority of organic compounds exhibiting large SHG efficiencies are polarizable dipolar molecules with a π-conjugated electron-donor-acceptor arrangement. In this respect, sesquifulvalene molecule and its derivatives should be good NLO candidates. And, indeed, substantial first molecular hyperpolarizabilities β have been predicted for sesquifulvalene derivatives based on theoretical calculations[5].

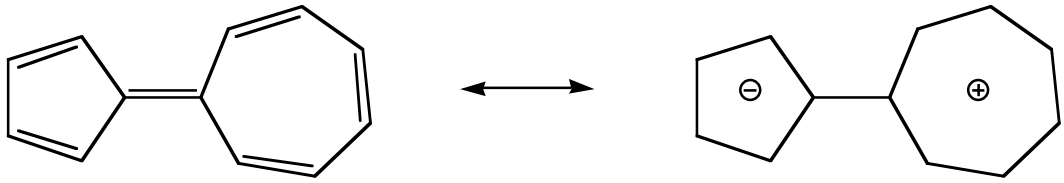

Figure 1. Canonical presentations for sesquifulvalene

Unfortunately, the sesquifulvalene molecule is instable[6]. Therefore no experimental studies of the nonlinear optical properties of sesquifulvalene or relative organic derivatives could be undertaken. In contrast, the sesquifulvalene moiety is stabilized if complexed with a transition metal ion[7, 8]. The resulting complexes are currently the subject of considerable attention in the field of nonlinear optics[9, 10].

Heck and coworkers have synthesised and studied a large number of those mono- and dinuclear sesquifulvalene complexes[3, 8, 11]. Some of them exhibit first molecular hyperpolarizabilities that are among the highest values ever measured for organometallic complexes.

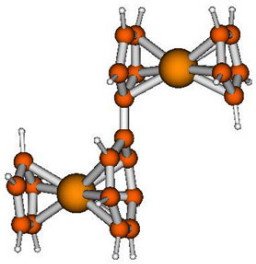

Figure 2. Exemple of dinuclear sesquifulvalene compexe

In this work, we used, in collaboration with professor Heck's group in Hamburg, a computational chemistry approach to predict second-order NLO. Thus, using time-dependent density functional theory (TDDFT), we did obtain good results for molecule of the family of para-nitroaniline. In a second part, we extended our work to the computation of NLO properties of dipolar bimetallic sandwich-like complexes, as synthesised by Heck's group. These complexes are composed of sesquifulvalenes and other metal-ligand fragments.

6.2 Computational methods

The Density Functional Theory (DFT) within the Kohn-Sham formalism has been used throughout this work. The ADF[12, 13] program package has been employed in all the calculations. The Vosko, Wilk and Nusair[14] (VWN) functional for exchange and correlation energies was used in the Local Density Approximation (LDA). The nonlocal corrections using the Becke[15] exchange and Perdew[16] correlation (B88P86) have been used in all the gradient corrected calculations (GGA or Generalized Gradients Approximations). We used basis functions present in the program database. All atoms were described by a triple-ζ STO basis set and the core electrons of Fe(1s-2p), Ru(1s-3d), C(1s), H(1s) were kept frozen.

In the time-dependent density functional theory (TDDFT) formalism, the calculations were performed with the RESPONSE module of the ADF program. In this regard, excitation energies and oscillator strengths have been computed using the iterative DAVIDSON method. In TDDFT, either the B88P86 functional or the « asymptotically correct » Van Leeuwen-Baerends potential[17] (LB94) have been used.

6.3 Nonlinear optics

When a beam of light interacts with a material, it induces polarization in that material. In case of linear optics, there is an instantaneous displacement (polarization) of the electron density of an atom by the electric field E of the light wave. This instantaneous displacement of electron density results in charge separation. With small fields, the amount of charge displacement (induced dipole) is proportional to the instantaneous magnitude of the electric field

$$P_M = \mu = \alpha E$$

where α is the linear polarizability of the molecule or of the atom, and P_M stands for molecular polarization.

When we consider matter at a macroscopic scale, the linear polarizabiliy will be replaced by the linear susceptibility χ of a collection of molecules.

$$P = \chi E$$

When a molecule is exposed to a very intense electric field, as it is the case for lasers, a nonlinear response is observed. The nonlinear molecular polarization P_M can then be expressed in the following way

$$P_M = \alpha E + \beta E^2 + \gamma E^3 + \mathrm{K}$$

where β is the first molecular hyperpolarizability (second order effect) and γ is the second molecular hyperpolarizability (third order effect).

On a macroscopic scale, the induced polarization of a material is again given by an analogous expression

$$P = \chi^{(1)} E + \chi^{(2)} E^2 + \chi^{(3)} E^3 + \mathrm{K}$$

where $\chi^{(n)}$ is the nth order NLO susceptibility and is analogous to the molecular coefficients α, β, γ, … (except that with the χ terms, local field effects, which are consequences of the surrounding medium, are also taken into account).

A point which is important to emphasize is that for β (or $\chi^{(2)}$) to be non-zero, the molecules (or material) have to be non-centrosymmetric. This can be explained by the fact that if a field +E is applied to a molecule, then from the equation above, the first nonlinear term will induce a polarization of $+\beta E^2$. If a field of –E is applied, the predicted polarization would still be $+\beta E^2$, but this should be $-\beta E^2$ if the molecules are centrosymmetric. This contradiction can only be rationalized if β=0 in centrosymmetric media.

One of the most interesting NLO feature is frequency doubling, or second harmonic generation (SHG), of incident light. This can be shown mathematically by expressing the electric field E as a plane wave.

$$E = E_0 \cos(\omega t)$$

This wave will induce the following polarization

$$P = \chi^{(1)} E_0 \cos(\omega t) + \chi^{(2)} E_0^2 \cos^2(\omega t) + \chi^{(3)} \cos^3(\omega t) + \mathrm{K}$$

Using the relation that $\cos^2(\omega) = 1/2 + 1/2 \cos(2\omega)$ we obtain

$$P = \frac{1}{2}\chi^{(2)} E_0^2 + \chi^{(1)} E_0 \cos(\omega t) + \frac{1}{2}\chi^{(2)} E_0^2 \cos(2\omega t) + \mathrm{K}$$

Mathematically, β (or $\chi^{(2)}$) is a third-rank tensor with 3^3=27 tensor components. In order to be able to compare with the experimental measurement in solution, the hyperpolarizability β is calculated as[18]

$$\beta_i = \frac{1}{3}\sum_j \left(\beta_{ijj} + \beta_{jji} + \beta_{jij}\right)$$

where i is the orientation of the dipole moment. When the dipole moment is parallel to the z axis, β can be calculated as[19]

$$\beta_z = \beta_{zzz} + \beta_{zxx} + \beta_{zyy}$$

Second order NLO effects can also involve the interaction of two distinct waves with electric fields E_1 and E_2 respectively with the electrons of the NLO materials. The two light beams of frequencies ω_1 and ω_2 interact then with the NLO material and the induced polarization (ω_3) occurs at sum ($\omega_1 + \omega_2$) and difference ($\omega_1 - \omega_2$) frequencies. The different terms for the first hyperpolarizability β are then noted :

$$\beta(-\omega_3;\omega_2,\omega_1)$$

with β(0 ;0,0) the static hyperpolarizability, β(-2ω ; ω,ω) the hyperpolarizability responsible for the second-order generation (SHG), and β(-ω ; ω,0) the hyperpolarizability responsible for the « de Pockels » effect

For more in-depth discussion, please consult references[1. 9. 10. 20].

6.4 Results and discussion

6.4.1 p-nitroaniline

The design of NLO materials is now quite advanced, as over the years, criteria have been discovered that are essential for exhibition of large hyperpolarizabilities. Basic rules are universally accepted and are as follows[9. 10] :

1. polarizable material
2. asymetric charge distribution (incorporation of donor-acceptor molecules)
3. a pathway of π-conjugated electrons
4. non-centro symmetric crystal packing

The good example for a material which presents non-linear optical property is p-nitroaniline. It is an highly polarizable molecule. p-nitroaniline has one site which is

electron rich, centered on the nitrogen atom of the amino group, and one site which is electron poor, centered on the nitrogen of the nitro group. Those two groups are connected by a conjugated π-system.

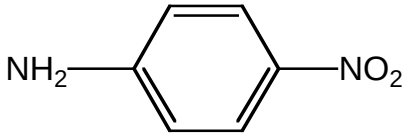

Figure 3. p-nitroaniline

In Table 1 are written the hyperpolarizability responsible for SHG at 1060nm and 1910nm and the static hyperpolarizability for the p-nitroaniline.

	λ [nm]	TDDFT/LB94	HRS[21]	EFISH[22]	EFISH[23]
β(0 ;0,0)	-	13.9	-	-	-
β(-2ω ; ω,ω)	1060	32.7	30 (DMF)	36 (MeOH)	16.9 (dioxane)
β(-2ω ; ω,ω)	1910	17.2	-	-	9.6

Table 1. First hyperpolarizability β of the p-nitroaniline (values are expressed in 10^{-30} esu)

	λ [nm]	LB94	MP2[19]	PPP-CI	CNDO-CI	HF[18]	2Level[24]
β(0 ;0,0)	-	13.9	8.55	-	-	4.37	-
β(-2ω ; ω,ω)	1060	32.7	12.0	15.5[25] 35.3[26]	7.7[23] 12.2[27]	6.20	23.0
β(-2ω ; ω,ω)	1910	17.2	9.6	-	5.7	4.84	5.7

Table 2. First hyperpolarizability β of the p-nitroaniline compared to previous calculations (values are expressed in 10^{-30} esu)

We can see in Table 1 that the value we obtained using the TDDFT/LB94 method and the response theory as implemented in the ADF program package is in good agreement with experimental values for the first hyperpolarizability of the p-nitroaniline.

This method yields better results than previous model, or methods, as can be seen in Table 2.

We then performed the same calculation with several various substituted benzene molecules. Results that can be seen in Table 3 show the trend that we expected.

	λ [nm]	aniline	nitrobenzene	p-nitroaniline	N,N-dimethyl-p-nitroaniline
β(0 ;0,0)	-	1.1	3.4	13.9	23.1
β(-2ω ; ω,ω)	1060	2.6	6.1	32.7	74.6

Table 3. First hyperpolarizability of the p-nitroaniline compared to other substituted benzene molecules (values are expressed in 10^{-30} esu)

For molecules like aniline and nitrobenzene, hyperpolarizabilities are by far lower than for the p-nitroaniline. This can be easily understood by the fact that p-nitroaniline possesses both a donor and an acceptor group and corresponds to the rules for good NLO materials as explained previously. It is also interesting to note that the substitution of the two hydrogenes by two methyl groups in the amino group does multiply by two the hyperpolarizability terms.

Conforted by this good prediction of β values for those small test molecules, we started to study new types of NLO materials that are currently investigated by the group of professor Heck in Hamburg, i.e. organometallic sesquifulvalene bimetallic complexes.

6.4.2 $[Ru_2C_{22}H_{20}]^{2+}$ bimetallic sesquifulvalene complexe

Whereas the study of organic compounds with interesting NLO properties started about 30 years ago with the work of Davydov et al.[28], the introduction of metals into NLO chromophores was first referred by Green et al. in 1987[29]. These results were the motivation for organometallic and coordination chemists to create new NLO chromophores.

As a result of the basic trends of NLO materials that we mentioned earlier, a simplified theoretical approach for calculating the first hyperpolarizability β elucidates the

correlation between the molecular electronic properties and the NLO properties. This so called two-level-approximation[30, 31] suggests that molecules must possess a) excited states close in energy to the ground state, b) large oscillator strengths for electronic transitions from ground to excited states, and c) a large difference between ground and excited state dipole moments. The formulation of this two-level-approximation reads

$$\beta(0) \propto \left(\vec{\mu}_{ee} - \vec{\mu}_{gg}\right)\frac{\vec{\mu}_{ge}^{2}}{E_{ge}^{2}}$$

where $\vec{\mu}_{ee}$ and $\vec{\mu}_{gg}$ are excited and ground-state dipole moments, respectively, $\vec{\mu}_{ge}$ is the transition dipole moment, and E_{ge} is the transition energy.

6.4.2.1 Structural parameters

Taking these rules into considerations, we began the study of the following sesquifulvalene bimetallic complexe : $Ru_2C_{22}H_{20}$. A picture of this complex is drawn in Fig. 4.

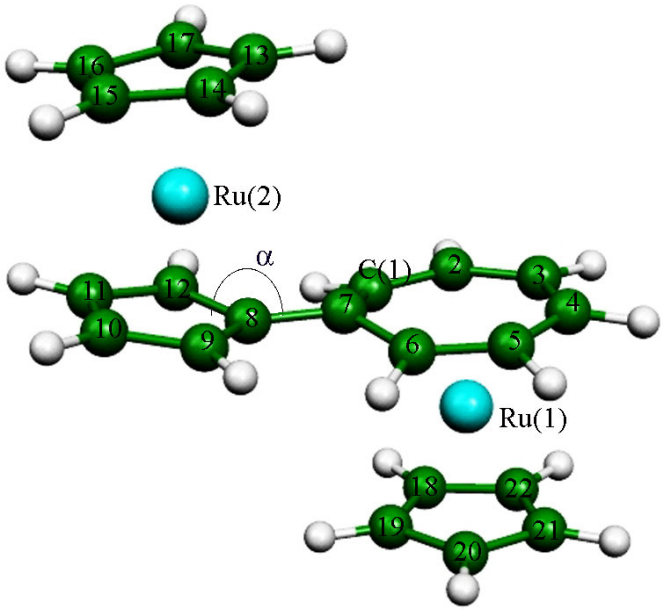

Figure 4. Sesquifulvalene $RuC_{10}H_9$-$RuC_{12}H_{11}$

	Exp.[11]	LDA optimization	GGA optimization
Ru(1)-C(19)	2.184(3)	2.189	2.234
Ru(1)-C(18)	2.184(3)	2.192	2.236
Ru(1)-C(22)	2.186(3)	2.212	2.255
Ru(1)-C(20)	2.192(3)	2.192	2.236
Ru(1)-C(21)	2.198(3)	2.212	2.255
Ru(1)-C(5)	2.226(3)	2.236	2.285
Ru(1)-C(3)	2.233(4)	2.233	2.285
Ru(1)-C(4)	2.234(4)	2.233	2.285
Ru(1)-C(2)	2.247(3)	2.236	2.285
Ru(1)-C(6)	2.271(3)	2.273	2.338
Ru(1)-C(1)	2.281(3)	2.273	2.338
Ru(1)-C(7)	2.462(3)	2.537	2.618
Ru(2)-C(8)	2.145(3)	2.183	2.252
Ru(2)-C(9)	2.171(3)	2.177	2.224
Ru(2)-C(10)	2.204(3)	2.195	2.241
Ru(2)-C(11)	2.208(3)	2.195	2.241
Ru(2)-C(12)	2.176(3)	2.177	2.224
Ru(2)-C(13)	2.180(3)	2.213	2.260
Ru(2)-C(14)	2.178(3)	2.197	2.242
Ru(2)-C(15)	2.178(3)	2.163	2.206
Ru(2)-C(16)	2.192(3)	2.163	2.206
Ru(2)-C(17)	2.194(3)	2.197	2.242
C(8)-C(7)	1.449(4)	1.414	1.429
α	165.7	169.7	174.1

Table 4. Comparison between calculated and experimental structural parameters for the sesquifulvalene complexe $[Ru_2C_{22}H_{20}]^{2+}$ with atom labeling in Fig. 4 (bond lengths in Å, angle in °)

We first performed a DFT calculation to optimize the structure of this complex ion. In order to reduce the computational effort, we optimized the structure in C_s symmetry. The plane of symmetry σ_h of the C_s point group contains both Ruthenium atoms and is orthogonal to the plane spaned by the sesquifulvalene moiety. In agreement with experimental results, we set the charge of the ion to +2. Moreover, based on experimental evidence as well, we began the computation with a transoid conformation of the $[Ru_2C_{22}H_{20}]^{2+}$ sesquifulvalene complexe. Indeed, it has been found that, without any exception, all archetype dinuclear sesquifulvalene complexes without an additional π-spacer adopt a transoid conformation, independent of the electronic nature of the donor an the acceptor. In contrast to it, all of the dinuclear complexes containing an additional π-bridge between the donor and acceptor always take a cisoid conformation[3].
Results of the geometry optimization can be found in Table 4. The best results are obtained with the LDA method, especially for the metal to ligand bond lengths. Our calculations are thus in agreement with the conclusion, often pointed out, that for Werner type complexes, GGA functionals lead to structural parameters in worse agreement with the experiment than the LDA[32]. The angle α appearing in Table 4 and in Fig. 4 is the angle enclosed by the vector which bisects the five-membered ring and contains the bridge-head atom of the Cp ring, and the bonding vector of the bridging bond between the five and seven-membered rings (C(8)-C(7)). This angle α appears to be very dependant on the acceptor and donor parts of the sesquifulvalene bimetallic complex, and thus finally on the NLO properties of the complex[3]. For this angle again, the LDA optimization gives a value in better agreement with experiment than GGA does.

6.4.2.2 Electronic properties

As mentionned previously for the two-level-approximation, electronic structure of a compound is very important with respect to its potential NLO properties. For the $[Ru_2C_{22}H_{19}]^{2+}$ sesquifulvalene complex, the molecular orbital scheme as well as the composition of the molecular orbital can be found in Fig. 5 and in Table 5 respectively.

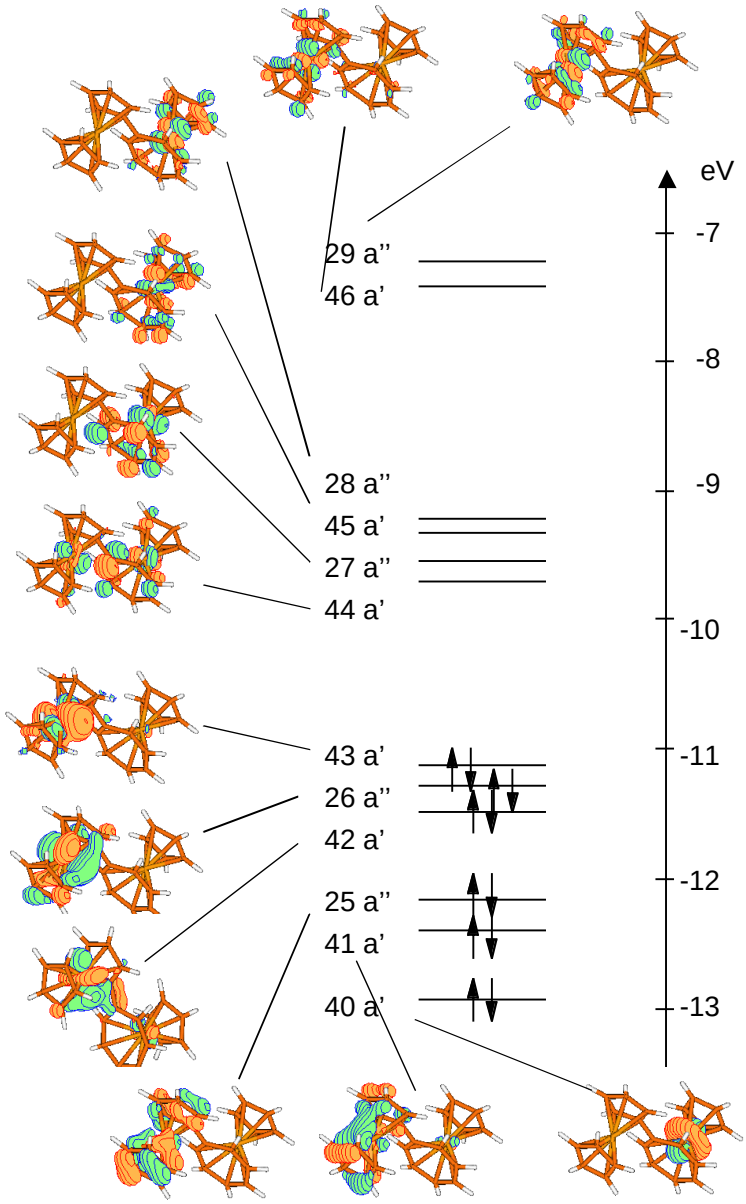

Figure 5. Frontier molecular orbitals of the [Ru2C22H20]2+ sesquifulvalene complexe with 3D representation of the MOs

	Ru(1)	Ru(2)	sesqu(7)	sesqu(5)	Cp(2)	Cp(1)	E (eV)
29a'' (0)	-	48% d_{xz}	-	-	25%	-	-7.2352
46a' (0)	-	41% d_{yz}	11%	19%	20%	-	-7.4143
28a'' (0)	47% d_{xz}	-	8%	-	-	32%	-9.2688
45a' (0)	36% d_{yz}	-	27%	-	-	25%	-9.2946
27a'' (0)	20% d_{xy}	-	68%	-	-	-	-9.5329
44a' (0)	8% d_{x2-y2} 8% d_{yz}	8% d_{x2-y2} 5% d_{z2}	37%	5%	5%	6%	-9.6996
43a' (2)	-	62% d_{z2} 16% d_{x2-y2}	-	-	-	-	-11.1086
26a'' (2)	-	75% d_{xy}	-	8%	10%	-	-11.2744
42a' (2)	5% d_{x2-y2}	54% d_{x2-y2} 6% d_{z2}	-	5%	5%	-	-11.4876
25a'' (2)	-	7% d_{xy}	-	32%	46%	-	-12.1847
41a' (2)	-	11% d_{z2}	-	23%	34%	-	-12.4091
40a' (2)	82% d_{z2}	-	-	-	-	-	-12.9440

Table 5. Orbital contributions to the $[Ru_2C_{22}H_{20}]^{2+}$ complexe

In Table 5, Ru(1) and Ru(2) refer to the labeling used in Fig. 4. Ru(1) is the metal coordinated to the seven-membered ring (sesqu(7)) of the sesquifulvalene moiety, and to the cyclopentadienyl ligand labeled Cp(1) as shown in Table 5. This part of the complex acts as the electron acceptor part[3]. Ru(2) is the metal coordinated to the five-membered ring (sesqu(5)) of the sesquifulvalene moiety, and to the cyclopentadienyl ligand labeled Cp(2) (cf. Table 5). This part of the complex acts as the electron donor part.

In our model, the highest molecular orbitals are mainly metal centered orbitals on Ru(2) : d_{z2}, d_{x2-y2}, d_{xy}. These orbitals, which are very close in energy, are all centered on the donor part of the complex, in agreement with experience and with a previous theoretical study[33]. The next highest occupied orbital is the HOMO-3 orbital. It results from a combination of the highest occupied cyclopentadienyl (Cp(2)) orbital and of the highest occupied π-bridge orbital (sesqu(5)), both are located on the donor part.

In contrast, the LUMO is largely localized on the acceptor moiety, but has also a small extension to the donor. In molecules with C_s symmetry, the z-axis is conventionally orthogonal to the σ-plane. It is to note that in our case, and for the sake of clarity, the σ-plane is defined by the yz plane. Thus, the z-axis is then parallel to the Ruthenium-cyclopentadienyl « bond » for each donor and acceptor part.

6.4.2.3 Excited states of the $[Ru_2C_{22}H_{20}]^{2+}$

More than the electronic structure of a complexe, its optical transition energies are very important for its NLO properties. To develop guidelines to design new metallocene dyes, it is helpful to know which transitions contribute significantly to the NLO response and to understand the molecular origin of these contributions.

		E (TDDFT)	f (TDDFT)
^{1}A’	43 a’ → 44 a’	797	$0.7\cdot10^{-2}$
^{3}A’		931	0
^{1}A’’	26 a’’ → 44 a’	735	$0.5\cdot10^{-3}$
^{3}A’’		822	0
^{1}A’’	25 a’’ → 44 a’	490	$0.3\cdot10^{-5}$
^{3}A’’		506	0
^{1}A’	42 a’ → 44 a’	480	0.1793
^{3}A’		770	0
^{1}A’	41 a’ → 44 a’	412	0.3402
^{3}A’		472	0

Table 6. Excited state energies for the $[Ru_2C_{22}H_{20}]^{2+}$ (values given in nm)

The UV-VIS spectra of the sesquifulvalene complexes consists generally of two absorption bands in the visible region or in the near UV. They are comparable to the spectra of metallocene – (π-bridge) – acceptor-type of compounds. In the case of the $[Ru_2C_{22}H_{20}]^{2+}$ complexe, the first band has been found to have its maximum around 462 nm (21645 cm^{-1}) in $MeNO_2$ solvent[3, 11]. The energy of the second band, which is shifted

towards the near UV, is not known exactly. The information we can find in the litterature is that λ_{max} is smaller than 370nm in $MeNO_2$[3, 11].

Within the time-dependent density functional theory framework (TDDFT), we computed some of the lowest transition energies (Table 6). We observe two transitions with a high oscillator strength amongst the lowest ones. These can correspond to the two bands experimentally observed. In our model, the two bands are predicted to lie energetically closer to each other than observed. We got a good prediction for the lower energy band which appears experimentally at 462nm and which has been calculated at 480nm in our work. However, it is important to be careful in analyzing those results, as it has been shown experimentally that the electronic excitations are governed by a strong negative solvatochromism for such complexes.

The assignment of those two bands has for a long time be subject of debates and discussions. Over the years, three model have been set up.

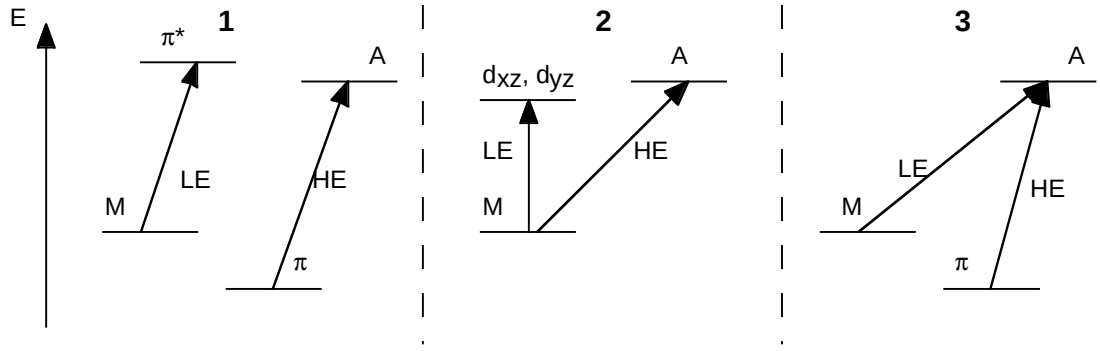

Figure 6. Schematic representation of the orbitals involved in the two bands of the UV-VIS spectra of metallocene – (π-bridge) – acceptor type of compounds for three different models

In the Fig. 6, M represents the set of quasi-degenerate highest occupied molecular orbitals mainly centered on the metal of the donor part. In our case, M consists of three orbitals : 43 a' (d_{z2}), 26 a'' (d_{xy}) and 42 a' (d_{x2-y2}) as can be seen in Table 5. The two next lower occupied molecular orbitals, i.e. the 25 a'' and 41a' in our case, are denoted as π in the different models. « A » represents the lowest unoccupied molecular orbital largely

localized on the acceptor, and π* the lowest unoccupied molecular orbital with substantial bridge contribution.

In the first model, 1 in Fig. 6, that has been proposed by Calabrese et al.[34], the lower energy (LE) of the two transitions was assigned to a charge-transfer transition between the HOMO M and the bridge-localized LUMO+1. The possibility of a direct HOMO-LUMO transition was considered less likely because of the small spatial overlap between these orbitals. The higher energy (HE) transition was assigned to a transition from π to LUMO.

In the second model, 2 in Fig. 6, that has been proposed by Kanis et al.[35], the LE transition was assigned to be a metal-localized ligand field (d-d) transition without significant contribution to β. Whereas the HE transition was identified as carrying a major contribution to β and was described as a metal-acceptor transition.

In the latest model, 3 in Fig. 6, that has been proposed by Barlow et al.[33], the LE absorption is a M → A transition, while the HE absorption is a π → A transition.

Our results are very close to model 3. Both intense electronic transitions arrise from the promotion of one electron out of an occupied orbital into the LUMO. The LE absorption is due to the promotion of one electron occupying initially the 42 a' orbital which belongs to M in our definition, and the HE absorption is due to the promotion of one electron occupying initially the 41 a' orbital which has been assigned as π.

The difference between our model and the model 3 originates from the assignement of the character of the LUMO. If our LUMO is mainly located on the acceptor part, it has a non-negligeable π* contribution localised on the bridge. In comparison, as can be seen in Table 5, LUMO+1, LUMO+2 and LUMO+3 have higher contribution from the acceptor and a lower contribution from the bridging part. Thus, our LUMO should carry the label A-π*. This is also in agreement with a high oscillator strength which requires a substantial spatial overlap between orbitals. A transition between an orbital located on the donor part and another orbital located on the acceptor part would result in a weak transition intensity.

6.4.2.4 Dipole moments of the $[Ru_2C_{22}H_{20}]^{2+}$

Up to know we have found two excited states relatively low in energy and with a large oscillator strength, among the lowest excited. Following the two-level-approximation, we still need a large difference between ground and excited states dipole moments in order to clearly predict that those two transitions contribute significantly to the observed NLO response.

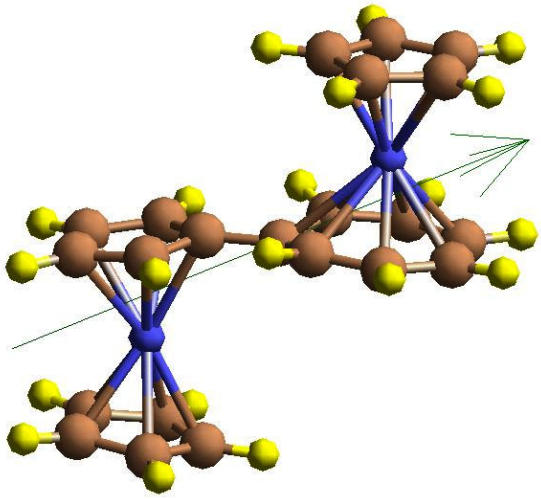

Figure 7. Dipole moment of the $[Ru_2C_{22}H_{20}]^{2+}$ ground state

The dipole moment of the ground state has been calculated to be

$$\vec{\mu}_{gg} = (0 \quad -9.2201 \quad -4.3925) \Rightarrow \left\|\vec{\mu}_{gg}\right\| = 10.2129 \text{ Debye}$$

The largest difference between the ground and excited state dipole moment has been found for the 43a' to 45a' transition. This latter one amounts to

$$\vec{\mu}_{ee(43a' \to 45a')} = (0 \quad -2.2578 \quad 1.1190) \Rightarrow \left\|\Delta\vec{\mu}\right\| = 8.8798 \text{ Debye}$$

For both of the transitions we assigned to the absorption bands, we did obtain the following dipole changes

$$\vec{\mu}_{ee(42a' \to 44a')} = (0 \quad -3.8703 \quad -0.6972) \Rightarrow \left\|\Delta\vec{\mu}\right\| = 6.5020 \text{ Debye}$$

$$\vec{\mu}_{ee(41a' \to 44a')} = (0 \quad -6.1335 \quad -2.6488) \Rightarrow \left\|\Delta\vec{\mu}\right\| = 3.5451 \text{ Debye}$$

The substantial dipole moment changes for both transitions, together with their low energies and high oscillator strengths, suggest that both transitions should contribute to the observed NLO response.

6.4.2.5 Hyperpolarizability computation of the $[Ru_2C_{22}H_{20}]^{2+}$

Keeping in mind that we have a model that gives a good description of the geometry and of the electronic structure of the $[Ru_2C_{22}H_{20}]^{2+}$ bimetallic sesquifulvalene complex, we performed a computation of the first hyperpolarizability at 1060nm and of the static hyperpolarizability.
As it was the case for p-nitroaniline, where we got results in good agreement with experience, we used the TDDF RESPONSE Theory to compute hyperpolarizability tensor elements. The results thus obtained are given in Table 7 below.

	TDDFT/LDA	Exp.
β_0	$39.5 \cdot 10^{-30}$	$53 \cdot 10^{-30}$
$\beta(-2\omega ; \omega,\omega)$ (1060nm)	$3805 \cdot 10^{-30}$	$264 \cdot 10^{-30}$

Table 7. Calculated static and first hyperpolarizabilities of $[Ru_2C_{22}H_{20}]^{2+}$

For those hyperpolarizability calculations, the LDA/VWN functional has been used. It would have certainly been better to compute hyperpolarizabilities with a functional like the LB94, but this was not possible due to the size of the complex.

6.5 Conclusion

This work has been done in collaboration with professor Jürgen Heck and his group from the Institute of Inorganic and Applied Chemistry of the University of Hamburg, Germany. For one of their research projects on NLO, they were interested in the modelization of NLO properties of some organometallic complexes. We got both, good results and challenging tasks for further work and collaboration.

Using TDDFT and the response theory as implemented in the ADF code, we got good hyperpolarizability values for small organic molecules with sufficiently high symmetry. For big systems e.g. bimetallic sesquifulvalene complexes however, the results we did obtain for the hyperpolarizability tensors are not yet satisfactory.
Other parameters like geometry, excited states in TDDFT and electronic structures are well reproduced in our model. This is very helpful to understand the UV-VIS spectra of such complexes, and enables us to then assign bands responsible for the NLO properties. In a near future, this will help synthetic chemists to setup novel strategies for the design and synthesis of compound with nonlinear optical properties. It is thus a domain were theory can, or shoud, be applied together with experiment.

6.6 References

(1) Williams, D. J., *Angew. Chem.* **1984**, *96*, 637.

(2) Burland, D. M., *Chem. Rev.* **1994**, *94*, 1.

(3) Heck, J.; Dabek, S.; Meyer-Friedrichsen, T.; Wong, H., *Coord. Chem. Rev.* **1999**, *190-192*, 1217.

(4) Lambert, C.; Stadler, S.; Bourhill, G.; Bräuchle, C., *Angew. Chem.* **1996**, *108*, 710.

(5) Morley, J. O., *J. Am. Chem. Soc.* **1988**, *110*, 7660.

(6) Bingmann, H.; Beck, A.; Fritz, H.; Prinzbach, H., *Chem. Ber.* **1981**, *114*, 1679.

(7) Cais, M.; Eisenstadt, A., *J. Am. Chem. Soc.* **1967**, *89*, 5468.

(8) Behrens, U.; Brussard, H.; Hagenau, U.; Heck, J.; Hendrickx, E.; Körnich, J.; van der Linden, J. G. M.; Persoons, A.; Spek, A. L.; Veldman, N.; Voss, B.; Wong, H., *Chem. Eur. J.* **1996**, *2*, 98.

(9) Long, N. J., *Angew. Chem.* **1995**, *107*, 37.

(10) Long, N. J., *Angew. Chem. Int. Ed. Engl.* **1995**, *34*, 21.

(11) Meyer-Friedrichsen, T., Dissertation, Hamburg, **1999**, pp. 172.

(12) Baerends, E. J.; Bérces, A.; Bo, C.; Boerrigter, P. M.; Cavallo, L.; Deng, L.; Dickson, R. M.; Ellis, D. E.; Fan, L.; Fischer, T. H.; Fonseca Guerra, C.; van Gisbergen, S. J. A.; Groeneveld, J. A.; Gritsenko, O. V.; Harris, F. E.; van den Hoek, P.; Jacobsen, H.; van Kessel, G.; Kootstra, F.; van Lenthe, E.; Osinga, V. P.; Philipsen, P. H. T.; Post, D.; Pye, C.; Ravenek, W.; Ros, P.; Schipper, P. R. T.; Schreckenbach, G.; Snijders, J. G.; Sola, M.; Swerhone, D.; te Velde, G.; Vernooijs, P.; Versluis, L.; Visser, O.; van Wezenbeek, E.; Wiesenekker, G.; Wolff, S. K.; Woo, T. K.; Tiegler, T.,
(13) Fonseca Guerra, C.; Snijders, J. G.; te Velde, G.; Baerends, E. J., *Theor. Chem. Acc.* **1998**, *99*, 391.

(14) Vosko, S. H.; Wilk, L.; Nusair, M., *Can. J. Phys.* **1980**, *58*, 1200.

(15) Becke, A. D., *Phys. Rev. A* **1988**, *38*, 3098.

(16) Perdew, J. P., *Phys. Rev. B* **1986**, *33*, 8822.

(17) van Leeuwen, R.; Baerends, E. J., *Phys. Rev. A* **1994**, *49*, 2421.

(18) Karna, S. P.; Prasad, P. N.; Dupuis, M., *J. Chem. Phys.* **1991**, *94*, 1171.

(19) Sim, F.; Chin, S.; Dupuis, M.; Rice, J., *J. Phys. Chem.* **1993**, *97*, 1158.

(20) Shelton, D. P.; Rice, J. E., *Chem. Rev.* **1994**, *94*, 3.

(21) Stähelin, M.; Burland, D.; Rice, E. J., *Chem. Phys. Lett.* **1992**, *191*, 245.

(22) Oudar, J. L.; LePerson, H., *Opt. Commun.* **1975**, *18*, 410.

(23) Teng, C. C.; Garito, A. F., *Phys. Rev. Lett.* **1983**, *50*, 350.

(24) Levine, B. F., *Chim. Phys. Lett.* **1976**, *37*, 516.

(25) Li, D.; Ratner, M. A.; Marks, J. T., *J. Am. Chem. Soc.* **1988**, *110*, 1707.

(26) Dirk, C. W.; Twieg, R. J.; Wagnière, G., *J. Am. Chem. Soc.* **1986**, *108*, 5387.

(27) Docherty, V. J.; Pugh, D.; Morley, J. O., *J. Chem. Soc. Faraday Trans.* **1985**, *81*, 1179.

(28) Davydov, B. L.; Derkacheva, L. D.; Dunina, V. V.; Zhabotinskii, M. E.; Zolin, V. F.; Koreneva, L. G.; Samokhina, M. A., *Opt. Spectrosc.* **1970**, *30*, 274.

(29) Green, M. L. H.; Marder, S. R.; Thompson, M. E.; Bandy, J. A.; Bloor, D.; Kolinsky, P. C.; Jones, R. J., *Nature* **1987**, *330*, 360.

(30) Oudar, J. L.; Chemla, D. S., *Chem. Phys.* **1977**, *66*, 2664.

(31) Hendrickx, E.; Clays, K.; Persoons, A.; Dehu, C.; Brédas, J. L., *J. Am. Chem. Soc.* **1995**, *117*, 3547.

(32) Bray, M. R.; Deeth, R. J.; Paget, V. J.; Sheen, P. D., *Int. J. Quant. Chem.* **1996**, *61*, 85.

(33) Barlow, S.; Bunting, H. E.; Ringham, C.; Green, J. C.; Bublitz, G. U.; Boxer, S. G.; Perry, J. W.; Marder, S., *J. Am. Chem. Soc.* **1999**, *121*, 3715.

(34) Calabrese, J. C.; Cheng, L.-T.; Green, J. C.; Marder, S. R.; Tam, W., *J. Am. Chem. Soc.* **1991**, *113*, 7227.

(35) Kanis, D. R.; Ratner, M. A.; Marks, T. J., *Chem. Rev.* **1994**, *94*, 195.

BUCHS Matthieu

adresse:	rue Jean-Grimoux 13, 1700 Fribourg
téléphone (prof.):	026/300 87 49
téléphone (priv.):	026/322 63 49
e-mail:	matthieu.buchs@unifr.ch
né le:	09.05.1973
nationalité:	suisse
état civil:	célibataire
adresse internet:	http://www-chem.unifr.ch/ac/phd/mbuchs

EDUCATION

1997 – 2000 **Doctorant à l'institut de chimie inorganique et analytique de la Faculté des Sciences Naturelles de l'Université de Fribourg dans le groupe du professeur Claude Auguste Daul**
sujet : *Etudes de propriétés de complexes métalliques à l'aide de la Théorie de la Fonctionnelle de Densité.*

1992 - 1996 **Université**
Université de Fribourg, Faculté des Sciences Naturelles, section chimie

1988 - 1992 **Gymnase – Lycée**
Collège St-Michel, Fribourg

DIPLOMES OBTENUS

19.12.1996 **Diplôme de chimie** sujet principal: chimie physique (isolation de radicaux, spectroscopie en matrice gelée)
sujet secondaire: chimie inorganique (chimie théorique, théorie de la fonctionelle de la densité)

20.06.1992 **Certificat de Maturité de type C** (scientifique)

EXPERIENCE PROFESSIONNELLE

2000 - **Secrétaire auxiliaire**
Service Presse et Communication de l'université de Fribourg

1999 - **Chroniqueur scientifique pour le quotidien romand édité à Fribourg « La Liberté »**

1998 - **Assistant informatique pour l'institut de chimie inorganique**
Participation à l'établissement du budget, Webmestre de la section de chimie de l'Université de Fribourg, responsable du bon fonctionnement des PCs,…

CONNAISSANCES UTILES

Informatique: systèmes IRIX (Unix), LINUX, DOS, Windows 95, MacOS x.x
Pack Microsoft Office (de 5.0 à 98), traitement de texte LaTex, Logiciel intégré Claris, Matlab, Photoshop et autres ; ADF, Cerius2, Hyperchem, Gaussian

Langues: **Français** : langue maternelle
Deutsch: gute schriftliche und mündliche Kenntnis (Vater Sprache)
English: good knowledge for writing and speaking english

PUBLICATIONS

- 'Geometry Optimization and Excited States of Tris(2,2'-bipyridine)ruthenium(II) using Density Functional Theory'.
  M.Buchs and C.Daul, *Chimia*, **1998**, *52*, 163.
- 'DFT Investigation of Metal Complexes Containing a Nitrosyl Ligand. Part I : Ground State and Metastable States.'
  P. Boulet, M. Buchs, H. Chermette, C. Daul, F. Gilardoni, F. Rogemond, C.W. Schläpfer and J. Weber, *en préparation*.
- 'DFT Investigation of Metal Complexes Containing a Nitrosyl Ligand. Part II : Excited States.'
  P. Boulet, M. Buchs, H. Chermette, C. Daul, F. Gilardoni, F. Rogemond, C.W. Schläpfer and J. Weber, *en préparation*.

PRESENTATIONS

- 'The Electronic Structure of Tris(2,2'-bipyridine)Ruthenium(II) using Density Functional Theory'
  poster lors du meeting Suisse-Alsace, Mulhouse, 15-16.05.**1997**.
- 'Geometry Optimisation and Excited States of Tris(2,2'-bipyridine)Ruthenium(II) using Density Functional Theory'
  poster présenté lors de la conférence IUPAC, Genève,17-22.08.**1997**.
- 'Study of Bis(2,2,6,6-tetramethylheptane-3,5-dionato)Nickel(II) and the addition product with bipyridine using DFT'
  poster lors de la '7th International Conference on the Applications of Density Functional Theory', Vienne, 2-6.09.**1997**.
- 'The Electronic Structure of Tris(2,2'-bipyridine)Ruthenium(II) using Density Functional Theory'
  présentation orale lors de l'Assemblée d'automne de la Nouvelle Société Suisse de Chimie, Lausanne, 15.10.**1997**.
- 'The electronic structure of Pentacyanonitrosylferrate (II) (Nitroprusside) using DFT'
  poster à l'occasion du 34ème Symposium de Chimie Théorique, Gwatt (CH), 20-24.09. **1998**.
- 'Study of Bis(2,2,6,6-tetramethylheptane-3,5-dionato)Nickel(II) and the addition product with bipyridine using DFT'
  présentation orale lors de l'Assemblée d'automne de la Nouvelle Société Suisse de Chimie, Zürich,15.10.**1998**.
- 'Density Functional Study of the Photodissociation of $[Ru(bpy)_3]^{2+}$'

poster à l'occasion d'un meeting COST du groupe de travail D9/0002/1997, Genève, 3-5. 07.**1999**.

- 'Density Functional Study of the Photodissociation of $[Ru(bpy)_3]^{2+}$'
  poster à l'occasion du congrès WATOC (World Association of Theoretically Oriented Chemists), Londre, 1-6.08.**1999**.
- 'Excited States of $[Ru(bpy)_3]^{2+}$'
  poster lors de la '8th International Conference on the Applications of Density Functional Theory', Rome, 6-9.09.**1999**.
- 'Excitation energies in DFT using response theory and ΔSCF for different types of molecule'
  poster à l'occasion de l'Assemblée d'automne de la Nouvelle Société Suisse de Chimie, Bâle, 12.10.**1999**.
- 'A density functional study of sesquifulvalene complexes : results and perspectives'
  séminaire donné dans le groupe du professeur Jürgen Heck, Hamburg, 16-18.03.**2000**.
- 'A density functional study of sesquifulvalene complexes : results and perspectives'
  présentation orale à l'occasion d'une réunion TMR (Training and Mobility Researchers) du réseau 'Organometallic dipoles with NLO properties, Norwich (UK), 12-16.4.**2000**.